

M.Sc. Marine Biology

Master Thesis

---

**The physiological response of the Arctic haptophyte  
*Phaeocystis pouchetii* to marine heatwaves**

---

Submitted by:

Naomi Urbschat

Supervisors:

Prof. Dr. Björn Rost

Alfred Wegener Institute – Helmholtz Centre for Polar and Marine Research,  
Bremerhaven

Prof. Dr. Kai Bischof

Universität Bremen

Bremen, 08.03.2022

Naomi Urbschat

3210481

---

Name:

Enrolment number:

### Declaration of copyright

Hereby I declare that my Master's Thesis was written without external support and that I did not use any other sources and auxiliary means than those quoted. All statements which are literally or analogously taken from other publications have been identified as quotations.

Bremen, 08.03.2022



---

Date:

Signature

### Declaration with regard to publishing theses

Two years after the final degree, the thesis will be submitted to the University of Bremen archive and stored there permanently.

Storage includes:

- 1) Master's Theses with a local or regional reference, as well as 10 % of all theses from every subject and year
- 2) Bachelor's Theses: The first and last Bachelor degrees from every subject and year

I agree that for research purposes third parties can look into my thesis stored in the University archive.

I agree that for research purposes third parties can look into my thesis stored in the University archive after a period of 30 years (in line with §7 para. 2 BremArchivG).

I do not agree that for research purposes third parties can look into my thesis stored in the University archive.

Bremen, 08.03.2022



---

Date:

Signature

## Acknowledgements

First of all I would like to thank Prof. Dr. Björn Rost and Prof. Dr. Kai Bischof for evaluating this thesis and for supporting me in this very special situation.

To the whole Phytochange group at AWI, I want to say thank you for welcoming me so kindly in your group. Being part of this team was very enriching, not only professionally but also personally.

Very special thanks go to Prof. Dr. Björn Rost, Dr. Klara Wolf, Dr. Clara Hoppe and Dr. Sebastian Rokitta. It has really been a pleasure to work with all of you and to dive deeper into phytoplankton ecophysiology! Thank you for always taking the time to answer my questions and inspiring and lively discussions. Although I didn't know much about this research field when I started with my Master's degree, I can now say I definitely found the field of research that truly fascinates me!

I am deeply grateful to Björn and Klara, for their guidance and constructional criticism and for supporting me in this race against time. Especially Klara, I want to thank for her outstanding supervision, support in the lab, for infecting me with her enthusiasm for phytoplankton research, but also for just a wonderful time together.

Further I would like to thank Tina Brenneis for the kind support and indispensable help with measurements and Laura Wischnewski, Jil Sonka, Daniel Scholz, Klaus-Uwe and Ulrike Richter for technical assistance.

I thank Eva-Maria Nöthig for taking the time to marvel with me at microscopy samples of *Phaeocystis*, her help in identification and sharing the fascination of this peculiar phytoplankton species.

A big thank you also goes to my Phyto-Girls Antonia, Jasmin and Linda for keeping me sane in lunch and coffee breaks, providing me with sufficient sugar, encouraging me and supporting me on crazy lab days.

Last but not least, I would like to thank my family for always supporting me in my career choice and believing in me and Timo for being my rock and haven of peace.

# Table of Contents

<b>List of Figures</b> .....	I
<b>List of Tables</b> .....	II
<b>List of Abbreviations</b> .....	III
<b>Summary</b> .....	V
<b>Zusammenfassung</b> .....	VII
<b>1. Introduction</b> .....	1
1.1. Phytoplankton shape the biogeochemistry of the oceans .....	1
1.2. Physiological processes in unicellular photoautotrophs.....	3
1.2.1. Photosynthesis and respiration.....	3
1.2.2. Allocation of energy and carbon between metabolic pathways.....	5
1.3. Temperature as a master driver of physiological processes .....	6
1.4. Reactive oxygen species .....	8
1.5. Primary production in the Arctic Ocean.....	9
1.6. Warming of the Arctic Ocean and marine heatwaves .....	11
1.7. Aim of study .....	14
<b>2. Materials and Methods</b> .....	16
2.1. Culturing conditions .....	16
2.2. Experimental setup and timeline.....	17
2.4. Growth rates.....	21
2.5. Elemental analysis.....	22
2.6. Measurement of chlorophyll <i>a</i> by fluorometric analysis.....	23
2.7. Fast Repetition Rate Fluorometry (FRRF) .....	24
2.8. Flow cytometric analysis of reactive oxygen species .....	28
2.9. Statistical analysis .....	31
<b>3. Results</b> .....	33
3.1. Carbonate chemistry.....	33
3.2. Growth rates.....	33
3.3. Cellular composition and production rates .....	35
3.4. Photophysiological response.....	38
3.5. Intracellular levels of reactive oxygen species .....	43
<b>4. Discussion</b> .....	45
4.1. Acute response to rapidly increasing temperature .....	45
4.2. Warming triggers accumulation of reactive oxygen species .....	46
4.3. MHWs reduce photosynthetic efficiency .....	48

4.4. Stress responses are enhanced during longer MHWs .....	49
4.5. Acclimated response to continued heat stress.....	51
4.6. Impact of the post-MHW cooling – a relief or additional stressor?.....	52
4.7. Performance of <i>Phaeocystis pouchetii</i> in the future Arctic Ocean and implications for future research .....	55
<b>References</b> .....	<b>60</b>

## List of Figures

<b>Figure 1.</b> Schematic illustration of the biological carbon pump .....	1
<b>Figure 2.</b> Schematic representation of the mechanisms of photosynthesis .....	4
<b>Figure 3.</b> Major generation sites of the reactive oxygen species superoxide anion radical ( $O_2^{\bullet-}$ ) and hydrogen peroxide ( $H_2O_2$ ) in phytoplankton.....	9
<b>Figure 4.</b> Images of <i>Phaeocystis pouchetii</i> cells under a light microscope .....	10
<b>Figure 5.</b> Projected change in annual mean surface temperature until the end of the century under the RCP2.6 and RCP8.5 scenarios .....	12
<b>Figure 6.</b> Simulated changes in the probability of MHWs for different levels of global warming .....	13
<b>Figure 7.</b> Experimental timeline.....	18
<b>Figure 8.</b> Overview of the timepoints of harvest, fast repetition rate fluorometry (FRRF) and reactive oxygen species (ROS) measurements during the MHW treatments.....	19
<b>Figure 9.</b> Fluorescence spectra of Chlorophyll <i>a</i> and Pheophytine <i>a</i> .....	23
<b>Figure 10.</b> The concept of energy allocation after light absorption and chlorophyll fluorescence transients from light and dark-regulated states .....	25
<b>Figure 11.</b> Photosynthesis vs irradiance curve .....	27
<b>Figure 12.</b> Absorption- and emission spectra of the fluorochromes Dihydroethidium (HE) and Dihydrorhodamine123 (DHR123) .....	29
<b>Figure 13.</b> Application of the gating tool on plots of detected fluorescence emission.....	30
<b>Figure 14.</b> Overview of the study design.....	31
<b>Figure 15.</b> Specific growth rates $\mu$ .....	34
<b>Figure 16.</b> Elemental composition and pigmentation.....	36
<b>Figure 17.</b> FRRF measurement of PSII quantum yield efficiency $F_v/F_m$ .....	39
<b>Figure 18.</b> Temporal changes of relative electron transport rate (rETR), connectivity ( $\rho$ ), absorption cross-section of photosystem II ( $\sigma_{PII}$ ) and reopening rate of PSII ( $\tau$ ) .....	40
<b>Figure 19.</b> Capacity for non-photochemical quenching .....	42
<b>Figure 20.</b> Intracellular levels of reactive oxygen species .....	43

## List of Tables

<b>Table 1.</b> Summary of the abbreviations and units of photophysiological parameters.....	28
<b>Table 2.</b> Carbonate chemistry parameters .....	33
<b>Table 3.</b> Growth rates $\mu$ , POC production rates and cellular quota of POC and PON as well as their ratio .....	37
<b>Table 4.</b> Chl <i>a</i> production, cellular Chl <i>a</i> quota and Chl <i>a</i> :POC ratio .....	38
<b>Table 5.</b> PSII photochemistry measurements .....	41

## List of Abbreviations

ANOVA	Analysis of variance
AO	Arctic Ocean
ATP	Adenosine triphosphate
C	Carbon
CCM	CO <sub>2</sub> concentrating mechanisms
Chl <i>a</i>	Chlorophyll <i>a</i>
ChlF	Chlorophyll <i>a</i> fluorescence
CO <sub>2</sub>	Carbon dioxide
DHR123	Dihydrorhodamine 123
DIC	Dissolved inorganic carbon
DMSO	Dimethylsulfoxide
End	Timepoint at the end of the marine heatwave
F <sub>0</sub>	Minimal fluorescence in the dark
F'	Minimal fluorescence in the light
F <sub>m</sub>	Maximal fluorescence in the dark
F <sub>m</sub> '	Maximal fluorescence in the light
F <sub>q</sub> '/F <sub>m</sub> '	Quantum yield (efficiency) of electron transport through PSII in the light
FRRF	Fast repetition rate fluorometry
F <sub>v</sub>	Variable fluorescence in the dark
F <sub>v</sub> /F <sub>m</sub>	Quantum yield (efficiency) of electron transport through PSII in the dark
HE	Dihydroethidium
H <sub>2</sub> O <sub>2</sub>	Hydrogen peroxide
IPCC	Intergovernmental Panel on Climate Change
LMM	Linear mixed-effect model
MHW	Marine heatwave
Mid	Timepoint during marine heatwave
NADP <sup>+</sup>	Nicotinamide adenine dinucleotide phosphate
NADPH	Reduced form of NADP <sup>+</sup>
NPQ	Non-photochemical quenching
O <sub>2</sub>	Oxygen
O <sub>2</sub> <sup>•-</sup>	Superoxide anion radical
P680	Photochemical reaction centre of PSII

P700	Photochemical reaction centre of PSI
PC	Plastocyanin
pCO <sub>2</sub>	Carbon dioxide partial pressure
pCR	Timepoint post-cooling ramp
pH	Negative logarithm of the hydrogen ion activity
pHR	Timepoint post-heating ramp
PI-curve	Photosynthesis-irradiance curve
POC	Particulate organic carbon
PON	Particulate organic nitrogen
ppm	Parts per million
PQ	Plastoquinone
Pre	Timepoint pre-marine heatwave
PSI/II	Photosystem I/II
RCP	Representative Concentration Pathways
Rec	Timepoint during recovery
rETR	Relative PSII electron transfer rate
ROS	Reactive oxygen species
RuBisCO	Ribulose-1,5-bisphosphate carboxylase/oxygenase
RuBP	Ribulose-1,5-bisphosphate
SOD	Superoxide dismutase
SST	Sea surface temperature
TA	Total alkalinity
TCA cycle	Tricarboxylic acid cycle
Y(NPQ)	Quantum yield of regulated non-photochemical energy loss in PS II
Y(NO)	Quantum yield of non-regulated non-photochemical energy loss in PS II
μ	Growth rate
ρ	Connectivity between PSII reaction centres in the dark
σ <sub>PII</sub>	Absorption cross section for PSII photochemistry in the dark
τ	Time constant for PSII re-oxidation in the dark

## Summary

Due to the ongoing global warming extreme weather events like marine heatwaves (MHWs) have already become more frequent and intense as well as longer lasting, and their probability of occurrence is projected to increase in the future, especially in the Arctic Ocean. MHWs can rapidly push a species beyond their usually experienced temperature range, often exceeding physiological tolerance thresholds. Furthermore, fluctuation between higher and lower temperatures associated with MHWs can induce metabolic mismatches between physiological subprocesses. Thus, MHWs could have worse effects on the performance of a species than those emanating from the mean temperature rise due to global warming. Despite this potential threat, knowledge on the impact of MHWs on Arctic phytoplankton is still scarce.

In this master thesis project, I designed a laboratory experiment to investigate the physiological capacity of the Arctic key phytoplankton species *Phaeocystis pouchetii* to physiologically acclimate to heatwave scenarios. After pre-acclimation to experimental conditions at 3 °C, cells were rapidly exposed to two MHWs with an intensity of 6 °C for varying durations (MHW1: 6 days, MHW2: 10 days), followed by a 5-day recovery phase at 3 °C. The non-acclimated response to the MHW treatments was further compared to the acclimated response of cells experiencing continuous heat exposure of 6 °C for 3 weeks. The physiological performance of cells was investigated by assessing specific growth rates, elemental composition and cellular chlorophyll *a* content. Furthermore, photophysiology was assessed by fast repetition rate fluorometry (FRRF) measurements of variable chlorophyll fluorescence and intracellular levels of O<sub>2</sub><sup>•-</sup> and H<sub>2</sub>O<sub>2</sub> were determined by flow cytometric analysis.

The results demonstrated that warming strongly stimulated growth rates in the short-term and reduced photosynthetic efficiency and triggered production of reactive oxygen species (ROS) in the long-term. Intracellular ROS levels reached a maximum after 6 days and declined thereafter, which was likely enabled by a highly effective antioxidant scavenging system and the water-water cycle. In the long-term, *P. pouchetii* was not able to maintain the stimulated growth rates observed shortly after the temperature rise, which could be explained by a reallocation of energy into ROS detoxification. Longer MHWs exerted more thermal stress on cells than shorter ones, as indicated by lower  $F_v/F_m$  values and decreased POC quota. Thermal acclimation of cells to continuous heat exposure (6 °C control) involved enhanced light absorption capacity by increasing cellular Chl *a* content, increased POC quota and rebalancing of intracellular ROS levels. A high capacity for ROS scavenging, but also elevated thresholds towards oxidative stress may thus play a pivotal role in this species' resilience to increased

thermal stress. However, thermal plasticity comes at a metabolic cost and reduced performance in the long-term, as indicated by lower growth rates of cultures acclimated to 6 °C compared to 3 °C. During the recovery at 3 °C after the MHWs, Chl *a* content decreased as an adjustment to reduce excitation pressure. In combination with the still upregulated detoxification mechanisms during MHW exposure, ROS levels declined. The cooling post-MHW therefore represented a relief to cells in regard to oxidative stress, but it nevertheless required re-acclimation and reduced performance as indicated by the trend of declining growth rates during recovery.

The overall effect of MHWs on the fitness of *P. pouchetii* was nevertheless only marginal and even though 6 °C seems to be positioned above its optimum temperature, it is still within its thermal tolerance range. The resilience of this species towards MHWs with an intensity of 6 °C might be explained by the adaptation to the warmer and fluctuating temperatures of the Fram Strait, where this strain was originally isolated or advection of this strain into the Arctic from lower latitudes. Even though maximizing growth does not seem to be the ecological strategy of *P. pouchetii*, it may nonetheless outcompete other species with lower thermal thresholds. In addition, the heteromorphic life cycle and high capacity for protection against oxidative stress may represent valuable strategies, that enable the ecological success of this species in the future Arctic Ocean.

## Zusammenfassung

Der Klimawandel verursacht nicht nur eine Erwärmung der Meeresoberfläche, sondern erhöht auch die Wahrscheinlichkeit von Wetterextremen wie marinen Hitzewellen (MHWs). Im Arktischen Ozean treten diese Extreme bereits heute vermehrt auf, jedoch werden deren Häufigkeit, Dauer und Intensität in Zukunft noch weiter zunehmen. MHWs können Arten Temperaturen außerhalb ihres gewohnten Temperaturbereich aussetzen, die oft auch außerhalb ihrer physiologischen Toleranzschwelle liegen. Zudem können die durch MHWs hervorgerufenen Fluktuationen zwischen niedrigen und hohen Temperaturen ein Ungleichgewicht zwischen physiologischen Teilprozessen verursachen. Somit könnten MHWs schwerwiegendere Auswirkungen auf die Physiologie und Konkurrenzfähigkeit einer Art haben als diejenigen, die von dem mittleren Temperaturanstieg herrühren. Trotz dieser potenziellen Bedrohung ist die Kenntnis über die möglichen Auswirkungen von MHWs auf arktisches Phytoplankton bislang sehr begrenzt.

Im Zuge dieser Masterarbeit, untersuche ich experimentell die physiologische Kapazität der arktischen Phytoplankton-Schlüsselart *Phaeocystis pouchetii* sich an Hitzewellen Szenarios zu akklimatisieren. Nach einer Vorakklimatisierung der Zellkulturen an 3 °C wurden diese zwei unterschiedlich langen MHWs mit einer Intensität von 6 °C ausgesetzt (MHW1: 6 Tage, MHW2: 10 Tage), gefolgt von einer fünftägigen Erholungsphase bei 3 °C. Die unakklimatisierte Reaktion zu den MHWs wurde zudem mit der akklimatisierten Reaktion von Zellen verglichen, die einer konstanten Temperatur von 6 °C für 3 Wochen ausgesetzt waren. Die physiologische Leistung der Zellen wurde durch die Bestimmung von Wachstumsraten, zelluläre Elementarzusammensetzung und Chlorophyll *a*-Gehalt, sowie die Analyse der Photophysilogie durch fast repetition rate fluorometry (FRRF)-Messungen der variablen Chlorophyllfluoreszenz beschrieben. Zudem wurden intrazelluläre Superoxidanion ( $O_2^{\cdot-}$ )- und Wasserstoffperoxid ( $H_2O_2$ )-Konzentrationen mithilfe von Durchflusszytometrie bestimmt.

Die Ergebnisse zeigen, dass eine Temperaturerhöhung kurzfristig die Wachstumsraten stark stimuliert und langfristig die photosynthetische Kapazität reduziert und eine Akkumulierung reaktiver Sauerstoffspezies (engl. reactive oxygen species, ROS) innerhalb der Zellen verursacht, welche ihr Maximum nach 6 Tagen erreichte. Während der längeren MHW fielen die ROS-Level wieder ab, womöglich bedingt durch ein effektives antioxidatives Scavenging-System und den Wasser-wasser-Zyklus. Diese Umleitung an Energie in ROS-Entgiftung erklärt möglicherweise, warum *P. pouchetii* die kurz nach der Hitzerampe beobachteten stimulierten Wachstumsraten unter verlängerter Hitzeexposition nicht aufrecht erhalten konnte. Eine

Verringerung der  $F_v/F_m$  und POC-Werte während MHW2 lassen darauf schließen, dass längere MHWs im Vergleich zu kürzeren MHWs mehr Hitzestress auf Zellen auslösten. Thermische Akklimatisierung von Zellen, die dauerhaften Hitzestress ausgesetzt waren (6 °C), involvierte erhöhte Lichtabsorptionskapazität durch gesteigerten Chl *a*-Gehalt, höhere POC-Quoten und einen Wiederausgleich von intrazellulärem ROS-Gehalt. Eine hohe Kapazität für ROS-Scavenging, aber auch ein erhöhter Schwellenwert an tolerierbarem oxidativem Stress spielen wahrscheinlich eine entscheidende Rolle für die Widerstandsfähigkeit dieser Art in Reaktion auf erhöhten Temperaturstress. Jedoch erforderte diese thermische Plastizität erhebliche zelluläre energetische Kosten und verringerte die Leistungsfähigkeit auf lange Sicht, angezeigt durch die niedrigeren Wachstumsraten bei 6 °C im Vergleich zu 3 °C. Während der Erholungsphase bei 3 °C nach den MHWs, verringerte sich der zelluläre Chl *a*-Gehalt als Anpassung zur Reduzierung überschüssiger Anregungsenergie. In Kombination mit den noch immer durch die MHW-Exposition hochregulierten ROS-Entgiftungsmechanismen, sanken intrazelluläre ROS-Konzentrationen. Die Temperaturverringerung nach den MHWs stellte daher in Bezug auf oxidativen Stress eine Entlastung für die Zellen dar, jedoch erforderte diese auch eine physiologische Re-Akklimatisierung und verringerte die Leistungsfähigkeit, wie durch die Tendenz sinkender Wachstumsraten während der Erholungsphase angezeigt wurde.

Ingesamt waren die Auswirkungen von MHWs auf die Fitness von *P. pouchetii* nur geringfügig und auch wenn 6 °C wahrscheinlich oberhalb des Temperaturoptimums dieser Art liegt, ist diese noch innerhalb des Temperatur-Toleranzbereiches. Eine mögliche Erklärung für die Resilienz dieser Art gegenüber MHWs mit einer Intensität von 6 °C ist die Anpassung an die wärmeren und fluktuierenden Temperaturen der Framstraße, in der diese Zelllinie ursprünglich isoliert wurde, oder die Advektion dieser Zelllinie in die Arktis von niederen Breiten. Auch wenn die Maximierung von Wachstumsraten vermutlich nicht der ökologischen Strategie von *P. pouchetii* entspricht, kann diese Mikroalge nichtsdestotrotz andere Arten mit niedrigeren Temperaturtoleranzen auskonkurrieren. Zudem stellen der heteromorphe Lebenszyklus und die hohe Kapazität für den Schutz vor oxidativem Stress wertvolle Strategien für den ökologischen Erfolg dieser Art im zukünftigen arktischen Ozean dar.

# 1. Introduction

## 1.1. Phytoplankton shape the biogeochemistry of the oceans

The sunlit layer of the world's oceans is teeming with microscopic organisms drifting with the currents. These unicellular photoautotrophs are called phytoplankton. By using the solar energy in the euphotic zone of the oceans, they fix carbon dioxide ( $\text{CO}_2$ ) and turn it into organic matter in the process of photosynthesis. In this way, these minute microalgae have permanently altered Earth's atmosphere over two billion years through the drawdown of  $\text{CO}_2$  and the accompanied rise of atmospheric oxygen levels (Bekker *et al.*, 2004). Even though they only make up  $<1\%$  of the global primary producer biomass, they still provide half of the oxygen on Earth today (Falkowski *et al.*, 1998; Field *et al.*, 1998).

Moreover, phytoplankton form the base of the aquatic food web by supplying organic matter for all organisms of higher trophic levels in the ecosystem. Particulate organic carbon (POC)

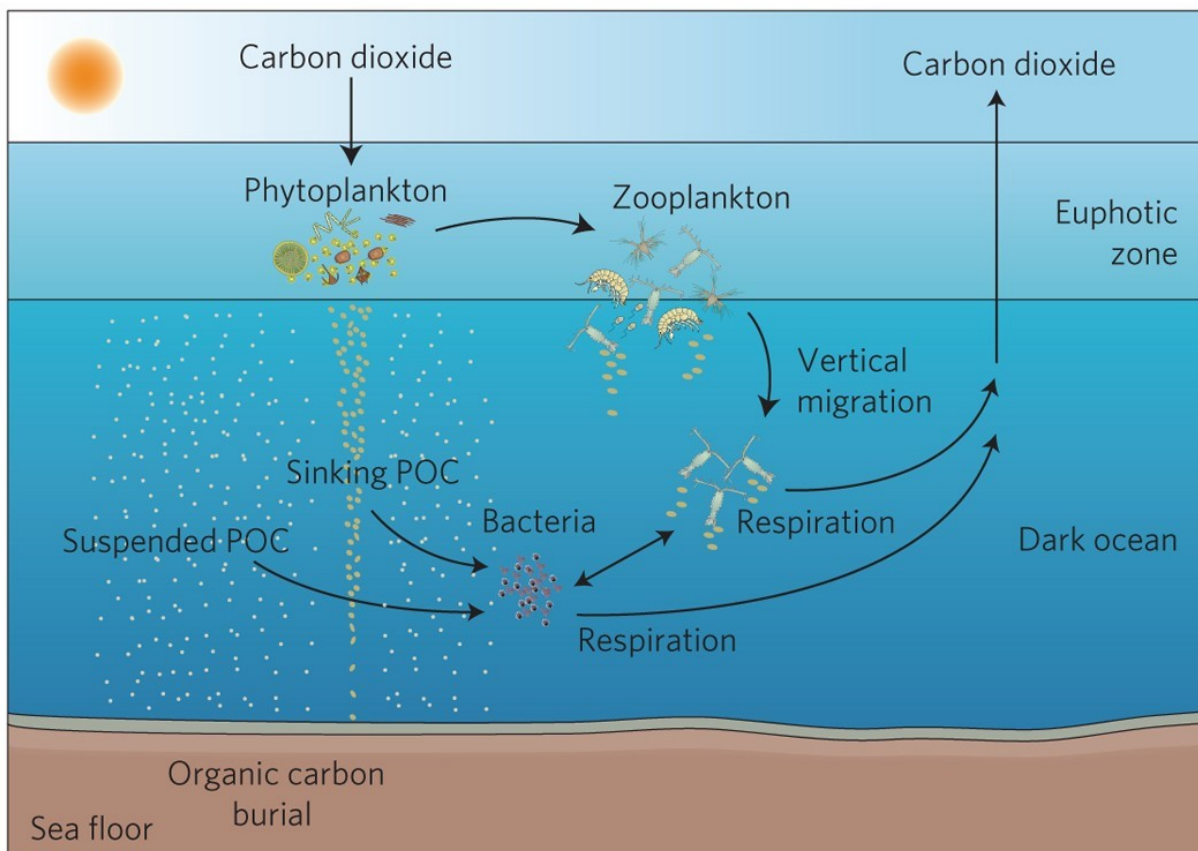


**Figure 1.** Schematic illustration of the biological carbon pump. Atmospheric carbon dioxide diffuses into seawater and is converted to particulate organic carbon (POC) by phytoplankton in the process of photosynthesis. Zooplankton feed on this POC and a part of the resulting faecal pellets, but also detritus and dead cells sink down to the ocean interior. The subsequent remineralization of the exported carbon enriches the deep ocean reservoir with inorganic carbon. Reprinted from Herndl and Reinthaler (2013).

such as dead cells are converted into aggregates and zooplankton faecal pellets (Basu and Mackey, 2018; Fig. 1). The downward flux of this so-called export production from the euphotic zone drives the exchange of carbon between the upper ocean and the ocean interior (Berger *et al.*, 1987). Exported production is subsequently remineralized on the way down by heterotrophic microbes and zooplankton, thereby enriching the deep ocean reservoir with dissolved inorganic carbon (DIC; Fig. 1). The fixation of CO<sub>2</sub> at the surface ocean, the transport to depth as POC and the subsequent conversion back to DIC are the processes underlying the so-called biological carbon pump (Falkowski *et al.*, 1998; Volk and Hoffert, 1985). Most of the exported carbon in the deep water masses returns to the atmosphere on millennial timescales through upwelling and the thermohaline circulation. However, the timescale of this carbon exchange depends on the depth of remineralisation. Less than 1 % of the exported carbon is even buried in the sediment over geological timescales. In this way, the biological carbon pump plays an extraordinary role in regulating atmospheric CO<sub>2</sub> levels and thus the climate.

Key factors controlling the formation of phytoplankton biomass in the euphotic zone are light and nutrient availability. In order to form carbohydrates, proteins, nucleic acids and lipids, cells not only need to assimilate carbon (C), but also other nutrients like nitrogen (N), phosphorus (P), silicate, sulphur and trace metals like iron and zinc. Particulate organic matter in the sea exhibits a specific elemental ratio of approximately 106 C : 16 N : 1 P called the Redfield ratio (Redfield, 1934). That same elemental stoichiometry can be found in the dissolved inorganic pool of the deep ocean, which emphasises the coupling between phytoplankton physiology and ocean biogeochemistry. Hence, phytoplankton not only influence the global cycle of carbon (Riebesell *et al.*, 2007; Rost and Riebesell, 2004; Smetacek, 1999), but furthermore impact the elemental cycles of nitrogen, phosphorus and other elements (Falkowski *et al.*, 1998; Litchman *et al.*, 2015; Redfield, 1958).

Even though phytoplankton compete for the same limited resources, there is not a single dominating species, but rather an astonishing diversity of co-existing planktonic forms. This apparent contradiction has been referred to as the paradox of the plankton (Hutchinson, 1961). The term “phytoplankton” describes a diverse agglomerate of over 25 000 different species spanning over several phyla (Falkowski *et al.*, 2004). One of these taxonomic groups are the cyanobacteria, which are the only prokaryotic organisms capable of oxygenic photosynthesis. Among the eukaryotic taxa, diatoms are one of the dominating phytoplankton groups. They are characterized by their siliceous cell walls (Falkowski *et al.*, 2004). More prominent taxa are haptophytes, which comprise the calcareous coccolithophores and the colony-forming

*Phaeocystis* and dinoflagellates, which are not exclusively autotrophic, but also include heterotrophic and symbiotic species (Simon *et al.*, 2009).

## 1.2. Physiological processes in unicellular photoautotrophs

### 1.2.1. Photosynthesis and respiration

The production of organic matter depends on the successful realization of various subcellular physiological processes. Photosynthesis can be divided into two parts: the light and the dark reactions. In a nutshell, solar energy is converted into chemical energy during the light reactions in the thylakoid membranes. The resulting energy carrier adenosine triphosphate (ATP) and reducing equivalent nicotinamide adenine dinucleotide phosphate (NADPH) are then used in the dark reactions (carbon fixation reactions) in the stroma for the synthesis of sugars (Taiz and Zeiger, 2006; Fig. 2).

The site of photosynthesis are the chloroplasts - special organelles with an extensive system of internal membranes called the thylakoids that are often arranged in stacks called grana. All pigments and proteins that are essential to photosynthesis are embedded in these thylakoid membranes. Essential for the light reactions are the two protein complexes, photosystem I and II (PSI and PSII), which can operate in series and are linked by the electron transport chain. Each PS is a structural and functional unit containing light-harvesting antennas and a specialized chlorophyll-protein complex known as reaction centre. Inspired by the wavelength of their absorption maxima, the reaction centre of PSII is called P680 and the one of PSI is named P700.

When chlorophyll and accessory pigments in the light-harvesting complex of PSII absorb photons, chlorophyll reaches an excited state. The resulting high energy electron is transferred to the specialized chlorophyll of the reaction centre and is further passed on to the electron carrier phaeophytin. The resulting electron gap in P680 is filled by the oxidation of water at PSII, which produces O<sub>2</sub> and releases protons into the lumen. The electron that was passed on from PSII travels energetically 'downhill' and is transferred to several carriers of the electron transport chain in the thylakoid membrane (Fig. 2). Phaeophytin reduces the electron carrier plastoquinone (PQ), which diffuses within the thylakoid membrane until it reaches the cytochrome-b<sub>6</sub>f-complex. This complex passes electrons on to plastocyanin (PC), which eventually delivers them to P700 of PSI. In PSI, the electron is once again excited by a

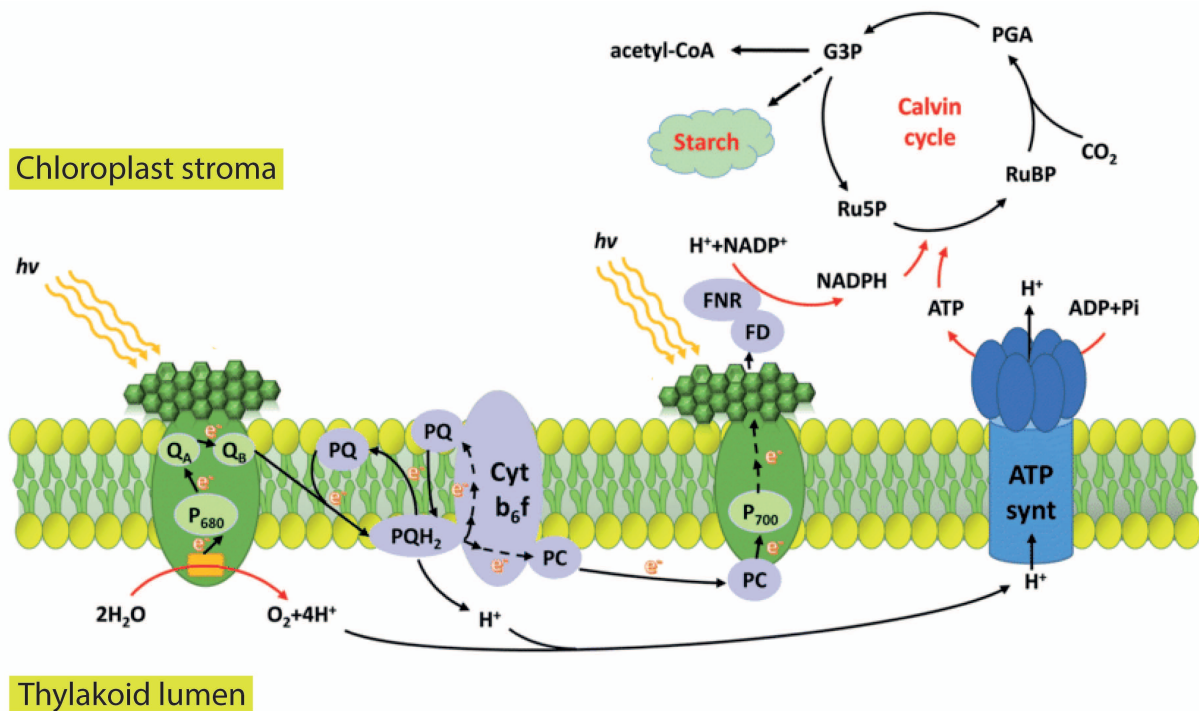


**Figure 2.** Schematic representation of the mechanisms of photosynthesis. During the light reactions solar energy is converted into chemical energy, which involves photosystems I and II and several electron carriers of the electron transport chain in the thylakoid membrane. The resulting ATP and NADPH are used in the dark reactions in the stroma to reduce inorganic carbon and synthesise carbohydrates through the reactions of the Calvin cycle. Modified after Yang *et al.* (2020).

photon and then passed on to  $\text{NADP}^+$  to form the reducing agent NADPH (Falkowski and Raven, 2007). The electron flow is accompanied by proton transfer across the thylakoid membrane, thereby creating an electrochemical proton gradient. This gradient drives the diffusion of protons from the lumen back into the stroma by which the ATP synthase enzyme generates ATP.

ATP and NADPH produced in the light reactions provide the energy to reduce inorganic carbon in the dark reactions. In the stroma of chloroplasts, the enzymatic reactions of the Calvin cycle fix  $\text{CO}_2$  by combining it with ribulose-1,5-bisphosphate (RuBP), which is catalysed by the enzyme ribulose-1,5-bisphosphate carboxylase/oxygenase (RuBisCO) and forms two molecules of 3-phosphoglycerate (Falkowski and Raven, 2007; Fig. 2). These molecules are reduced and converted to the three-carbon sugar Glyceraldehyde-3-phosphate (G3P) with the help of ATP and NADPH from the light reactions (Fig. 2). A fraction of the G3P leaves the Calvin cycle as a precursor compound for the hexose glucose and other organic compounds, while the rest is used for the regeneration of RuBP, thereby ensuring the continued operation of the cycle. In total, each turn of the Calvin cycle uses two NADPH plus three ATP per  $\text{CO}_2$  assimilated (Beardall and Raven, 2020).

In parallel to photosynthesis, the generated cellular carbohydrates can be oxidized to CO<sub>2</sub> and water by respiration. There are several metabolic pathways that contribute to this process: glycolysis, the citric acid cycle and oxidative phosphorylation. In the glycolysis pathway in the cytosol of cells, carbohydrates are converted into two molecules of pyruvate and a small amount of ATP is generated. The produced pyruvate enters the tricarboxylic acid (TCA) cycle in the mitochondrial matrix and is aerobically oxidized to CO<sub>2</sub> in the process of which a large number of NADPH is formed (Falkowski and Raven, 2007). The TCA cycle furthermore produces important intermediates for biosynthetic processes. During oxidative phosphorylation, electrons from the NADPH generated in the TCA cycle pass through the electron transport chain in the mitochondrial matrix to reduce oxygen. A proton gradient is established that drives the ATP synthase complex and produces a large amount of ATP (Falkowski and Raven, 2007).

### 1.2.2. Allocation of energy and carbon between metabolic pathways

The allocation of energy and carbon between metabolic pathways determines the growth rate of phytoplankton (Halsey and Jones, 2015), which is commonly used as a measure of cell fitness. It is often assumed that species optimize the allocation of photosynthetic resources among cellular processes to maximize growth (Behrenfeld *et al.*, 2008; Halsey and Jones, 2015). However, more rapid cell division may be limited by increases in cellular damage in the long-term (Collins, 2016), putting growth as a direct proxy for fitness into question. Furthermore, microalgae may allocate carbon and energy differently depending on their physiological abilities and ecological strategies. Produced biomass may also be channelled into increased biovolume, i.e. particulate organic carbon (POC) quota, instead of allocating it into growth (Falkowski and Raven, 2007). This is especially true under nitrogen limitation, because balanced growth is not possible and thus carbon and energy is accumulated as carbohydrates or lipids (Breuer *et al.*, 2012; Zhu *et al.*, 2014).

ATP and NADPH are not only needed for carbon fixation, but also many other cellular activities. Nitrogen assimilation, for example, also requires reductant and ATP, whereby the assimilation of nitrate demands even more electrons from NADPH than the assimilation of ammonium (Coruzzi and Last, 2000; Sanz-Luque *et al.*, 2015). Moreover, an enhanced investment of energy and reductant into cellular maintenance like repairing damaged proteins and turnover of nucleic acid may become necessary under certain conditions (Geider *et al.*, 2009). To meet these demands, only a fraction of ATP and NADPH from the light reactions may be allocated into carbon fixation and the remaining into other cellular activities, or ATP

and NADPH are obtained from mitochondrial respiration (Behrenfeld *et al.*, 2008). Furthermore, phytoplankton have evolved multiple mechanisms for generating ATP to match the production ratio of ATP and reductant to cellular requirements, including cyclic electron flow around PSI, the water-water cycle and the malate valve (Kramer and Evans, 2011).

### 1.3. Temperature as a master driver of physiological processes

Growth and productivity of algal populations are directly affected by the physical changes of their growth environment. Key influential factors are the availability of light and nutrients and the temperature they are exposed to (Behrenfeld *et al.*, 2008). Temperature is a fundamental control on biological processes, because it affects molecular motion (Pearle *et al.*, 2010). While a temperature increase results in accelerated molecular motion and as a consequence, an increase of biochemical reactions and metabolic rates, these effects are reversed at colder temperatures (Brown *et al.*, 2004; Raven and Geider, 1988). The so-called  $Q_{10}$  factor describes how much reactions are accelerated with a temperature increase of 10 °C and is commonly assumed to be  $\sim 2$  for phytoplankton maximum growth (Eppley, 1972; Goldman and Carpenter, 1974). Phytoplankton growth response to different temperatures is often described by a bell-shaped curve called thermal performance curve or thermal growth curve (Boyd *et al.*, 2013). With increasing temperature, the growth of microalgae is stimulated until the maximum growth rate is reached at the species specific optimum temperature  $T_{opt}$  (Beardall and Raven, 2004; Li, 1980). Warming beyond  $T_{opt}$ , however, results in a sharp decline of performance and can even be lethal for the organism. The temperature range over which positive growth occurs is defined as the thermal niche width of an organism and is situated between the thermal limits  $T_{min}$  and  $T_{max}$  (Chen, 2015).

The overall temperature dependency of growth is determined by the net effect of all subcellular physiological processes that enable growth. These differ in their thermal response, depending on whether purely biochemical (enzymatic) or biophysical phenomena like diffusion processes, photochemistry and membrane fluidity are involved (Falkowski and Raven, 2007). While biochemical reactions are stimulated until a specific thermal optimum, biophysical processes show a rather continuous stimulation. Even though the photosynthetic and respiratory sub-processes like the Calvin cycle, glycolysis and the TCA cycle consist to a large degree of enzymatic reactions, and are as such accelerated by rising temperatures, they can be affected by temperature to different degrees. Respiration, for example, appears to increase stronger with

temperature than photosynthesis (Brown *et al.*, 2004; Regaudie-de-Gioux and Duarte, 2012). Moreover, the catalytic rate of RuBisCO, the key enzyme of the Calvin cycle, is accelerated with increased temperature, but at the same time the affinity for CO<sub>2</sub> is decreasing (Galmés *et al.*, 2015; Jordan and Ogren, 1984). In combination with the decreased CO<sub>2</sub>/O<sub>2</sub> solubility ratio (Ku and Edwards, 1977), the oxygenase activity of RuBisCO may be favoured and the risk of photorespiration is increased (Hermida-Carrera *et al.*, 2016; Jordan and Ogren, 1984). To compensate for this property of RuBisCO and to ensure high CO<sub>2</sub> fixation rates, phytoplankton evolved CO<sub>2</sub>-concentrating mechanisms (CCMs) that accumulate CO<sub>2</sub> at the site of carboxylation (Badger *et al.*, 1998; Rokitta *et al.*, 2021). With decreasing temperatures, on the other hand, the rate of carbon fixation may be constrained by the reduced enzymatic activity and thus slow the carboxylation rate of RuBisCO (Young *et al.*, 2015).

The response of the light-dependent reactions of photosynthesis to temperature are more complex. True photochemical reactions like the absorption of solar energy and photosynthetic charge separation are not depend on intermolecular collisions and are therefore rather temperature-independent (Falkowski and Raven, 2007). The photosynthetic electron transport chain, on the other hand, is influenced by temperature due to the diffusion of electron carriers and the fluidity of membranes, which both increase under higher temperatures (Los *et al.*, 2013; Raven and Geider, 1988). At colder temperatures, the viscosity of biological membranes increase up to a point where movement of membrane components is hampered (Falkowski and Raven, 2007). For this reason, and decreasing diffusion rates, electron chain transfer is reduced with decreases in temperature (Raven and Geider, 1988).

The exposure to sub- or supraoptimal temperatures can cause energetic imbalances, because the different physiological sub-processes are not equally affected by temperature changes. This can induce multiple intracellular stress and compensatory responses, which can take place through physiological adjustments by acclimation within one or a few generations or evolutionary adaptation over longer time scales. Temperature tolerance can differ between phylogenetic groups (Huertas *et al.*, 2011) and even within the same species due to intraspecific diversity (Boyd *et al.*, 2013; Wolf *et al.*, 2018).

## 1.4. Reactive oxygen species

In general, the rate of reactive oxygen species (ROS) production is enhanced under environmental conditions when imbalances arise, e.g. when light absorption exceeds the utilization for carbon fixation (Asada, 2006). Elevated temperatures can also lead to the accumulation of ROS in the cell (Allakhverdiev *et al.*, 2008; Sun and Guo, 2016), as well as the exposure to other suboptimal environmental conditions like high light (Niyogi, 1999), UV radiation (Kováčik *et al.*, 2010), nutrient deficiency (Goiris *et al.*, 2015), pH (Liu *et al.*, 2007) and toxic compounds (Prado *et al.*, 2012).

Owing to the reductive nature of aerobic metabolic processes such as respiration and photosynthesis, the formation of ROS species like superoxide anion radical ( $O_2^{\cdot-}$ ) and hydrogen peroxide ( $H_2O_2$ ) is inevitable. As a matter of fact, ROS even have beneficial effects by functioning as sensors and signal molecules, that enable adjustments to gene expression and initiate acclimation responses depending on environmental cues (Foyer and Noctor, 2000, 2005). High intracellular ROS concentrations, however, induce harmful effects on proteins, lipids and DNA and are involved in programmed cell death (Asada and Takahashi, 1987; Fridovich, 1998; Halliwell, 2015). These deleterious effects are often summarised under the term ‘oxidative damage’.

In microalgae, major sites of ROS generation are the chloroplasts, the mitochondrial electron transport chain (Moller, 2001), peroxisomes and the cell surface (Diaz and Plummer, 2018; Fig. 3). During the photosynthetic reactions in the chloroplasts, ROS production occurs in the Calvin cycle in association with the enzyme RuBisCO (Kim and Portis, 2004) and at both photosystems PSI and PSII (Asada, 1999, 2006). At the electron acceptor side of PSII,  $O_2^{\cdot-}$  is generated by the leakage of electrons to molecular oxygen (Ananyev *et al.*, 1994; Cleland and Grace, 1999), while the incomplete oxidation of water on the electron donor side forms  $H_2O_2$  (Pospíšil, 2009).  $O_2^{\cdot-}$  production at PSI occurs through the reduction of  $O_2$  by the Mehler reaction (Mehler, 1951).

To protect the cell from oxidative damage, photosynthetic organisms have evolved an antioxidant defence system comprising non-enzymatic antioxidants such as ascorbate and glutathione (Noctor and Foyer, 1998) and enzymatic scavengers like superoxide dismutase (SOD) and catalase. The antioxidant enzyme SOD catalyses the disproportionation of  $O_2^{\cdot-}$  to  $H_2O_2$  (Foyer *et al.*, 1994; Navari-Izzo *et al.*, 1999), however this reaction also occurs spontaneously (Klimov *et al.*, 1993; Pospíšil *et al.*, 2004). The  $H_2O_2$  generated this way

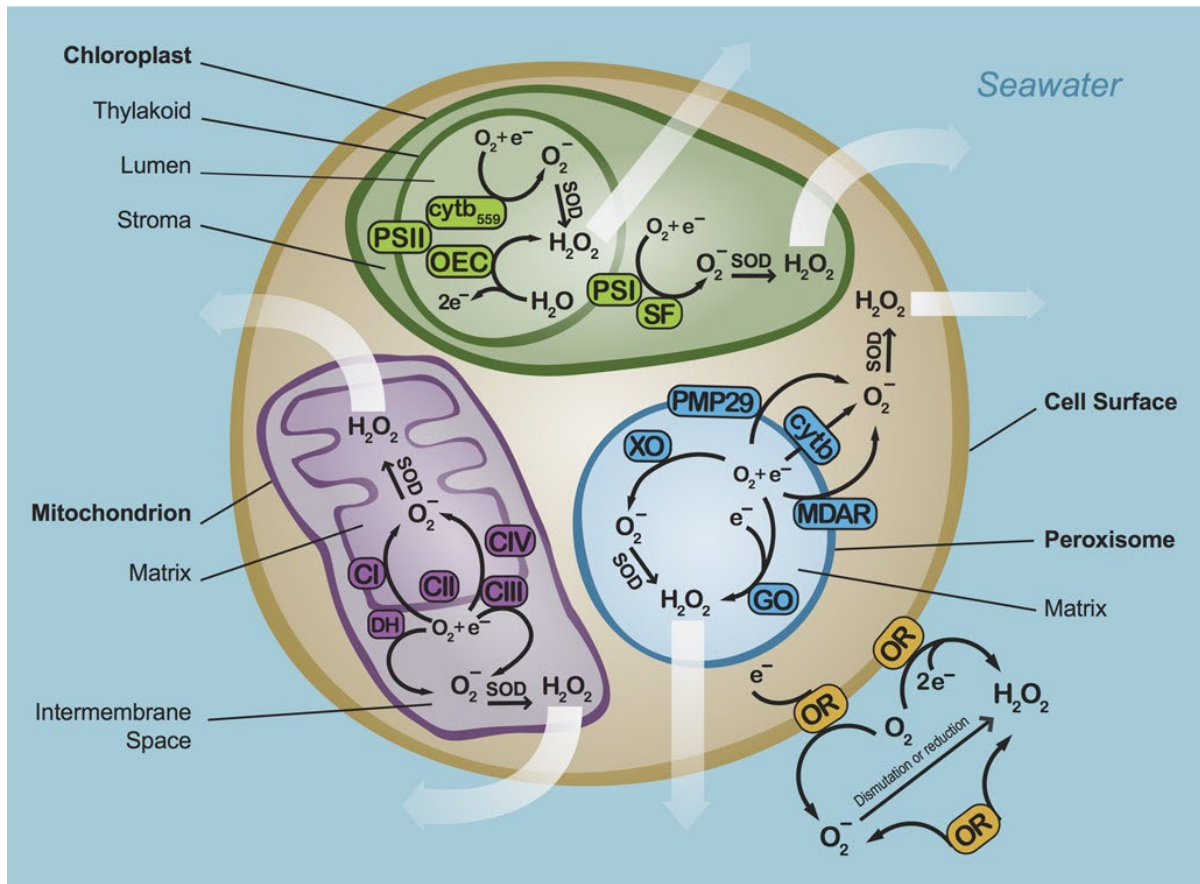


**Figure 3.** Major generation sites of the reactive oxygen species superoxide anion radical ( $\text{O}_2^-$ ) and hydrogen peroxide ( $\text{H}_2\text{O}_2$ ) in phytoplankton. In the chloroplasts,  $\text{H}_2\text{O}_2$  is formed by the oxygen-evolving complex at PSII and  $\text{O}_2^-$  is generated by the reduction of oxygen at PSII and by the Mehler reaction at PSI. Reprinted from Diaz and Plummer (2018).

following the Mehler reaction at PSI is further detoxified to water as part of the so-called water-water cycle (Asada, 1999). Further, non-photochemical quenching (NPQ) processes contribute to the prevention of ROS formation in the first place by dissipating excess excitation energy as heat (Horton *et al.*, 1994; Müller *et al.*, 2001).

### 1.5. Primary production in the Arctic Ocean

The Arctic Ocean (AO) is a unique ecosystem characterized by some of the harshest environmental conditions on Earth. Not only are organisms faced with freezing sea surface temperatures (SSTs) with an annual average around  $1.3^\circ\text{C}$  (Carvalho and Wang, 2020), but they are also subjected to an extreme seasonal change of light and nutrient availability. Moreover, the extent of the Arctic sea-ice varies depending on a change in temperature, reaching its maximum extent in March and its minimum extent in September. With the end of the polar night in spring, the return of sufficient sunlight in combination with winter-



**Figure 4.** Images of *Phaeocystis pouchetii* cells under a light microscope. **(A)** Lugol fixated solitary *P. pouchetii* cells showing two prominent anterior flagella. Scale bar represents 10  $\mu\text{m}$ . **(B)** *P. pouchetii* colony during the spring bloom in Kongsfjord, Svalbard in 2021 (© Klara Wolf).

accumulated nutrients and the stratifying water column due to warming and freshwater input from melting sea-ice, enables a rapid increase in primary production (Barber *et al.*, 2015; Wassmann *et al.*, 2006). This ultimately leads to the formation of the spring bloom from March-May, which is the most important primary production event in Arctic waters (Sakshaug, 2004). The species composition of phytoplankton associated with the Arctic spring bloom are usually dominated by diatom genera such as *Thalassiosira* spp., *Chaetoceros* spp., *Fragilariopsis* spp. and the prymnesiophyte *Phaeocystis pouchetii* (Barber *et al.*, 2015; Degerlund and Eilertsen, 2010). *P. pouchetii* is part of the seasonal succession towards summer, but sometimes it also dominates earlier in spring, resulting in an alternation between diatom- and *Phaeocystis*-dominated spring blooms from year to year (Degerlund and Eilertsen, 2010). However, there have been several reports on an increased *Phaeocystis* dominance in Arctic phytoplankton assemblages in recent years (Assmy *et al.*, 2017; Lafond *et al.*, 2019; Nöthig *et al.*, 2015; Orkney *et al.*, 2020).

*Phaeocystis pouchetii* has a complex life cycle that comprises a motile flagellated stage and a colonial stage with nonmotile aggregated cells embedded in mucilage (Eikrem *et al.*, 2016; Rousseau *et al.*, 1994; Fig. 4). The solitary cells are round or oval in shape and have an average size of 5  $\mu\text{m}$  (Jacobsen, 2002). Under the light microscope two golden-brown chloroplasts and two flagella at the anterior end of the cell are visible (Fig. 4A). In between these flagella, a much shorter haptonema is attached at the cell (Jacobsen, 2002), which is a characteristic feature of the haptophyte phylum this species belongs to (Eikrem *et al.*, 2016). Colonies are several mm in size and contain hundreds to thousands of cells embedded in a polysaccharide

gel matrix (Hamm, 2000; Rousseau *et al.*, 1994; Fig. 4B). This is also the life cycle stage during which they form massive blooms (Schoemann *et al.*, 2005).

The high productivity of *Phaeocystis* blooms may act as a relevant sink for atmospheric CO<sub>2</sub> (Smith *et al.*, 1991) and therefore play a significant role in the biogeochemical cycles of the ocean and regulation of climate (Schoemann *et al.*, 2005). Moreover, *Phaeocystis* is known to influence the Earth's sulfur cycle, by producing high concentrations of dimethylsulfoniopropionate (DMSP) and dimethylsulfide (Pfaff *et al.*, 2016; Verity and Medlin, 2003), the latter playing a crucial role as cloud condensation nuclei (Beck *et al.*, 2021). Increased cloud formation changes the albedo and can result in a cooling of Earth's climate.

## 1.6. Warming of the Arctic Ocean and marine heatwaves

In the last 200 years, human activities like fossil fuel combustion and land use changes have already caused a rise in atmospheric CO<sub>2</sub> by ~50 % from approximately 277 parts per million (ppm) in 1750 (Joos and Spahni, 2008) to 414 ppm in 2021 (Dlugokencky and Tans, 2022). The elevated concentration of CO<sub>2</sub> and other greenhouse gases (e.g. methane and nitrous oxide) in the atmosphere causes increased absorption of longwave radiation, thereby generating thermal energy in the Earth's atmosphere. This energy imbalance drives global warming, which has already reached 1.1 °C compared to the average of pre-industrial times (period 1850-1900) and is projected to continue at an unprecedented rate (IPCC, 2021).

The consequences of climate change are nowhere as pronounced and progress at such a rapid rate as they are in the Arctic (Burrows *et al.*, 2011). During 1982–2017 the temperature of the summer upper mixed layer of the AO increased at 0.5 °C per decade (IPCC, 2019) and is therefore warming two to three times faster than the rest of the planet – a phenomenon known as Arctic amplification (Cohen *et al.*, 2014; Serreze and Barry, 2011). The melting of the highly reflective ice and snow cover exposes more seawater surfaces and leads to a decline in albedo (Perovich *et al.*, 2007), which in turn amplifies the warming of the Arctic as a positive feedback. More seawater surface absorbs more solar energy leading to further warming and diminishing of the cryosphere (Serreze and Barry, 2011). Arctic sea ice extent and thickness have decreased noticeably over the last few decades (IPCC, 2019) and the heat transport towards the AO has increased by the inflow of warm Atlantic water masses (Oziel *et al.*, 2016) resulting in even warmer ocean temperatures and further reduced sea ice cover (Asbjørnsen *et al.*, 2020; Polyakov *et al.*, 2012). This increased influence of Atlantic water on the AO is termed

Atlantification (Årthun *et al.*, 2012; Polyakov *et al.*, 2017). With the warmer Atlantic water masses, also associated subarctic-boreal species from lower latitudes are intruding further into the Arctic (Hegseth and Sundfjord, 2008; Oziel *et al.*, 2020).

Different greenhouse gas emission scenarios called Representative Concentration Pathways (RCPs) have been modelled, which project different levels of global warming. RCP2.6 represents a low greenhouse gas emission scenario in which global warming is kept well below 2 °C by 2100 compared to pre-industrial temperatures (IPCC, 2019; Fig. 5). Under the high greenhouse gas emission scenario RCP8.5 without any climate mitigation policies, which is currently the most realistic scenario, global mean surface temperature is projected to increase by 4.3 °C by the end of the century relative to the pre-industrial period (IPCC, 2019; Fig. 5). Over 90 % of the excess heat in the climate system is taken up by the global ocean (Cheng *et al.*, 2017), which is leading to increasing sea surface temperatures (SSTs). For the end of the century, global mean SST is projected to increase by 0.73 °C under RCP2.6 and 2.58 °C under RCP8.5 scenario relative to the time period from 1986-2005 (IPCC, 2019).

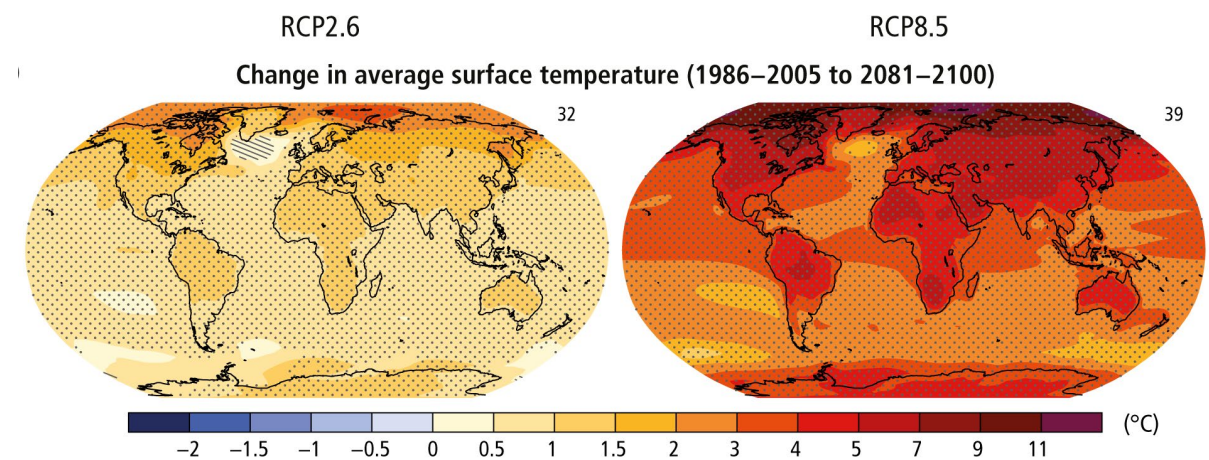


**Figure 5.** Projected change in annual mean surface temperature until the end of the century under the RCP2.6 (left) and RCP8.5 (right) scenarios in relation to the time period 1986-2005. Reprinted from IPCC, 2014.

Climate change also increases the risk of extreme weather events like marine heatwaves (IPCC, 2019; Fig. 6). A MHW is defined as an anomalously warm event during which seawater temperatures exceed the 90th percentile threshold for at least five consecutive days (Hobday *et al.*, 2016). These extreme warm water events can be characterised by their duration (time in days from start to end of MHW), intensity (temperature anomaly above average) and spatial extent. In the last decades, MHWs have occurred in all ocean basins and they have doubled in frequency over the period 1982 to 2016 (Frölicher *et al.*, 2018; IPCC, 2019). This trend will

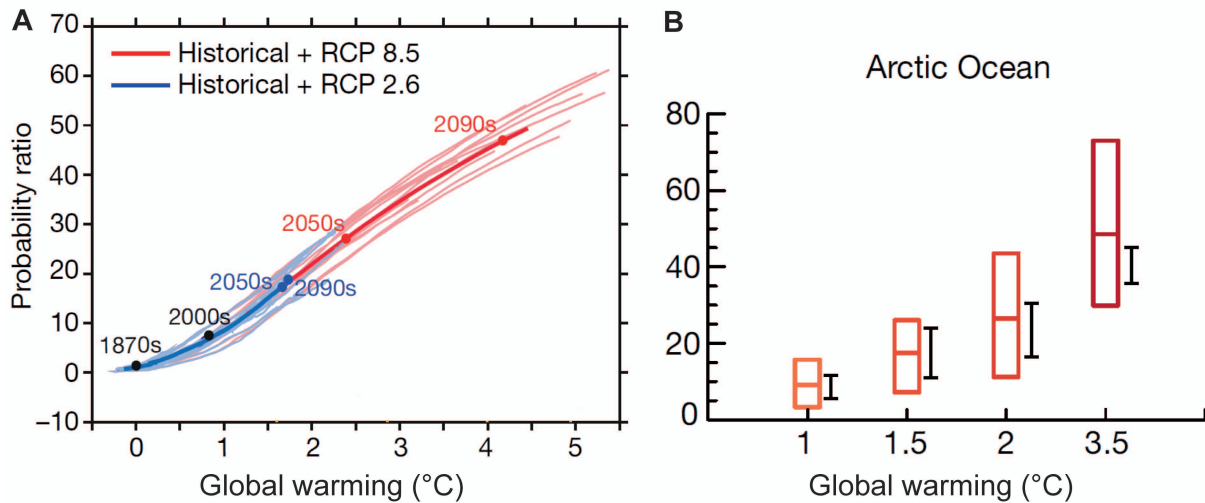


**Figure 6.** Simulated changes in the probability of MHWs for different levels of global warming. **(A)** Global aggregated annual mean probability ratio for the RCP 8.5 and RCP 2.6 scenarios. **(B)** Changes in probability of MHWs over the Arctic Ocean (>75° N). Adjusted from Frölicher *et al.* (2018).

intensify with ongoing global warming and will cause MHWs to be longer-lasting, more frequent, extensive and intense in the future (Frölicher *et al.*, 2018; Oliver *et al.*, 2019). The largest increase in the probability of MHWs is projected for the AO (Frölicher *et al.*, 2018; Fig. 6B). Between 1988-2017, the occurrence of MHWs in the Arctic has already increased to 1-4 events annually with an intensity of 10-40 °C/event (i.e., the cumulative SST anomaly over the duration of the event, SST anomaly (°C) x duration in days) and lasted for 9-25 days (Hu *et al.*, 2020).

The ongoing climatic changes in the AO are drastically altering phytoplankton productivity, phenology and species composition (Ardyna and Arrigo, 2020). Expanded open water areas and a prolonged growing season have caused an increase in Arctic primary production by ~57 % between 1998-2018 (Ardyna and Arrigo, 2020; Arrigo *et al.*, 2008; Lewis *et al.*, 2020). How phytoplankton will respond to warming in the future strongly depends on their ability to acclimate or adapt to the projected environmental changes. Even though the optimum growth temperatures of microalgae are strongly related to their geographical location with higher  $T_{opt}$  at warmer latitudes (Thomas *et al.*, 2012), the realized niche of a species might deviate from this. For most Arctic phytoplankton,  $T_{opt}$  seems to be positioned above the temperatures they currently experience (Coello-Camba and Agustí, 2017). Nevertheless, a poleward shift of species can be observed as a response to global warming (Lovejoy *et al.*, 2017) and thus, the competition between species advected to the AO from lower latitudes and resident communities will become a strong selection factor. However, not only the response of Arctic phytoplankton to the mean temperature rise, but also how they perform under increased MHW occurrence will

impact ecosystem functioning in the AO. In other environments, MHWs have been shown to cause coral bleaching, collapse of mangrove and kelp forests and mass mortalities of invertebrates, fishes, seabirds and marine mammals (Smale *et al.*, 2019). Knowledge on the impacts on phytoplankton is still sparse, apart from a few studies that found changed community composition and reduced biodiversity (Rasconi *et al.*, 2017; Remy *et al.*, 2017; Stefanidou *et al.*, 2019). The response of Arctic phytoplankton in particular has yet not been investigated.

### 1.7. Aim of study

Most studies on the temperature-dependence of biological processes in phytoplankton assess the performance of fully acclimated cultures to constant temperatures or focus on the determination of the optimum growth temperature (Bissinger *et al.*, 2008; Boyd *et al.*, 2013; Eppley, 1972). The performance in variable thermal environments, however, cannot be simply inferred from studies investigating performance under constant conditions (Bernhardt *et al.*, 2018). In the course of a MHW, organisms are not only exposed to sudden warming, but also cooling. While enzyme activity, membrane fluidity and electron chain transfer are increased with rising temperature, this effect is reversed when temperatures are lowered again (Raven and Geider, 1988) and may induce energetic, metabolic, and redox imbalances that trigger intracellular stress (Liang *et al.*, 2019). MHWs are extreme events that can rapidly push a species beyond its usually experienced temperature range and the limits of their resilience. In addition, they arise and disappear faster than the timeframes needed for acclimation or adaptation. Thus, MHWs could have worse effects on the performance of a species than those emanating from the mean temperature rise due to global warming.

The Arctic is the region with the fastest rate of warming and the highest probability for MHWs (Frölicher *et al.*, 2018). Nonetheless, knowledge on the impact of MHWs on Arctic phytoplankton is still scarce. To address this knowledge gap, this master thesis investigates the physiological capacity and resilience of the Arctic key species *Phaeocystis pouchetii* to respond to MHW scenarios as projected for the future Arctic Ocean. This undertaking was realized by cultivating *P. pouchetii* at two different temperatures (3 and 6 °C). Low temperature acclimated cultures were exposed to two MHWs with an intensity of 6 °C for varying durations (MHW1: 6 days, MHW2: 10 days), followed by a recovery phase at 3 °C for 5 days. By comparing these treatments with each other and with the 6 °C acclimated culture, this study aims to elucidate

whether the response of acclimated cells differs from the response to a sudden temperature increase and further, whether the duration of a MHW has an impact on the acclimatory capacity of cells. By monitoring the recovery phase after the MHW exposure, this study also aims to examine how reversible physiological adjustments are upon cooling and whether this post-MHW temperature drop is a relief or rather an additional stressor for cells exposed to MHWs.

The physiological state of cells was investigated by assessing specific growth rates, elemental composition and cellular chlorophyll *a* content. Furthermore, the plasticity of the photosynthetic capacity was assessed by variable chlorophyll fluorescence measurements (FRRF). It was hypothesized, that fluctuating temperatures entail opposing requirements of physiological adjustments, causing a mismatch of photosynthetic reactions and leading to the accumulation of ROS. This might hamper the performance of cells due to the increased energetic costs associated with ROS detoxification mechanisms and the repair of cell damage. To test this hypothesis, intracellular levels of  $O_2^{\cdot-}$  and  $H_2O_2$  were measured by means of flow cytometry throughout the MHW treatments. The data collected during this project will help to understand the ability of *P. pouchetii* to withstand or recover from future extreme events like MHWs and to improve model projections for primary production in the Arctic Ocean under climate change.

## 2. Materials and Methods

### 2.1. Culturing conditions

Experiments were conducted with the *Phaeocystis pouchetii* strain PS78 from the stock culture collection of the Alfred Wegener Institute for Polar and Marine Research in Bremerhaven, Germany, which was originally sampled in the Fram Strait during the RV Polarstern cruise PS78 in June, July and August 2011. Cells were grown under nutrient-replete conditions in F/2 R medium as dilute-batch cultures in 1 L glass bottles. The growth medium was prepared by enriching sterile filtered (0.2  $\mu\text{m}$ ) Arctic seawater obtained from Fram Strait (78°58.859'N 05°21.688'W, salinity 29.6, alkalinity 2107  $\mu\text{mol L}^{-1}$ ) with nutrient stock solutions of nitrate and phosphate (final concentration of 100 and 6.25  $\mu\text{mol L}^{-1}$ , respectively) as well as trace metal and vitamin solutions according to Guillard and Ryther (1962). Throughout the experiment, cell densities were kept between 6 and 40  $\times 10^3$  cells  $\text{mL}^{-1}$  by re-inoculating cultures into fresh medium to prevent nutrient limitation and pH fluctuations due to shifts in the carbonate chemistry. Handling and sampling of cultures was carried out sterilely under a clean bench in a 6 °C cold laboratory to avoid temperature shocks and contamination of cultures.

To resemble light conditions during a spring bloom in the Arctic, cell cultures were exposed to a light level of  $30 \pm 2$   $\mu\text{mol photons m}^{-2} \text{ s}^{-1}$  for 24 h by illuminating the culturing bottles in the water tanks with daylight lamps (Biolux T8, 6500K, Osram, München, Germany). Water tanks and lamps were additionally covered with 298 0.15 Neutral Density filters (LEE, Andover, United Kingdom) and white reflective foil to adjust the light level and achieve a homogeneous light field. The correct irradiance was verified using a US-SQS Submersible Spherical Micro Quantum Sensor connected to the ULM-500 Universal Light Meter (Walz, Effeltrich, Germany).

Temperature stability during the treatments was ensured by immersing the culture bottles in water tanks that were placed in 2 °C and 6 °C cooling rooms. The water temperatures were adjusted to  $2.7 \pm 0.1$  °C and  $6.2 \pm 0.3$  °C with the help of the CORIO CD immersion thermostat (JULABO GmbH, Seelbach, Germany). The ascending and descending temperature ramps of the heatwaves were generated at a rate of 1 °C  $\text{h}^{-1}$  in the tanks, respectively, by the heating function of the thermostats, or by addition of ice in combination with the mixing function of the thermostat. Water temperatures in the tanks were continuously recorded with a sampling time of 600 s using Type K sensors attached to the digital thermometer and datalogger PCE-T390 (PCE Instruments, Meschede, Germany) and with the help of a handheld thermometer.

Measured temperatures were corrected with the calibration certified ebro® TFX 430 Pt100 thermometer (Thermo Fisher Scientific Inc, Waltham, USA).

Cultures were continuously aerated with a pCO<sub>2</sub> of 400 ppm, which roughly corresponds to the present global average pCO<sub>2</sub> of 413 ppm (Dlugokencky and Tans, 2022). Adjustment of the CO<sub>2</sub> concentration was facilitated by mixing CO<sub>2</sub> free air (< 1 ppm CO<sub>2</sub>; Dominick Hunter, Willich, Germany) with pure CO<sub>2</sub> (Air Liquide Deutschland, Düsseldorf, Germany) by a custom-made gas mixing system equipped with a mass flow controller-based system (CGM 2000 MCZ Umwelttechnik, Bad Nauheim, Germany). The mixed air was humidified and filtered through 0.2 µm air-filters (Midisart 2000, Sartorius stedim) before entering the culturing bottles for equilibration. The tubes of the gas supply were equipped with hose clamps, that enabled manual regulation of the air flow.

To accustom the stock culture of *P. pouchetii* to these experimental conditions, acclimation of the cultures to 24 h of light and a temperature of 2.5 °C started seven weeks and acclimation to the irradiance of ~30 µmol photons m<sup>-2</sup> s<sup>-1</sup> four weeks prior to the start of the experiment. During this acclimation period, regular dilutions of cell cultures ensured acclimation to the experimental conditions with stable exponential growth. Prior to dilutions, the growth medium was equilibrated with a pCO<sub>2</sub> of 400 µatm at the respective temperature of the treatment for at least 24 h to ensure stable carbonate chemistry (see section 2.3).

## 2.2. Experimental setup and timeline

Cell cultures of the Arctic haptophyte *Phaeocystis pouchetii* were exposed to two marine heatwave (MHW) treatments of different durations (6 and 10 days) at 6 °C. The experiment started with the incubation of high (6 °C) and low (3 °C) stable temperature controls as three replicates (A, B, C), which were monitored for the entire duration of the experiment (Fig. 7). To reduce the amount of culturing bottles and sampling effort, cultures were split into the different MHW treatments at certain timepoints (Fig. 7). After one week of incubation, the three 3 °C control cultures were split into a MHW culture with three replicates (MHW A, B, C) and three 3 °C controls (3 °C control A, B, C). The MHW cultures remained at 3 °C for 2 more days before they were exposed to a gradual temperature ramp from 3 to 6 °C with a warming rate of 1 °C per hour. After the MHW triplicates were exposed to 6 °C for two days, they were split into three MHW1 cultures and three MHW2 cultures (Fig. 7). MHW1 cultures were exposed to 6 °C for 6 days in total and MHW2 cultures to an extended MHW of 10 days before they were

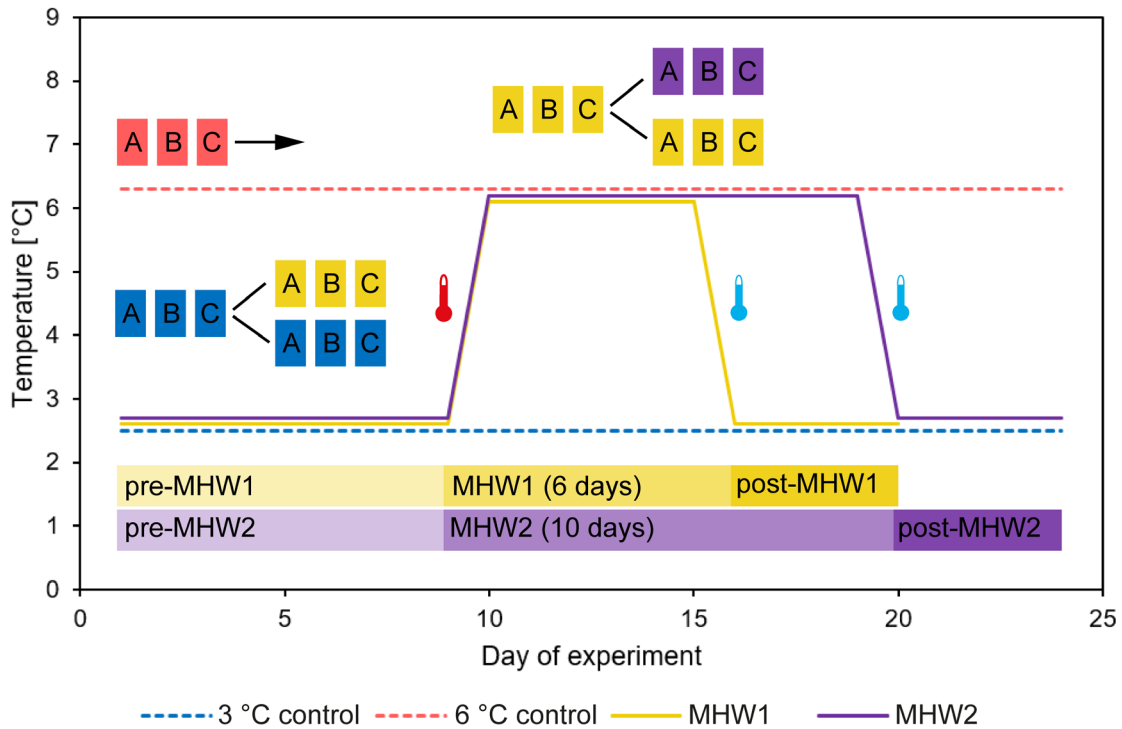


**Figure 7.** Experimental timeline of the 3 and 6 °C control, MHW1 and MHW2 treatments with indicated pre-, mid- and post-MHW timepoints. 3 °C control cultures were split into 3 °C control and MHW treatment before the temperature ramp and MHW cultures were later split into MHW1 and MHW2 cultures, which were exposed to a MHW with an intensity of 6 °C for 6 and 10 days respectively.

cooled down again to 3 °C (Fig. 7). The temperature ramp from 6 to 3 °C was performed with a cooling rate of 1 °C per hour. The recovery period at 3 °C after the MHW treatments (post-MHW) lasted five more days.

Throughout the experiment, growth rates were determined daily for all treatments. Chl *a* content, elemental quota, reactive oxygen species and photophysiology of the 3 and 6 °C control cultures were analysed at three timepoints during the experimental period. For the two MHW treatments, parameters of cellular composition were assessed at the end of the MHW (timepoint ‘MHW’) and after 5 days of recovery (timepoint ‘Rec’, Fig. 8). Data of the 3 °C control cultures were assumed to represent the physiological state of the MHW cultures prior to MHW exposure. The photophysiological response and ROS production in MHW cultures was analysed in higher temporal resolution, including measurement of these parameters shortly (1-2 hours) before and after the ascending and descending temperature ramps (Fig. 8). This resulted in the following measurement timepoints: pre-MHW (‘Pre’), post heating ramp (‘pHR’), during the MHW (‘Mid1, 2, 3’), at the end of the MHW (‘End’), post cooling ramp (‘pCR’) and after 2 and 5 days of recovery (‘Rec1’, ‘Rec2’). Furthermore, the gradual temperature rise or reduction was examined through continuous recording of the maximum quantum yield of electron transport through PSII ( $F_v/F_m$ , see section 2.7).

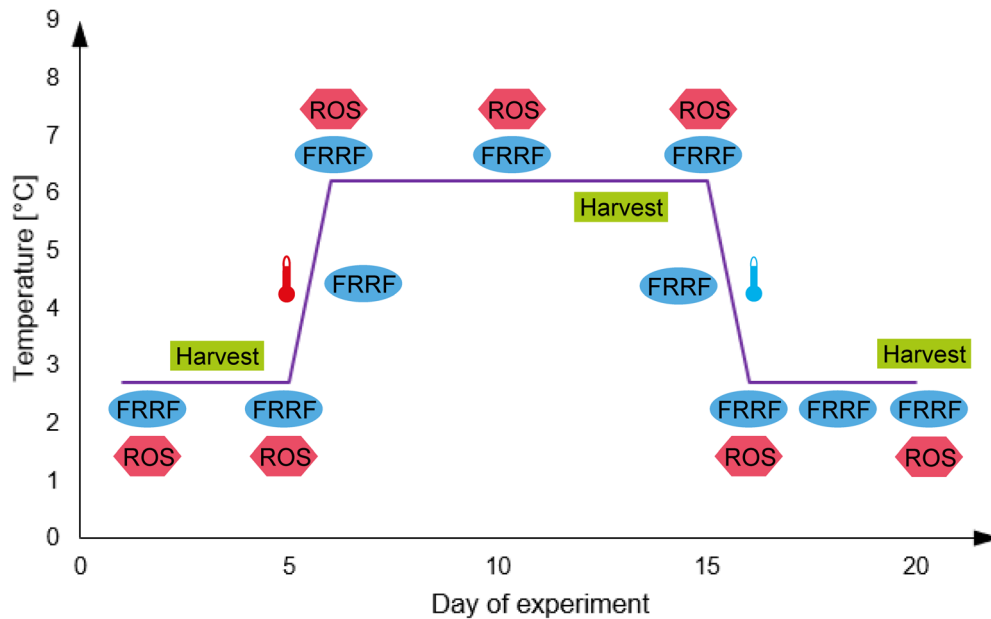


**Figure 8.** Overview of the timepoints of harvest, fast repetition rate fluorometry (FRRF) and reactive oxygen species (ROS) measurements during the MHW treatments exemplified for the MHW2 treatment. All parameters were determined pre-, mid- and post-MHW and the maximum quantum yield of electron transport through PSII ( $F_v/F_m$ ) was additionally recorded during the ascending and descending temperature ramps.

### 2.3. Carbonate chemistry

As  $\text{CO}_2$  equilibrates with seawater, it reacts with water and forms three different inorganic forms: aqueous carbon dioxide ( $\text{CO}_2(\text{aq})$ ), bicarbonate ( $\text{HCO}_3^-$ ) and carbonate ions ( $\text{CO}_3^{2-}$ ) (Zeebe and Wolf-Gladrow, 2005). The sum of these carbon species is called dissolved inorganic carbon (DIC). This carbonate system is a natural buffer for the pH of seawater and the relative proportions of the carbonate species influences the pH by the release or uptake of protons ( $\text{H}^+$ ). The proton buffering capacity of seawater can be described by the Total Alkalinity (TA), which is defined by the excess of proton acceptors over proton donors (Dickson, 1981; Wolf-Gladrow *et al.*, 2007; Zeebe and Wolf-Gladrow, 2005). An alternative definition of TA, the explicit conservative definition, contains major-ions and acid-base species that are unaffected by  $\text{CO}_2$  exchange, temperature or pressure (Wolf-Gladrow *et al.*, 2007).

Biological activity like photosynthetic carbon fixation or respiration may alter the carbonate chemistry of seawater (Rost *et al.*, 2008). Production of organic matter reduces DIC but also increases TA slightly, because charged ions like nitrate and phosphate are taken up as nutrients. Cultures with high cell densities can therefore cause a shift in carbonate chemistry, if the drawdown of inorganic carbon exceeds the supply with new  $\text{CO}_2$ . To rule out physiological constraints by varying carbonate chemistry and ensure controlled experimental conditions, I

worked with low cell densities and monitored the carbonate system parameters pH, TA and DIC throughout the experiment. To assess a potential drift in carbonate chemistry, two bottles of biomass-free culture medium were aerated with a pCO<sub>2</sub> of 400 ppm at 3 and 6 °C as a control.

pH was determined potentiometrically on the NBS scale by almost daily measurements with a glass reference electrode (Aquatrode plus Pt1000, Metrohm, Herisau, Switzerland). Temperature of the measured samples was simultaneously determined with the integrated Pt1000 temperature sensor of the combined pH electrode. To maintain temperatures as close as possible to experimental conditions, samples were kept on ice after sampling until they were measured. To ensure accurate results, three-point calibrations of the pH meter were performed weekly with NBS buffers (pH 4.0, 6.9, 9.2, ITW, USA).

Samples for TA analysis were taken on harvest days at the beginning and at the end of the experiment for all treatments. After cultures were filtered through 0.7 µm GF/F filters (Whatman, Maidstone, UK), the filtrate was transferred in borosilicate bottles and stored in darkness at 4 °C until measurement. TA was determined at room temperature by potentiometric titration (Brewer *et al.*, 1986) with precise quantities of 0.05 M HCl using a TitroLine alpha plus autosampler (Schott Instruments, Mainz, Germany). The Software TitrSoft then calculates the total alkalinity based on the amount of acid used during titration. For every sample, TA was determined in duplicates for 25 mL of sample. The obtained values were later corrected by a TA standard of filtered North Sea water. The drift in TA (%) was calculated by using the TA of the biomass-free control bottles as reference at the respective timepoints.

At the same timepoints, samples were collected for DIC analysis. Immediately after culture bottles were decoupled from the gas supply, duplicates of 5 mL of culture sample were filtered through 0.2 µm cellulose-acetate syringe-filters (NALGENE) into gastight borosilicate bottles and stored headspace-free at 4 °C until analysis. DIC was measured colorimetrically in technical duplicates after Stoll *et al.* (2001) using a QuaAatro autoanalyzer (Seal Analytical, Mequon, USA). In this method, the sample is first acidified with sulfuric acid (H<sub>2</sub>SO<sub>4</sub>) to a pH < 1, thereby converting all carbon species into the CO<sub>2</sub> gas phase. After the CO<sub>2</sub> diffuses across a semipermeable silicone membrane, an alkaline detector stream containing NaOH and phenolphthalein indicator absorbs the CO<sub>2</sub> gas and the indicator is discoloured. The amount of DIC in the sample can then be derived from the change of extinction in a flow cell at a wavelength of 550 nm. Obtained values were corrected with a standard (provided by A. Dickson) and the drift (%) of the measured DIC was determined with the DIC values of the biomass-free control bottles at 2.7 and 6.2 °C at the respective timepoints.

The aqueous pCO<sub>2</sub> and temperature correction of the measured pH were calculated with the program CO<sub>2</sub> sys (Pierrot *et al.*, 2006) assuming seawater with a salinity of 29.6, pressure of 0 dbars, 6.5 μmol kg<sup>-1</sup> seawater phosphate and 4 μmol kg<sup>-1</sup> seawater silicate. The program applied the dissociation constants by Mehrbach *et al.* (1973) refitted by Dickson and Millero (1987) and the dissociation constants for sulfuric acid from Dickson (1990). Depicted values for the aqueous pCO<sub>2</sub> were calculated with a combination of TA and pH values, which results in the lowest calculation inconsistencies according to Hoppe *et al.* (2010).

## 2.4. Growth rates

Cell densities were determined daily for all treatments using the Coulter Multisizer III cell-counter (Beckman-Coulter, Fullerton, USA). This instrument detects particles via electrical zone sensing according to the Coulter Principle. A tube with a small aperture and an internal electrode is immersed into a sample of cell culture. An electrical current is created between this internal electrode and a second electrode in the cell suspension outside the aperture tube. When particles pass through the sensing zone of the aperture, the impedance between the two electrodes is modulated. This change in electrical resistance across the aperture creates an electrical pulse that is directly processed into size distribution and particle count by the Multisizer software.

The determination of the cell densities was restricted to cells with a diameter of 3-8 μm. Specific growth rates of the *P. pouchetii* cultures were then calculated from the daily increments according to the formula:

$$\mu = \frac{\ln(N_t) - \ln(N_0)}{\Delta t} \quad (1)$$

where μ equals the specific growth rate in days, N<sub>0</sub> and N<sub>t</sub> refer to the cell concentrations at different timepoints and Δt represents the sum of days the culture has grown between the determination of N<sub>0</sub> and N<sub>t</sub>. Growth rates determined on the days following dilutions were removed from analysis, because cell growth always exhibited a short lag phase. With the obtained growth rates, the number of cell divisions per day was calculated with the division rate constant k (1/generation time) according to the formula:

$$k = \frac{\mu}{\ln(2)} \quad (2)$$

The average of the division rate constant  $k$  was used to calculate the production rates of particulate organic carbon and Chl *a*. Production rates of MHW1 and MHW2 treatments were determined with the mean  $k$  of the period of MHW exposure and the post-MHW phase respectively. Alternatively, the specific growth rate  $\mu$  can also be used to calculate production rates (Morel, 1987).

## 2.5. Elemental analysis

To investigate the elemental composition of *P. pouchetii*, the particulate organic carbon (POC) and particulate organic nitrogen (PON) quotas were assessed. Cells of all treatments were harvested at pre-, mid- and post-heatwave timepoints (Fig. 8) by filtration of 150-200 mL of cell culture onto pre-combusted (15 h at 500 °C) GF/F filters (0.7  $\mu\text{m}$  nominal pore size; Whatman, Maidstone, UK). For each biological replicate of the treatments, the cells were harvested in technical duplicates and the resulting samples were stored in petri dishes at -20 °C. Samples were then prepared for analysis by drying filters overnight at 60 °C, followed by wrapping in tin foil and compressing them into pellets.

The gas chromatograph CHNS-O elemental analyser (Euro EA 3000, HEKAtech) was used to analyse the elemental composition of the samples by the flash combustion technique. Samples sealed in tin capsules are oxidised in the oxidation reactor at  $\geq 1000$  °C due to the strong exothermic reaction of tin with oxygen. This flash combustion converts all organic carbon and nitrogen into the combustion gases  $\text{CO}_2$ ,  $\text{N}_2$  and various nitrous oxides ( $\text{NO}_x$ ). The vaporized sample is then transported by a carrier gas to the reduction reactor packed with copper wires, where excess oxygen is removed and  $\text{NO}_x$  is reduced to  $\text{N}_2$  at 650 °C. The sample stream then flows through a water trap of magnesium perchlorate to remove water vapour, before it reaches the gas chromatograph, in which the gas mixture is separated.  $\text{CO}_2$  and  $\text{N}_2$  are then measured by thermal conductivity detection.

Determined C and N values were corrected by MiliQ blanks and normalised to cell numbers to receive POC  $\text{cell}^{-1}$  and PON  $\text{cell}^{-1}$ . Production rates of POC were determined by multiplying the obtained POC quota with the average division rate constant  $k$  of the respective treatment.

## 2.6. Measurement of chlorophyll *a* by fluorometric analysis

With the same filtration setup as described for the elemental analysis (2.5), volumes of 100-150 mL of cell culture were filtered onto GF/F filters in technical duplicates. The accurate filtered volume was noted down for later calculations. Filters were folded in half twice, transferred into cryovials that were immediately shock-frozen in liquid nitrogen and stored at -80 °C until analysis to avoid degradation of chlorophyll *a* (Chl *a*). Pigments were extracted by inserting the filters in 6 mL cooled acetone and storing them overnight at -20 °C. After vortexing the sample, the pigment extract was decanted in a cuvette and Chl *a* concentration was measured fluorometrically with the TD-700 Fluorometer (Turner Designs, USA) as described by Knap *et al.* (1996). After excitement by blue wavelengths of light, Chl *a* fluoresces in the red wavelengths, which is detected by the photomultiplier of the fluorometer.

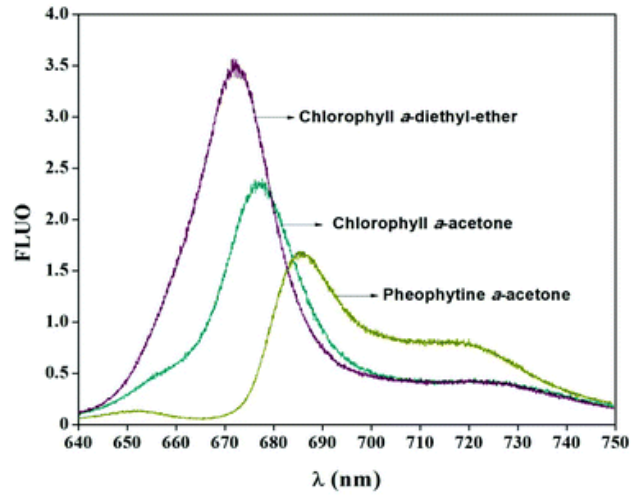


**Figure 9.** Fluorescence spectra of Chlorophyll *a* and Pheophytin *a*. From Sommer Márquez *et al.* (2014).

The Chl *a* degradation product phaeophytin fluoresces in the same spectral region as Chl *a* (French *et al.*, 1956; Fig. 9) and therefore reduces the accuracy of the fluorometric Chl *a* determination. To correct for the phaeophytin fluorescence, all Chl *a* was converted to phaeopigments by acidifying the sample with 3 drops of 1 M HCl and fluorescence was measured again. If the pigment concentration of samples were higher than the sensitivity maximum of the fluorometer, the sample concentration was adjusted by dilution with acetone. After correction with an acetone blank, the chlorophyll *a* and phaeopigment fluorescence can be used to calculate the absolute Chl *a* content in the sample according to the formula:

$$\text{Chl } a \text{ } [\mu\text{g/L}] = \left( \frac{F_m}{F_{m-1}} \right) \times (F_0 - F_a) \times K_x \times \left( \frac{\text{vol}_{\text{ex}}}{\text{vol}_{\text{filt}}} \right) \quad (3)$$

where  $F_0$  is the fluorescence reading before acidification,  $F_a$  the fluorescence reading after acidification,  $F_m$  the acidification coefficient ( $F_0/F_a$ ) for pure Chl *a*,  $K_x$  the linear calibration factor,  $\text{vol}_{\text{ex}}$  the extraction and  $\text{vol}_{\text{filt}}$  the sample volume.  $F_m$  and  $K_x$  values were derived from

the calibration of the fluorometer with a Chl *a* standard (*Anacystis nidulans*, C6144, Sigma-Aldrich). After dissolving the standard in 90% acetone for at least 2 hours, Chl *a* concentration was determined spectrophotometrically. A dilution series was prepared from the standard and fluorescence was determined before and after acidification with 3 drops of 1 M HCl. After correction by an acetone blank,  $F_m$  was calculated by averaging the ratio of non-acidified and acidified readings ( $F_0/F_a$ ). The slope of the unacidified fluorometric reading versus the Chl *a* concentration was defined as  $K_x$ .

Calculated Chl *a* values were normalized to cell concentrations and POC quotas to obtain the parameters Chl *a* cell<sup>-1</sup> and Chl *a* POC<sup>-1</sup>. Chl *a* production was determined by multiplying Chl *a* cell<sup>-1</sup> by the average division rate  $k$  of the respective treatment.

## 2.7. Fast Repetition Rate Fluorometry (FRRF)

Photosynthetic physiology was observed through measurement of variable chlorophyll fluorescence (ChlF) in photosystem II (PSII) using a fast repetition rate fluorometer (FRRF; FastOcean FRRf3 sensor, Chelsea Technologies) connected to the Act2 system (Chelsea Technologies). A list of the used abbreviations related to FRRF analysis is provided in Table 1. The theoretical concept behind variable ChlF is that light energy absorbed by Chl *a* pigments in PSII can be allocated into three competing pathways: photochemistry, dissipation as heat or re-emission at longer wavelengths as fluorescence (Klughhammer and Schreiber, 2008; Kramer *et al.*, 2004; Maxwell and Johnson, 2000). The distribution of energy among these three pathways is variable (Fig. 10) and by measuring the resulting ChlF, information can be gained about the changes in the efficiency of photochemistry and heat dissipation.

Sampling for FRRF measurements of the MHW treatments was performed pre-, mid- and post-MHW and during the temperature ramps as illustrated in Figure 8. Photophysiological assessments of the 3 and 6 °C control cultures were performed at three different timepoints evenly spread over the experimental period. The surrounding water jacket of the FRRF's sample chamber was connected to the aquarium of the respective temperature treatment through tubing and water pumps to keep the chamber at the correct temperature during measurements. For every biological replicate of a treatment, photophysiological parameters were assessed in technical triplicates. Prior to measurements, the triplicates of cell culture samples were dark-acclimated for 15 min (run 1), 40 min (run 2) and 65 min (run 3) at the respective temperature.

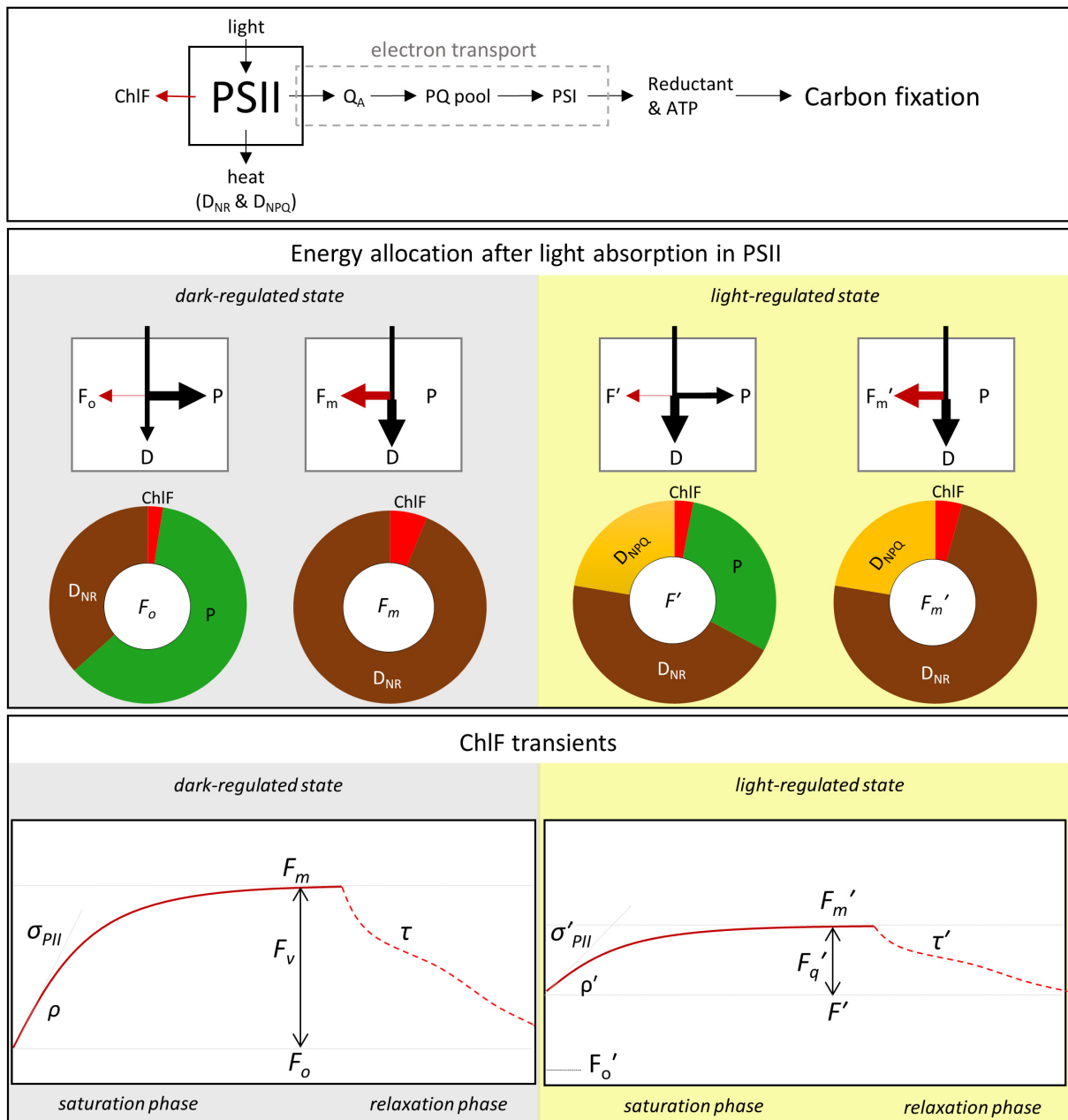


**Figure 10.** The concept of energy allocation after light absorption and chlorophyll fluorescence transients from light and dark-regulated states. ChlF: Chlorophyll fluorescence, P: Photochemistry, D: re-emission as heat, F: ChlF, D<sub>NR</sub>: non-regulated heat-dissipation, D<sub>NPQ</sub>: actively regulated heat-dissipation. From Schuback et al. (2021).

The FRRF applies a series of brief excitation flashlets with a blue LED at a wavelength of 450 nm to induce a change in ChlF (Kolber *et al.*, 1998). These ChlF transients consist of the saturation phase, in which ChlF increases to a maximum, and the following return of ChlF to the basal level in the so-called relaxation phase (Fig. 10). At the beginning of the ChlF transient all PSII reaction centres (RCII) are open, leading to a maximum fraction of absorbed photons to be allocated into photochemistry, which means ChlF is minimal ( $F_0$ ). Many brief flashlets of light are then applied by the FRRF during the saturation phase (70 flashlets at a 2  $\mu$ s pitch) until photosystems are transiently saturated by electrons and change from an open to a closed state

(Oxborough *et al.*, 2012). Since this causes photochemical quenching to decrease, the ChlF increases until it reaches a plateau called the maximum fluorescence ( $F_m$ ). The amplitude of the ChlF transient ( $F_v$ ) was used to calculate the maximum quantum efficiency of photochemistry by open PSII reaction centres (Genty *et al.*, 1989) as follows:

$$\frac{F_v}{F_m} = (F_m - F_0) / F_m \quad (4)$$

Furthermore, the absorption cross section for PSII photochemistry ( $\sigma_{\text{PSII}}$ ) and the connectivity among PSII units ( $\rho$ ) were determined from the saturation phase in a dark acclimated state.

After all RCII are closed and ChlF is maximal during the saturation phase, the intervals between the flashes become longer in the relaxation phase (40 flashlets at an 80  $\mu\text{s}$  pitch). This results in PSII to progressively open again (Kolber *et al.*, 1998) and ChlF to decrease back to a minimal level due to downstream photosynthetic electron transport (Schuback *et al.*, 2021). The time dependent decrease in ChlF is resolved by the time constant  $\tau$  for PSII reoxidation (Kolber *et al.*, 1998).

In addition to measurements in the dark, ChlF was also assessed after actinic light was applied for 5 min at the in-situ light level of 33  $\mu\text{mol photons m}^{-2} \text{s}^{-1}$  and the saturating irradiance of 450  $\mu\text{mol photons m}^{-2} \text{s}^{-1}$ . The minimum ( $F_0'$ ) and maximum ( $F_m'$ ) fluorescence was determined and the quantum yield of photochemistry at PSII ( $F_q'/F_m'$ ) calculated as:

$$\frac{F_q'}{F_m'} = (F_m' - F_0') / F_m' \quad (5)$$

The parameters described above were directly derived from the ChlF transients. From these, secondary parameters were calculated like the relative electron transport rate (rETR). rETR quantifies the relative photon flux in the photosynthetic electron transport chain and was determined by multiplying the photosynthetically active radiation (PAR,  $\mu\text{mol photons m}^{-2} \text{s}^{-1}$ ) by  $F_q'/F_m'$  according to Oxborough *et al.* (2012):

$$rETR = PAR \times \left( \frac{F_m' - F_0'}{F_m'} \right) \quad (6)$$

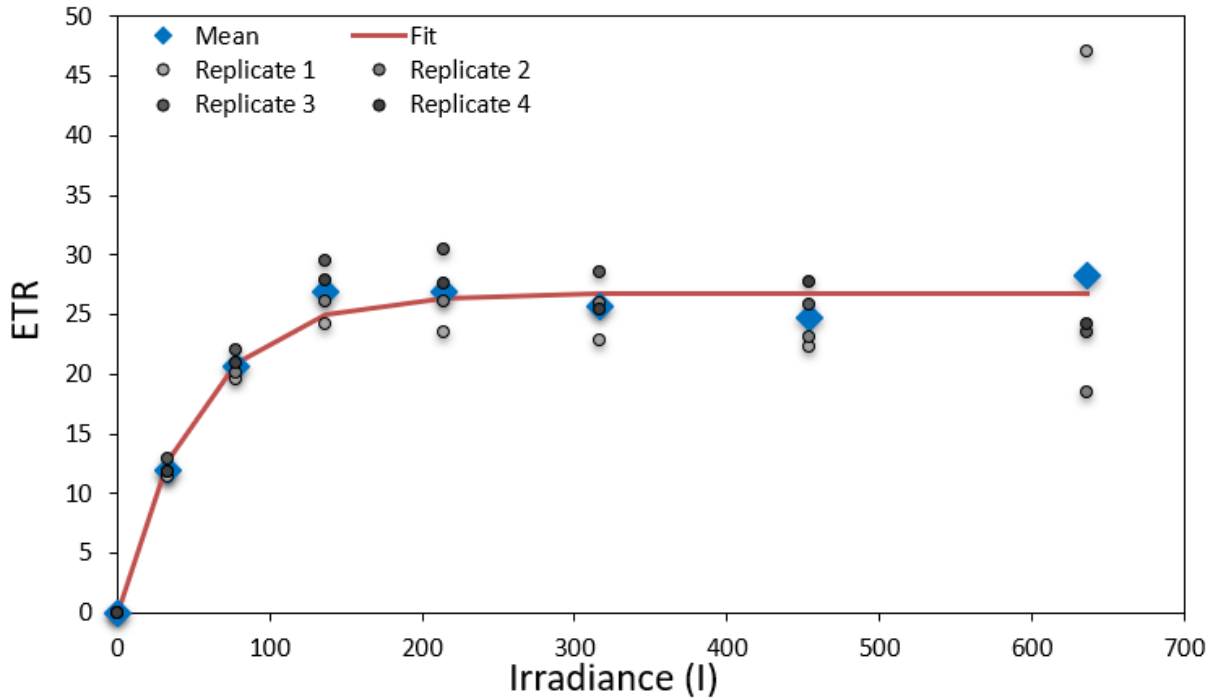


**Figure 11.** Photosynthesis vs irradiance curve of *Phaeocystis pouchetii* cultures (n = 4) acclimated to 2.5 °C and an irradiance of 30  $\mu\text{mol photons m}^{-2} \text{s}^{-1}$ .

The determination of the high irradiance level as 450  $\text{mol photons m}^{-2} \text{s}^{-1}$  was based on the plateau of photosynthesis versus irradiance (PI) curves that were recorded prior to the start of the experiments (Fig. 11). The PI curves were conducted at eight different irradiance levels from 0 to 636  $\mu\text{mol photons m}^{-2} \text{s}^{-1}$ . Calculated rETR values of these actinic light periods were fitted as described by Webb *et al.* (1974):

$$P = P_{max} \left[ 1 - e^{\left(\frac{-aI}{P_{max}}\right)} \right] \quad (7)$$

Potentially harmful excess excitation energy can be dissipated by the activation of non-photochemical quenching (NPQ) mechanisms resulting in a decrease of ChlF. Fractional yields of regulated (Y(NPQ)) and non-regulated energy dissipation processes (Y(NO)) were calculated for in-situ and high light as described in Klughammer and Schreiber (2008):

$$Y(NPQ) = \frac{F'}{F_m'} - \frac{F'}{F_m} \quad (8)$$

$$Y(NO) = \frac{F'}{F_m} \quad (9)$$

**Table 1.** Summary of the abbreviations and units of photophysiological parameters.

Parameter	Description	Unit
$F_0$	Minimal fluorescence in the dark	Relative units
$F_m$	Maximal fluorescence in the dark	Relative units
$F'$	Minimal fluorescence in the light	Relative units
$F_m'$	Maximal fluorescence in the light	Relative units
$F_v$	Variable fluorescence in the dark	Relative units
$F_v/F_m$	Quantum yield (efficiency) of electron transport through PSII in the dark	Dimensionless
$F_q'/F_m'$	Quantum yield (efficiency) of electron transport through PSII in the light	Dimensionless
$\sigma_{PII}$	Absorption cross section for PSII photochemistry in the dark	$\text{nm}^2 \text{PSII}^{-1}$
$\rho$	Connectivity between PSII reaction centres in the dark	Dimensionless
$\tau$	Time constant for PSII re-oxidation in the dark	$\mu\text{s}$
rETR	Relative PSII electron transfer rate	Dimensionless
Y(NPQ)	Quantum yield of regulated non-photochemical energy loss in PS II	Dimensionless
Y(NO)	Quantum yield of non-regulated non-photochemical energy loss in PS II	Dimensionless

## 2.8. Flow cytometric analysis of reactive oxygen species

Oxidative stress of *P. pouchetii* cells was evaluated based on flow cytometric analysis of intracellular levels of superoxide anion radical ( $\text{O}_2^{\cdot-}$ ) and hydrogen peroxide ( $\text{H}_2\text{O}_2$ ) based on methods of Prado *et al.* (2012). The fluorescent probe dihydroethidium (HE) has been commonly used as indicator for  $\text{O}_2^{\cdot-}$  (Bindokas *et al.*, 1996; Carter *et al.*, 1994; Rothe and Valet, 1990). This fluorochrome reacts with superoxide and forms the red fluorescent product ethidium, which binds to DNA and enhances the fluorescence to a maximum emission signal of 605 nm (Zhao *et al.*, 2003). A HE stock solution with a final concentration of 3.17 mM was prepared by dissolving HE (37291, Sigma-Aldrich®) in dimethylsulfoxide (DMSO, D8418, Sigma-Aldrich®). For the detection of  $\text{H}_2\text{O}_2$  the fluorogenic probe Dihydrorhodamine 123 (DHR123, D1054, Sigma-Aldrich®) was used. DHR123 is selectively oxidised by  $\text{H}_2\text{O}_2$  in the cell (Henderson and Chappell, 1993; Qin *et al.*, 2008) and forms the highly fluorescent Rhodamine 123, which emits green fluorescence with a maximum emission signal at 529 nm. A DHR123 stock solution with a final concentration of 5.77 mM was prepared by dissolving

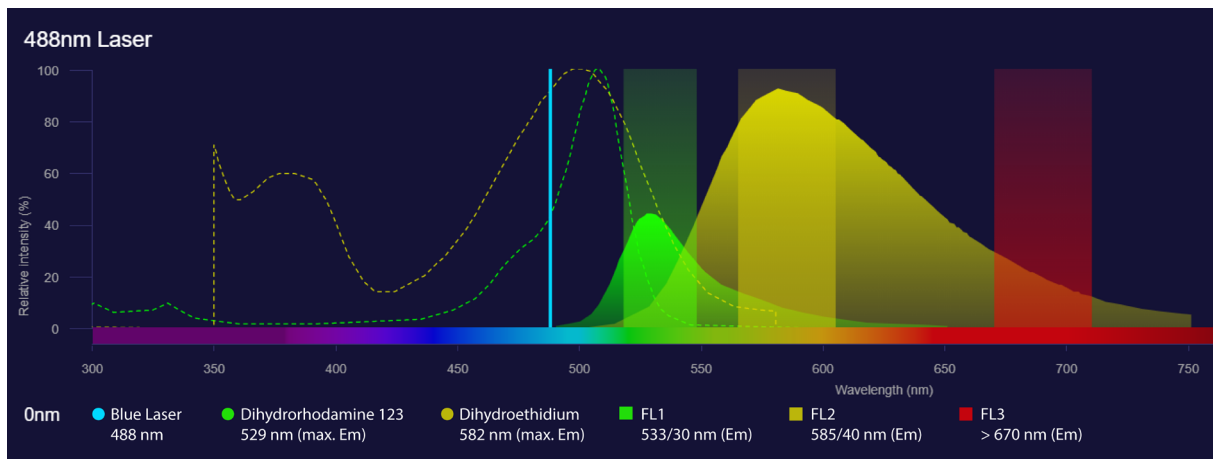


**Figure 12.** Absorption- (dashed lines) and emission spectra (shaded areas) of the fluorochromes Dihydroethidium (HE) and Dihydrorhodamine 123 (DHR123) normalized to the blue excitation laser of 488 nm. Emitted fluorescence is measured by the fluorescence detectors FL1 (533/30 nm), FL2 (585/40 nm) and FL3 (> 670 nm).

DHR123 in DMSO. Aliquots of both fluorochrome stock solutions were stored in the dark at  $-20\text{ }^{\circ}\text{C}$  until they were used for sample analysis.

ROS was determined at pre-, mid- and post-MHW timepoints in all temperature treatments and in addition shortly before and after the temperature ramps in the MHW treatments (Fig. 8). Samples for each biological replicate (A, B, C) were measured with both fluorochromes in technical duplicates. Suspensions of  $500\text{ }\mu\text{L}$  of cell culture were incubated for 15 min with  $10\text{ }\mu\text{L}$  HE stock solution to yield a final concentration of  $158.5\text{ }\mu\text{M}$  and for 20 min with  $2.5\text{ }\mu\text{L}$  DHR123 stock solution with a final concentration of  $28.87\text{ mM}$ . Incubation took place in the dark at the respective temperature of the treatment. Prior to the experiment, concentration and incubation time was optimized experimentally for each fluorescent marker in order to establish a staining protocol with the least concentration possible and shortest incubation time to prevent toxicity to cells. The effectiveness of the staining protocol was validated by incubating stained cells with  $\text{H}_2\text{O}_2$  as a positive control. In addition, the fluorescence of cell samples without any fluorochrome was measured in duplicates as negative controls for every replicate.

Flow cytometric analysis of stained and unstained samples was performed with the BD Accuri™ C6 Flow Cytometer (Becton, Dickinson and Company (BD), Franklin Lakes, USA). This instrument injects a sample of cell culture into the centre of a sheath fluid (filtered, deionized water), which confines the cells into a core stream by hydrodynamic focussing. The cells are then passed through a focused blue laser beam with a wavelength of 488 nm like beads on a string, which allows the analysis of individual cells. After excitation by the laser, light scattered from the cells is analysed by two detectors. One detector measures the forward scatter

(FSC), which is proportional to the size of the cell. The second detector at 90 degrees to the laser beam collects the side-scattered light (SSC), which is proportional to the shape and internal complexity of the cell. In addition, fluorescence emitted from particles is measured by four fluorescence detectors that are fitted by interference filters to transmit light in different wavelength ranges (Fig. 12): 533/30 nm (FL1), 585/40 nm (FL2), > 670 nm (FL3) and 675/25 nm (FL4). The passage of a cell through the measurement system produces a pulse. This so-called event is given a channel number depending on the fluorescence intensity, which are then visualized using one and two-dimensional plots (Fig. 13). The performance of the cytometer was evaluated at three occasions during the experiment by running Spherotech 6-Peak (653145, BD) and 8-Peak Validation Beads (653144, BD).

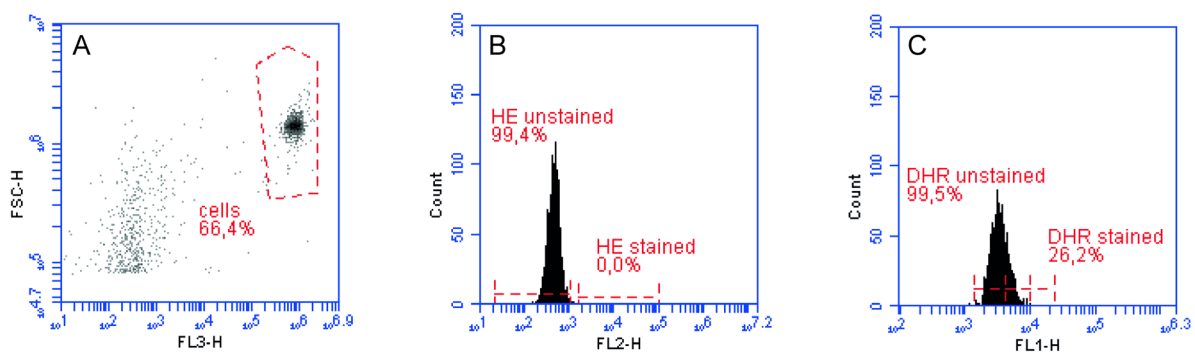


**Figure 13.** Application of the gating tool on plots of detected fluorescence emission to isolate (A) the cell population of interest and the range of stained and unstained cells for the fluorochromes (B) HE and (C) DHR123.

Forward scatter, side scatter and the FL3 histogram (Fig. 13), which displays the chlorophyll fluorescence, were used to characterise the microalgal population and discriminate cells from debris and noise. The cell population of interest was then segregated by the gating tool (Fig. 13A) and analysis was performed on 1000 gated cells of this isolated cluster. Fluorescence emission of HE was detected by the FL2 channel and DHR123 fluorescence by the FL1 channel (Fig. 12). For every fluorochrome, the range of stained and unstained cells were defined using gates (Fig. 13B+C). The FL1 histogram showed two stained peaks for some samples, but the second one was excluded from analysis because the majority of cells were represented in the first peak. Fluorescence values of the stained samples were later corrected by subtracting the autofluorescence of the unstained sample. Values were further corrected by forward scatter to account for the variability due to differences in cell size.

## 2.9. Statistical analysis

All statistical analyses and data visualization were performed with the Software R (version 4.0.3, © 2020 The R Foundation for Statistical Computing). In this study, several outcome variables are repeatedly measured over time in the same replicates (A, B, C). This so-called repeated-measures design was extended to a groups-by-trials design by including a treatment structure between the replicates (Quinn and Keough, 2012). Cell cultures were split into 4 x 3 replicates and randomly allocated to the four treatment groups 3 °C control, 6 °C control, MHW1 and MHW2 and their responses were measured at several timepoints (Fig. 14).

The overall effect of time, treatment and the interaction of the two on the outcome variable was analysed by mixed analysis of variance (ANOVA) with a linear mixed-effect model (LMM) using the *lme()* function of the package *nlme* (Pinheiro *et al.*, 2021). ‘Treatment’ was classified as the between-subjects-factor and ‘Timepoint’ as the within-subjects-factor of the mixed ANOVA. For the linear mixed-effects model, the timepoints within each treatment were defined as fixed effect, biological replicates within timepoints as random effect (random = 1|Replicate/Timepoint/Treatment). The between-group variable of ‘Treatment’ was added to

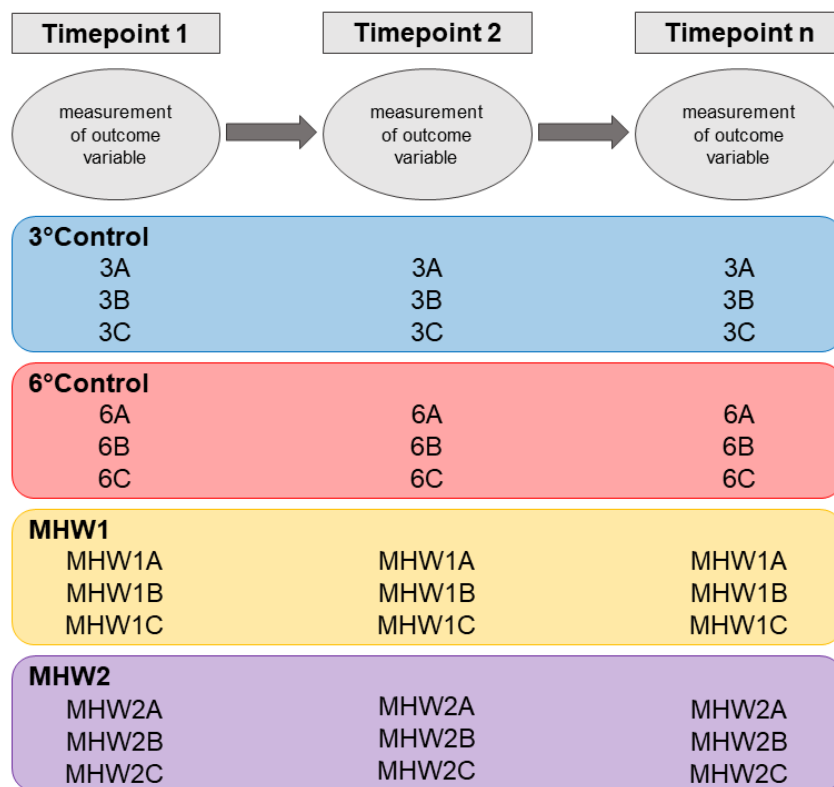


**Figure 14.** Overview of the study design with ‘Timepoint’ as the repeated-measures variable (within-subjects factor) and ‘Treatment’ as between-subjects variable.

the model as an additional predictor. After setting up a baseline model with only the intercept as predictor, further models were specified one predictor at a time to look at the overall main effects of time and temperature treatment separately and the interaction of the two (Field *et al.*, 2012). The fit of the full and the reduced models were compared by performing an ANOVA with the function *anova()*. If the ANOVA yielded significant results, the effect of the temperature treatment on the outcome variable or the change of this variable over the period of the treatment exposure was considered significant. Pairwise comparisons were computed with Tukey's post-hoc tests ( $p < 0.05$ ) with the help of the *emmeans* package (Lenth, 2021) to determine which specific timepoints were significantly different from one another. The assumption of normal distribution of the residuals and the random coefficients was checked using the Shapiro-Wilk normality test ( $p > 0.05$ ) and homogeneity of variance was analysed using Levene's test ( $p > 0.05$ ). LMMs of the FRRF and ROS data were set up slightly different, because the number of timepoints when data were collected varied between the four treatments and hence could not be compared. For the 3 and 6 °C controls, the LMM included the effect of the temperature treatment and time, whereas the LMM of the MHW1 and MHW2 treatments only included the predictor of time to analyse whether outcome variables changed significantly over the duration of the MHWs. NPQ data of the 3 and 6 °C controls were analysed by performing Welch's t-tests (data collection at only one timepoint) thereby comparing the means of the two independent experimental treatments.

The significance level of all statistical tests was set to 0.05 ( $p < 0.05$ ). Up to 0.001, exact p-values were reported, values below this level were indicated as  $p < 0.001$ . All data shown in the plots or tables are reported as raw data points ( $\mu$ ) or as means  $\pm$  standard deviations (SD) of the biological replicates ( $n = 3$ ).

### 3. Results

#### 3.1. Carbonate chemistry

During the entire experiment, the pCO<sub>2</sub> within the culture bottles remained close to the target pCO<sub>2</sub> of 400 μatm with slight deviations of up to 10 % (Table 2). The carbonate chemistry parameters of pH, DIC and TA also remained relatively stable during the complete duration of the experiment in all treatments. The drift in pH<sub>NBS</sub> and DIC remained <0.035 and <3.6 %, respectively. Also TA remained constant over the experiment and drifted less than 1 % , except for the final culturing days (t5) of the 6 °C control, where the drift was about 3 %. Hence, cells were neither exposed to physiological constraints by limited availability of inorganic carbon, nor to strongly distorted pH conditions.

**Table 2.** Carbonate chemistry parameters of the control and heatwave treatments (n = 3; mean ± SD) at different timepoints throughout the experiment.

Treatment	Temperature [°C]	Timepoint	pCO <sub>2</sub> [μatm] (pH + TA)	pH (NBS scale)	TA [μmol kg <sup>-1</sup> ]	DIC [μmol kg <sup>-1</sup> ]
3 °C control	2.7	t1	397.2 ± 4.1	8.126 ± 0.004	2165.8 ± 3.9	2058.2 ± 10.8
	2.7	t5	359.4 ± 4.3	8.166 ± 0.005	2169.7 ± 2.8	2031.0 ± 4.9
6 °C control	6.2	t1	415.0 ± 15.4	8.123 ± 0.013	2176.2 ± 9.8	2021.3 ± 30.9
	6.2	t5	364.0 ± 1.0	8.162 ± 0.002	2115.3 ± 8.3	1917.6 ± 3.9
MHW1	2.7	t1	397.2 ± 4.1	8.126 ± 0.004	2165.8 ± 3.9	2058.2 ± 10.8
	2.7	t4	365.0 ± 6.9	8.161 ± 0.010	2174.0 ± 22.5	2045.1 ± 44.1
MHW2	2.7	t1	397.2 ± 4.1	8.126 ± 0.004	2165.8 ± 3.9	2058.2 ± 10.8
	2.7	t6	358.9 ± 1.0	8.168 ± 0.001	2174.6 ± 1.3	2016.5 ± 20.7

#### 3.2. Growth rates

Specific growth rates of *P. pouchetii* differed between the two control treatments at constant high and low temperature. At 3 °C, the growth rate was  $0.40 \pm 0.14 \text{ d}^{-1}$  on average, while constant exposure to 6 °C resulted in a decline of the growth rates to  $0.34 \pm 0.11 \text{ d}^{-1}$  (Fig. 15A+B, Table 3). This decrease of ~18 % was statistically not significant, but close to the significance level (LMM,  $\chi^2(1) = 2.83$ ,  $p = 0.092$ ). Please note that the scale of the y-axis in Figure 15 covers a large range due to a high standard deviation of the growth rate values.

Growth rates of *P. pouchetii* cultures exposed to the MHW treatments changed significantly over the course of the MHWs (LMM, MHW1:  $\chi^2(10) = 46.37$ ,  $p < 0.001$ ; MHW2:  $\chi^2(12) = 45.73$ ,  $p < 0.001$ ; Fig. 15C+D). The abrupt temperature rise from 3 to 6 °C significantly

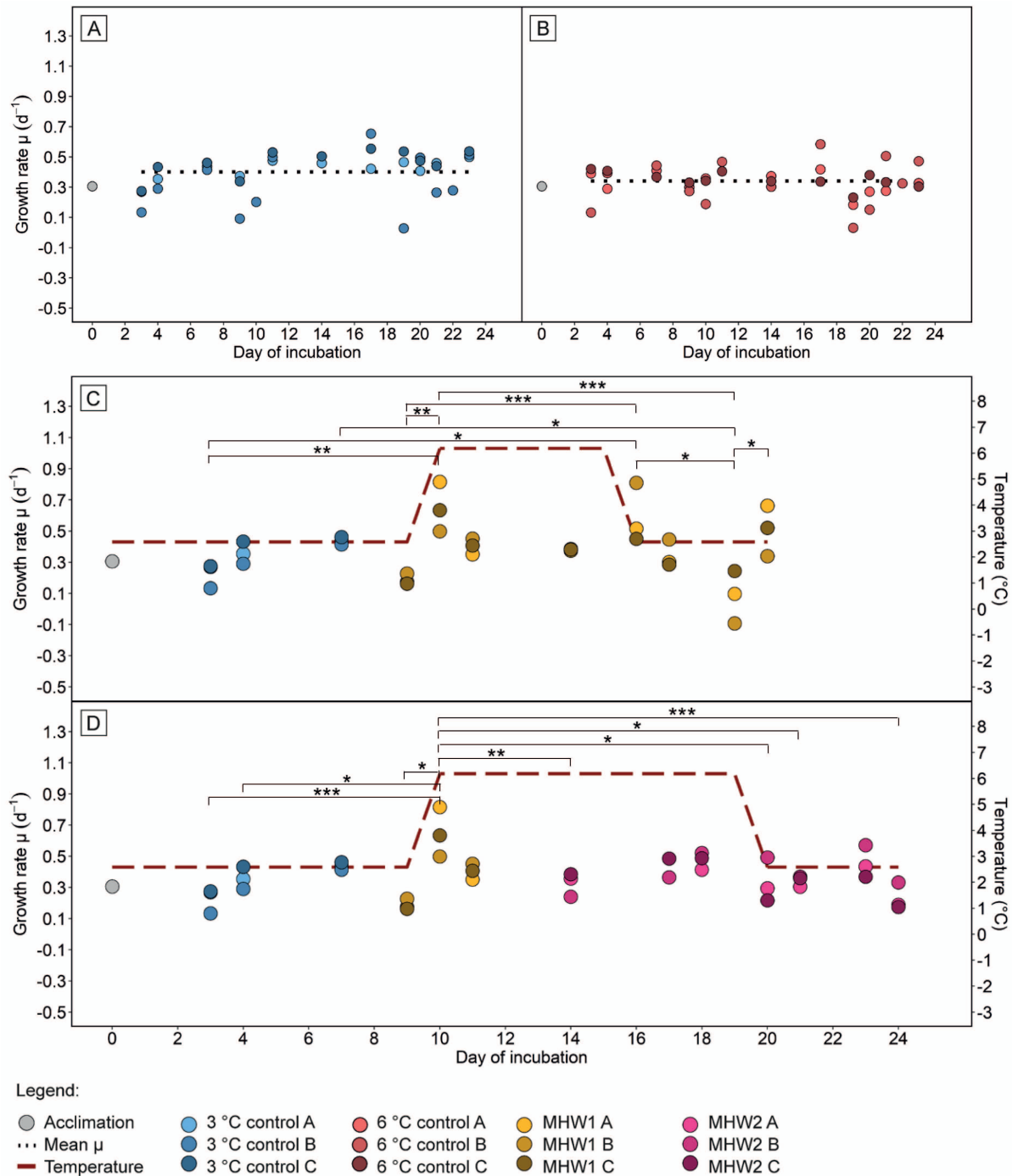


**Figure 15.** Specific growth rates  $\mu$  of *Phaeocystis pouchetii* for all three biological replicates A, B, C in (A) 3 °C control (B) 6 °C control (C) MHW1 and (D) MHW2 treatments. Bottles of the MHW1 cultures were split into MHW1 and MHW2 cultures on day 11 of the experiment. Mean growth rates during acclimation to 3 °C (grey) and of 3 and 6 °C control cultures (black dotted line) as well as the temperature profiles of the MHWs (red dashed line) are indicated on the plots. Statistical significance between the different timepoints revealed by post hoc tests is expressed in asterisks (\*:  $p \leq 0.05$ , \*\*:  $p \leq 0.01$ , \*\*\*:  $p \leq 0.001$ ).

increased growth rates of the MHW cultures by 242 % from pre- to post-heating ramp (post hoc tests,  $t = 4.50$ ,  $p = 0.003$ ). Already one day later, growth rates started to decrease again to an average of  $0.36 \pm 0.09$  d<sup>-1</sup> for the remaining period of MHW1 (Table 3). Cells exposed to the longer MHW revealed a mean growth rate of  $0.40 \pm 0.08$  d<sup>-1</sup> during the exposure to 6 °C, which

is similar to the mean growth rate of the low temperature control (Table 3). The sudden cooling at the end of the MHWs had no effect on growth rates in any of the treatments (post hoc tests, MHW1:  $t = -2.29$ ,  $p = 0.476$ ; MHW2:  $t = 1.94$ ,  $p = 0.757$ ). During the recovery period, growth rates of cultures ranged around  $0.33 \pm 0.24 \text{ d}^{-1}$  for MHW1 and  $0.34 \pm 0.12 \text{ d}^{-1}$  for MHW2 cultures (Table 3). While growth rates remained comparably stable during the recovery period of MHW2 cultures, they fluctuated more strongly during the recovery of MHW1 cultures.

### 3.3. Cellular composition and production rates

All parameters of the cellular composition (POC, PON, Chl *a*, as well as their production rates and ratios) determined during the MHWs and the recovery period are presented as boxplots in Figure 16 and in Tables 3 and 4. In addition, mean values of the control cultures constantly exposed to 3 or 6 °C are displayed as reference values.

Analysis of the data collected during the recovery period of the MHW1 cultures revealed that the biological replicate B was a clear outlier concerning all parameters of the elemental composition and Chl *a* content compared to the data obtained for replicates A and C at timepoint 'Rec'. Cells in this culture probably stopped dividing as indicated by the negative growth rates on the two days prior to harvest ( $\mu = -0.02 \text{ d}^{-1}$  and  $-0.09 \text{ d}^{-1}$ ). Based on this, data for replicate MHW1 B at the recovery timepoint was excluded from statistical analysis ( $n = 2$ ). In addition, a handling error caused the loss of POC samples of all treatments from the first harvest timepoint. Therefore, the elemental composition of cells could only be derived from the analysis of the other two sampling timepoints.

The constant exposure of *P. pouchetii* to elevated temperatures in the control treatments significantly increased cellular quota of POC and PON by ~20 % compared to the low temperature control (Fig. 16A, B; LMM, POC:  $\chi^2(3) = 19.55$ ,  $p < 0.001$ ; PON:  $\chi^2(3) = 18.33$ ,  $p < 0.001$ ). POC quota slightly increased after 6 days of heat exposure (MHW1) by 14 %, but after 10 days (MHW2) quota returned to initial values (post hoc tests, MHW1:  $t = -2.66$ ,  $p = 0.258$ ; MHW2:  $t = -0.31$ ,  $p = 1.000$ ; Fig. 16A). During recovery, POC quota of both MHW treatments ranged around pre-MHW values again (Table 3). A similar trend was observed for the cellular PON quota during MHWs, where neither the abrupt temperature rise (post hoc tests, MHW1:  $t = -2.61$ ,  $p = 0.274$ ; MHW2:  $t = 0.22$ ,  $p = 1.000$ ) nor the cooling post-MHW (post hoc tests, MHW1:  $t = 3.25$ ,  $p = 0.154$ ; MHW2:  $t = 0.81$ ,  $p = 0.986$ ) resulted in any significant

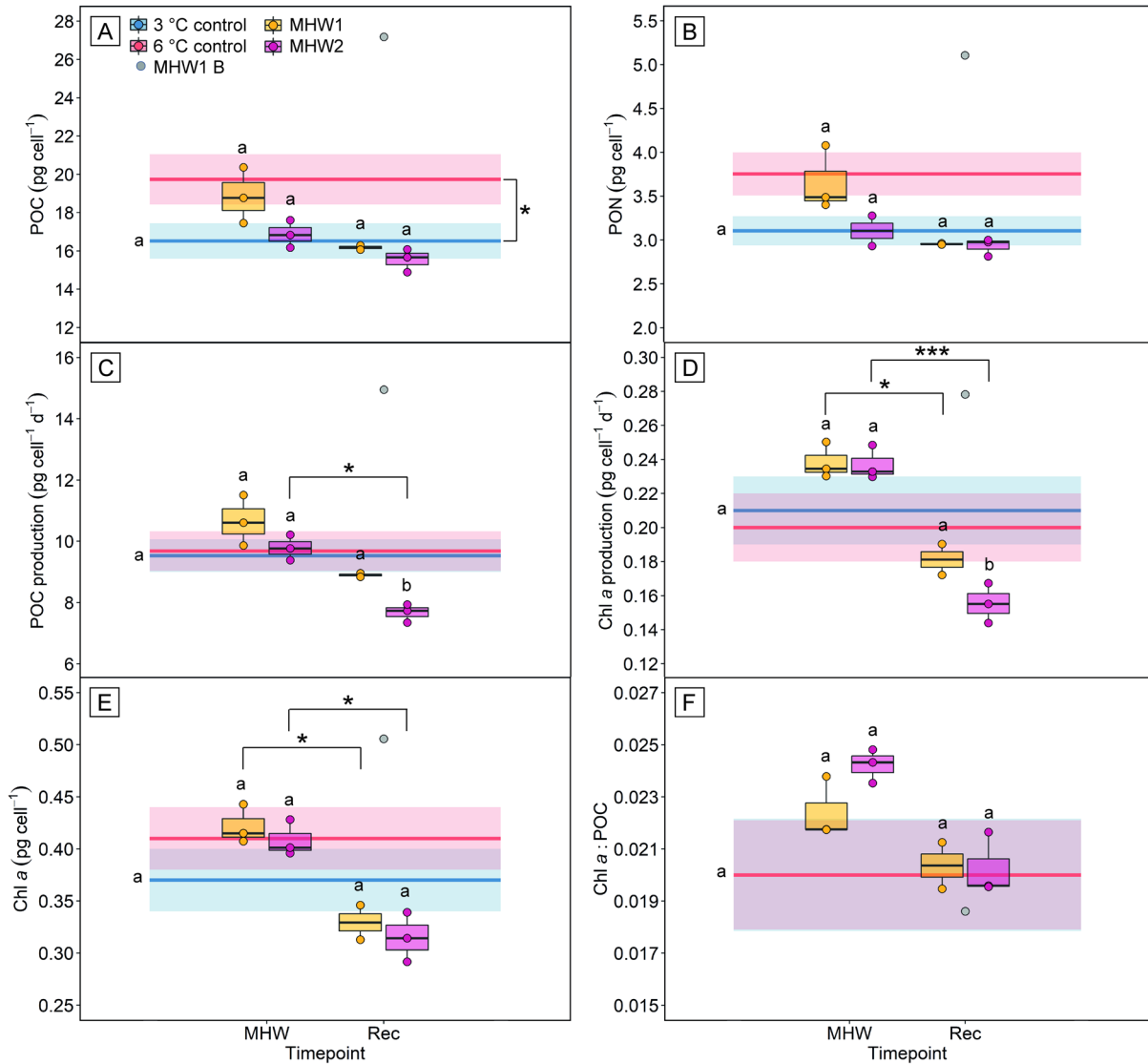


**Figure 16.** Elemental composition and pigmentation of *Phaeocystis pouchetii*. Values for (A) particulate organic carbon (POC) per cell, (B) particulate organic nitrogen (PON) per cell, (C) POC production, (D) Chl *a* production, (E) Chl *a* per cell and (F) Chl *a* per POC are shown for the 3 °C control (blue), 6 °C control (red), MHW1 (yellow) and MHW2 (violet) treatments. Data of the MHW cultures are separately displayed for the response during heat exposure (MHW) and during recovery (Rec). Mean (solid line)  $\pm$  SD (shaded area) of the 3 and 6 °C control cultures are depicted as baselines on the plots. Data of replicate MHW1 B (grey dot) at timepoint Rec was excluded from statistical analysis. Statistical significance between the different timepoints and between 3 and 6 °C control treatments revealed by post hoc tests is expressed in asterisks (\*:  $p \leq 0.05$ , \*\*:  $p \leq 0.01$ , \*\*\*:  $p \leq 0.001$ ). Statistical significance between timepoints of the MHW treatments and the 3 °C control is denoted with different letters.

changes (Fig. 16B). The C:N ratios of cells also remained unchanged during the temperature fluctuations of MHW1 and MHW2 as well as constant exposure to 6 °C (LMM,  $\chi^2(3) = 0.47$ ,  $p = 0.926$ ; Table 3).

Cells constantly exposed to 6 °C revealed Chl *a* quota 11 % higher than those of cells growing at 3 °C (Fig. 16E, Table 4). However, this increase was statistically not significant between the different timepoints (post hoc tests,  $t = -2.48$ ,  $p = 0.452$ ;  $t = -0.96$ ,  $p = 0.995$ ;  $t = -1.84$ ,  $p =$

0.767). Exposure of cells to the MHW treatments resulted in changed Chl *a* quotas (LMM,  $\chi^2(2) = 21.51$ ,  $p < 0.001$ ; Fig. 17E, Table 4). At the end of MHW1, cellular Chl *a* content was increased by 17 % and by 13 % at the end of MHW2, but this rise was not significant (post hoc tests, MHW1:  $t = -3.02$ ,  $p = 0.193$ ; MHW2:  $t = -2.37$ ,  $p = 0.475$ ). However, the decrease of Chl *a* quota during the recovery was significant (post hoc tests, MHW1:  $t = 4.71$ ,  $p = 0.034$ ; MHW2:  $t = 4.59$ ,  $p = 0.012$ ; Fig. 16E). The ratio of Chl *a*:POC did not differ between cultures exposed to 3 and 6 °C (Table 4). For the MHW treatments, neither the slight increase of Chl *a*:POC during the MHW (post hoc tests, MHW1:  $t = 1.32$ ,  $p = 0.869$ ; MHW2:  $t = -0.18$ ,  $p = 1.000$ ), nor the decrease post-MHW was significant (post hoc tests, MHW1:  $t = 1.54$ ,  $p = 0.768$ ; MHW2:  $t = 3.31$ ,  $p = 0.127$ ; Fig. 16F).

**Table 3.** Growth rates  $\mu$ , POC production rates and cellular quota of POC and PON as well as their ratio under the different temperature treatments ( $n = 3$ ; mean  $\pm$  SD). Data for 3 and 6 °C control cultures are shown as mean values for the whole incubation period. Data for the short (MHW1) and long marine heatwave treatments (MHW2) are displayed for the end of the MHW (MHW) and the recovery period (Rec). In the recovery period of MHW1, values are based on  $n = 2$  (<sup>1</sup>).

Treatment	Timepoint	Temperature (°C)	Growth rate $\mu$ (d <sup>-1</sup> )	POC production (pg cell <sup>-1</sup> d <sup>-1</sup> )	POC quota (pg cell <sup>-1</sup> )	PON quota (pg cell <sup>-1</sup> )	C:N
3 °C control	-	3	0.40 $\pm$ 0.14	9.5 $\pm$ 0.5	16.5 $\pm$ 0.9	3.1 $\pm$ 0.2	6.2 $\pm$ 0.2
6 °C control	-	6	0.34 $\pm$ 0.11	9.7 $\pm$ 0.6	19.7 $\pm$ 1.3	3.8 $\pm$ 0.2	6.1 $\pm$ 0.3
MHW1	MHW	6	0.39 $\pm$ 0.03	10.7 $\pm$ 0.8	18.9 $\pm$ 1.5	3.7 $\pm$ 0.4	6.0 $\pm$ 0.2
	Rec	3	0.38 $\pm$ 0.24	8.9 $\pm$ 0.1 <sup>1</sup>	16.2 $\pm$ 0.2 <sup>1</sup>	3.0 $\pm$ 0.0 <sup>1</sup>	6.4 $\pm$ 0.0 <sup>1</sup>
MHW2	MHW	6	0.40 $\pm$ 0.08	9.8 $\pm$ 0.4	16.9 $\pm$ 0.7	3.1 $\pm$ 0.2	6.2 $\pm$ 0.3
	Rec	3	0.34 $\pm$ 0.12	7.7 $\pm$ 0.3	15.5 $\pm$ 0.6	2.9 $\pm$ 0.1	6.2 $\pm$ 0.1

<sup>1</sup>  $n = 2$

Production rates of POC and Chl *a* were not significantly influenced by the long-term exposure to high temperature (LMM, POC:  $\chi^2(3) = 6.76$ ,  $p = 0.080$ ; Chl *a*:  $\chi^2(3) = 3.88$ ,  $p = 0.274$ ; Table 3+4). During the MHWs, POC production slightly increased in MHW1 (post hoc tests,  $t = -2.33$ ,  $p = 0.376$ ), but not in MHW2 cultures (post hoc tests,  $t = -0.45$ ,  $p = 0.999$ ). At the end of the recovery period, production rates of MHW1 cultures only declined slightly, while values for MHW2 decreased even below 3 °C control values (post hoc tests, MHW1:  $t = 34$ ,  $p = 0.113$ ; MHW2:  $t = 4.59$ ,  $p = 0.029$ ; Fig. 16C). Chl *a* production also slightly increased during MHW1 (post hoc tests,  $t = -2.73$ ,  $p = 0.297$ ) and MHW2 (post hoc tests,  $t = -2.61$ ,  $p = 0.350$ ) and significantly decreased after 5 days of recovery at 3 °C (post hoc tests, MHW1:  $t = 4.45$ ,  $p = 0.016$ ; MHW2:  $t = 7.32$ ,  $p < 0.001$ ; Fig. 16D).

**Table 4.** Chl *a* production, cellular Chl *a* quota and Chl *a*:POC ratio of *Phaeocystis pouchetii* during the different temperature treatments (n = 3; mean ± SD). Data for 3 and 6 °C control cultures are shown as mean values for the whole incubation period. Data for the short (MHW1) and long marine heatwave treatments (MHW2) are displayed for the end of the MHW (MHW) and the recovery period (Rec). In the recovery period of MHW1, values are based on n = 2 (<sup>1</sup>).

Treatment	Timepoint	Temperature (°C)	Chl <i>a</i> production (pg cell <sup>-1</sup> d <sup>-1</sup> )	Chl <i>a</i> quota (pg cell <sup>-1</sup> )	Chl <i>a</i> :POC
3 °C control	-	3	0.21 ± 0.02	0.37 ± 0.03	0.022 ± 0.002
6 °C control	-	6	0.20 ± 0.02	0.41 ± 0.03	0.021 ± 0.002
MHW1	MHW	6	0.24 ± 0.01	0.42 ± 0.01	0.022 ± 0.001
	Rec	3	0.18 ± 0.01 <sup>1</sup>	0.33 ± 0.02 <sup>1</sup>	0.020 ± 0.001 <sup>1</sup>
MHW2	MHW	6	0.24 ± 0.01	0.41 ± 0.01	0.024 ± 0.001
	Rec	3	0.16 ± 0.01	0.32 ± 0.01	0.020 ± 0.001

<sup>1</sup> n = 2

### 3.4. Photophysiological response

During the experiment, the water jacket pump of the FRRF stopped working for a few days. Even though the FRRF was located in the 2 °C culture room, this failure of the water jacket pump hindered the temperature regulation in the cuvette and a heat build-up in the sample during measurements cannot be ruled out. This technical error concerned measurements of MHW1 cultures at timepoint ‘Rec2’, MHW2 cultures at timepoint ‘Rec1’ and 3 and 6 °C control cultures at the final timepoint. Consequently, FRRF data of the mentioned timepoints were excluded from statistical analysis. Data of the non-photochemical quenching parameters were only assessed at two timepoints during the experiment for 3 and 6 °C control cultures. Due to the failure of the water jacket pump on one of these timepoints, mean NPQ values are only based on the measurement at one timepoint (n = 3).

Cultures acclimated to 3 and 6 °C showed only minor differences in the dark-acclimated quantum yield efficiency of PSII ( $F_v/F_m$ ; LMM,  $\chi^2(1) = 1.04$ ,  $p = 0.307$ ; Fig. 17), with an average value of  $0.54 \pm 0.01$  for the 3 °C and  $0.52 \pm 0.00$  for the 6 °C cultures (Table 5). rETR,  $\rho$  and  $\sigma_{PII}$  all showed significantly elevated values under 6 °C compared to 3 °C (LMM, rETR:  $\chi^2(1) = 6.14$ ,  $p = 0.013$ ;  $\rho$ :  $\chi^2(1) = 14.48$ ,  $p < 0.001$ ;  $\sigma_{PII}$ :  $\chi^2(1) = 8.13$ ,  $p = 0.004$ ; Table 5). The time constant for PSII re-oxidation in the dark ( $\tau$ ) showed an opposing trend, with a significantly decreased value under elevated temperature (LMM,  $\chi^2(1) = 19.97$ ,  $p < 0.001$ ; Fig. 18G+H; Table 5). Regulated ( $Y(NPQ)$ ) and nonregulated non-photochemical quenching ( $Y(NO)$ ) were not affected by the long-term exposure to 6 °C compared to 3 °C (t-test,  $Y(NPQ)$ :  $t(2) = -1.05$ ,  $p = 0.401$ ;  $Y(NO)$ :  $t(2) = 1.06$ ,  $p = 0.396$ ; Table 5).

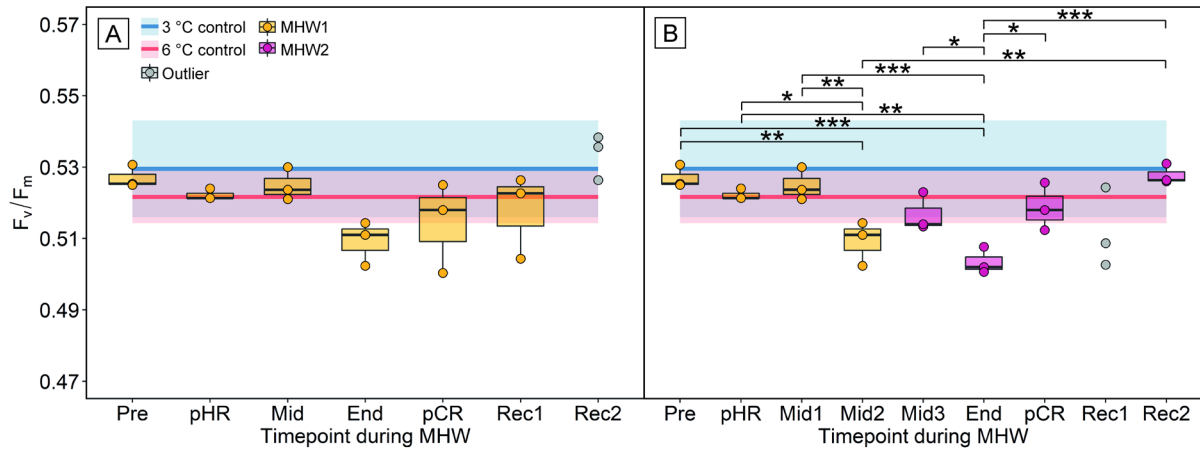


**Figure 17.** FRR fluorometrical measurement of PSII quantum yield efficiency  $F_v/F_m$  in *Phaeocystis pouchetii* during the 3 °C control (blue), 6 °C control (red) and the (A) MHW1 and (B) MHW2 treatments ( $n = 3$ ; mean  $\pm$  SD). Timepoints Rec2 of MHW1 and Rec1 of MHW2 were eliminated from statistical analysis due to an instrumental failure (grey dots). Statistical significance between the different timepoints revealed by post hoc tests is expressed in asterisks (\*:  $p \leq 0.05$ , \*\*:  $p \leq 0.01$ , \*\*\*:  $p \leq 0.001$ ). Abbreviations: Pre = pre-MHW, pHR = post heating ramp, Mid = during MHW, End = end of MHW, pCR = post cooling ramp, Rec = recovery.

In contrast to the constant exposure to 6 °C, the MHWs had an effect on  $F_v/F_m$  values (LMM, MHW1:  $\chi^2(5) = 11.84$ ,  $p = 0.037$ ; MHW2:  $\chi^2(7) = 42.85$ ,  $p < 0.001$ ; Fig. 17). While  $F_v/F_m$  decreased only slightly towards the end of MHW1, (post hoc tests,  $t = -2.52$ ,  $p = 0.205$ ), this trend was even more pronounced at the end of MHW2 (post hoc tests,  $t = -5.38$ ,  $p = 0.002$ ; Table 5). After the cooling ramp and during recovery, values approached the 3 °C baseline again in both MHWs treatments. The sudden increase in  $F_v/F_m$  directly after the cooling ramp was significant for MHW2 (post hoc tests,  $t = -4.36$ ,  $p = 0.011$ ; Fig. 17B), but not for MHW1 (post hoc tests,  $t = -0.84$ ,  $p = 0.953$ ; Fig. 17A). Continuous recording of  $F_v/F_m$  during the heating and cooling ramp revealed only minor changes, with an increasing trend with warming and a decreasing trend during cooling (data not shown). Directly after cell cultures experienced the abrupt temperature increase from 3 to 6 °C, there was a significant jump in rETR (post hoc tests,  $t = 5.11$ ,  $p = 0.004$ ; Fig. 18A), connectivity  $\rho$  (post hoc tests,  $t = 5.34$ ,  $p = 0.003$ ; Fig. 18C) and  $\sigma_{PII}$  (post hoc tests,  $t = 8.54$ ,  $p < 0.001$ ; Fig. 18E), while  $\tau$  decreased clearly with warming (post hoc tests,  $t = -19.09$ ,  $p < 0.001$ ; Fig. 18G). rETR and  $\rho$  remained around similar values than the 6 °C control for at least 2 days, but showed a significant decline after 6 days of exposure to the MHW (post hoc tests, rETR:  $t = -4.98$ ,  $p = 0.005$ ;  $\rho$ :  $t = -6.06$ ,  $p = 0.001$ ). After 5 days of recovery,  $\rho$  values returned to the 3 °C control, while rETR increased significantly again (post hoc tests,  $t = -10.75$ ,  $p < 0.001$ ; Table 5).  $\sigma_{PII}$  remained high during the exposure to the MHWs and decreased slightly with the cooling of the cultures back to 3 °C (post hoc tests, MHW1:  $t =$

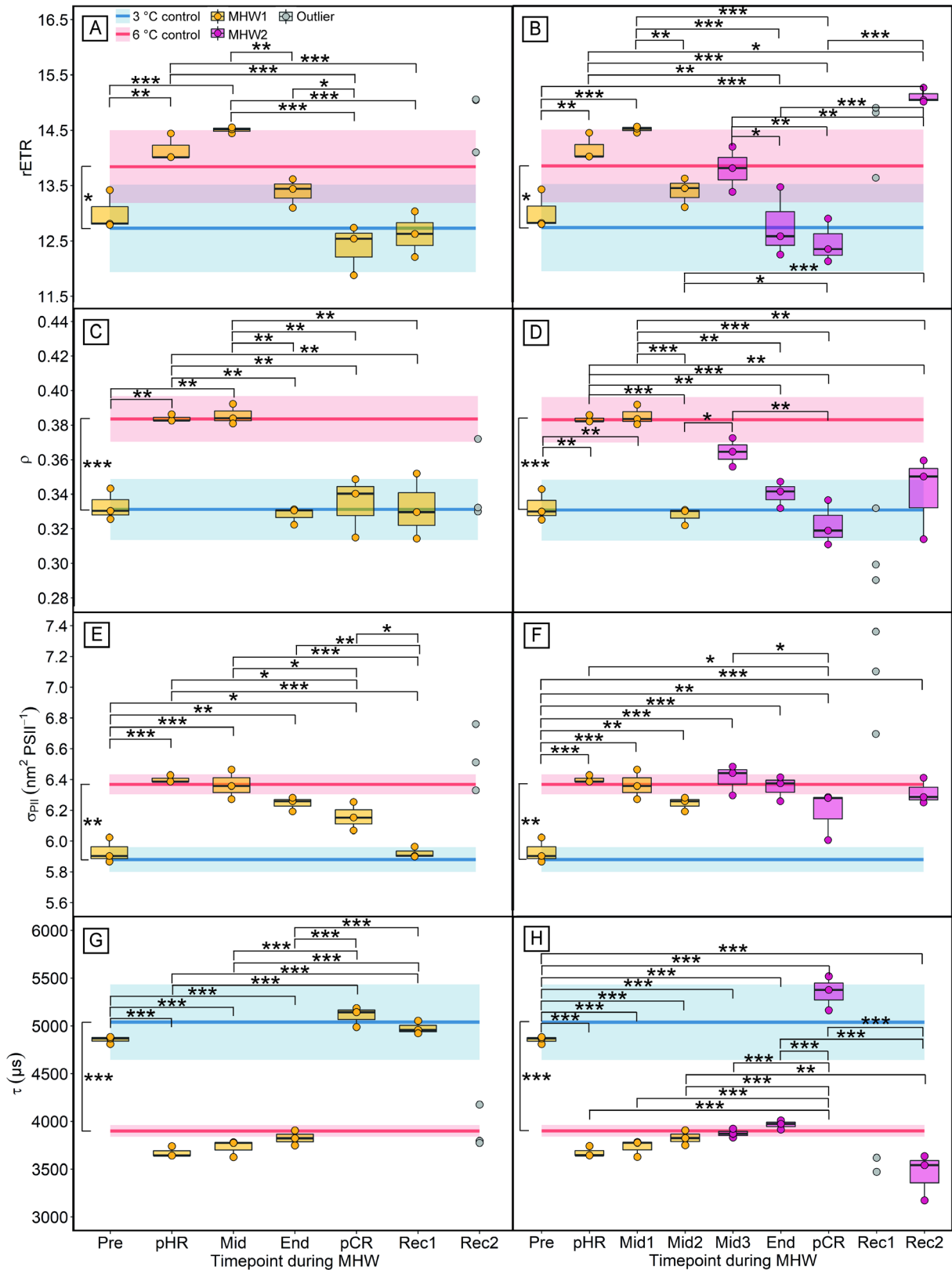


**Figure 18.** Temporal changes of relative electron transport rate (rETR; **A, B**), connectivity ( $\rho$ ; **C, D**), absorption cross-section of photosystem II ( $\sigma_{\text{PII}}$ ; **E, F**) and reopening rate of PSII ( $\tau$ ; **G, H**) in *Phaeocystis pouchetii* cells exposed to MHW1 (left panel) and MHW2 (right panel) treatments. Timepoints Rec2 of MHW1 and Rec1 of MHW2 were eliminated from statistical analysis due to an instrumental failure (grey dots). Mean (solid line)  $\pm$  SD (shaded area) of parameters are indicated as baselines on the plots for the 3 °C control (blue) and 6 °C control (red). Statistical significance between the different timepoints revealed by post hoc tests is expressed in asterisks (\*:  $p \leq 0.05$ , \*\*:  $p \leq 0.01$ , \*\*\*:  $p \leq 0.001$ ). Abbreviations: Pre = pre-MHW, pHR = post heating ramp, Mid = during MHW, End = end of MHW, pCR = post cooling ramp, Rec = recovery.

1.56,  $p = 0.639$ ; MHW2:  $t = 2.75$ ,  $p = 0.185$ ; Fig. 18E+F). Values reached the 3 °C-baseline after 2 days of recovery, but increased again after 5 days of recovery. This rise in  $\sigma_{\text{PSII}}$  was also visible in MHW2 cultures after a recovery period of 5 days (Fig. 18F). However, the significance of this increase could not be tested statistically, because timepoint Rec2 is excluded from MHW1 and Rec1 from MHW2 data for the reasons elaborated on above.  $\tau$  values remained low during the complete exposure to both MHWs, but showed a sudden increase during the cooling ramp (post hoc tests, MHW1:  $t = -20.72$ ,  $p < 0.001$ ; MHW2:  $t = -16.57$ ,  $p < 0.001$ ; Fig. 18G+H). After 5 days of recovery  $\tau$  experienced a decline again (post hoc tests,  $t = 22.74$ ,  $p < 0.001$ ).

**Table 5.** PSII photochemistry measurements of PSII quantum yield efficiency  $F_v/F_m$ , connectivity ( $\rho$ ), functional absorption cross section ( $\sigma_{\text{PSII}}$ ), PSII re-opening rate ( $\tau$ ), relative electron transfer rates through PSII (rETR) and the quantum yield of regulated (Y(NPQ)) and nonregulated non-photochemical energy loss in PSII (Y(NO)) in *Phaeocystis pouchetii* under the different temperature treatments ( $n = 3$ ; mean  $\pm$  SD). Data for 3 and 6 °C control cultures are shown as mean values for the whole incubation period. Data for the short (MHW1) and long marine heatwave treatments (MHW2) are separately displayed for the different timepoints prior, during and after the MHW. Abbreviations: Pre = pre-MHW, pHR = post heating ramp, Mid = during MHW, End = end of MHW, pCR = post cooling ramp, Rec = recovery.

Treatment	Time-point	Temp. (°C)	$F_v/F_m$	$\rho$	$\sigma_{\text{PSII}}$ (nm <sup>2</sup> PSII <sup>-1</sup> )	$\tau$ ( $\mu$ s)	rETR	Y(NPQ)	Y(NO)
3 °C control	-	3	0.53 $\pm$ 0.01	0.33 $\pm$ 0.02	5.88 $\pm$ 0.08	5039 $\pm$ 395	12.7 $\pm$ 0.8	0.13 $\pm$ 0.08 <sup>2</sup>	0.82 $\pm$ 0.08 <sup>2</sup>
6 °C control	-	6	0.52 $\pm$ 0.01	0.38 $\pm$ 0.01	6.37 $\pm$ 0.06	3900 $\pm$ 62	13.8 $\pm$ 0.7	0.14 $\pm$ 0.03 <sup>2</sup>	0.81 $\pm$ 0.03 <sup>2</sup>
MHW1	Pre	3	0.53 $\pm$ 0.00	0.33 $\pm$ 0.01	5.93 $\pm$ 0.08	4855 $\pm$ 40	13.0 $\pm$ 0.4	0.10 $\pm$ 0.05	0.86 $\pm$ 0.05
	pHR	6	0.52 $\pm$ 0.00	0.38 $\pm$ 0.00	6.40 $\pm$ 0.02	3675 $\pm$ 57	14.2 $\pm$ 0.2	0.16 $\pm$ 0.04	0.79 $\pm$ 0.04
	Mid	6	0.53 $\pm$ 0.01	0.39 $\pm$ 0.01	6.37 $\pm$ 0.10	3728 $\pm$ 89	14.5 $\pm$ 0.1	0.18 $\pm$ 0.04	0.77 $\pm$ 0.04
	End	6	0.51 $\pm$ 0.01	0.33 $\pm$ 0.01	6.25 $\pm$ 0.05	3826 $\pm$ 78	13.4 $\pm$ 0.3	0.19 $\pm$ 0.02	0.75 $\pm$ 0.02
	pCR	3	0.51 $\pm$ 0.01	0.34 $\pm$ 0.02	6.16 $\pm$ 0.02	5107 $\pm$ 105	12.4 $\pm$ 0.4	0.17 $\pm$ 0.04	0.79 $\pm$ 0.04
	Rec1	3	0.52 $\pm$ 0.01	0.33 $\pm$ 0.02	5.92 $\pm$ 0.04	4978 $\pm$ 69	12.6 $\pm$ 0.4	0.19 $\pm$ 0.01	0.76 $\pm$ 0.02
	Rec2	3	NA	NA	NA	NA	NA	NA	NA
MHW2	Pre	3	0.53 $\pm$ 0.00	0.33 $\pm$ 0.01	5.93 $\pm$ 0.08	4855 $\pm$ 40	13.0 $\pm$ 0.4	0.10 $\pm$ 0.05	0.86 $\pm$ 0.05
	pHR	6	0.52 $\pm$ 0.00	0.38 $\pm$ 0.00	6.40 $\pm$ 0.02	3675 $\pm$ 57	14.2 $\pm$ 0.2	0.16 $\pm$ 0.04	0.79 $\pm$ 0.04
	Mid1	6	0.53 $\pm$ 0.01	0.39 $\pm$ 0.01	6.37 $\pm$ 0.10	3728 $\pm$ 89	14.5 $\pm$ 0.1	0.18 $\pm$ 0.04	0.77 $\pm$ 0.04
	Mid2	6	0.51 $\pm$ 0.01	0.33 $\pm$ 0.01	6.25 $\pm$ 0.05	3826 $\pm$ 78	13.4 $\pm$ 0.3	0.19 $\pm$ 0.02	0.75 $\pm$ 0.02
	Mid3	6	0.52 $\pm$ 0.01	0.37 $\pm$ 0.01	6.41 $\pm$ 0.10	3874 $\pm$ 46	13.8 $\pm$ 0.4	0.18 $\pm$ 0.03	0.77 $\pm$ 0.03
	End	6	0.50 $\pm$ 0.00	0.34 $\pm$ 0.01	6.35 $\pm$ 0.08	3966 $\pm$ 48	12.8 $\pm$ 0.6	0.19 $\pm$ 0.02	0.76 $\pm$ 0.02
	pCR	3	0.52 $\pm$ 0.01	0.32 $\pm$ 0.01	6.19 $\pm$ 0.16	5356 $\pm$ 179	12.5 $\pm$ 0.4	0.13 $\pm$ 0.04	0.83 $\pm$ 0.03
	Rec1	3	NA	NA	NA	NA	NA	NA	NA
	Rec2	3	0.53 $\pm$ 0.00	0.34 $\pm$ 0.02	6.32 $\pm$ 0.09	3448 $\pm$ 246	15.1 $\pm$ 0.1	0.19 $\pm$ 0.01	0.72 $\pm$ 0.02

<sup>2</sup> Data collection at one timepoint instead of three.

NA Data excluded from statistical analysis.

The exposure to MHWs also had a significant effect on the capacity of *P. pouchetii* for non-photochemical quenching (LMM, MHW1: Y(NPQ):  $\chi^2(5) = 18.23$ ,  $p = 0.003$ , Y(NO):  $\chi^2(5) = 19.38$ ,  $p = 0.002$ ; MHW2: Y(NPQ):  $\chi^2(7) = 34.07$ ,  $p < 0.001$ , Y(NO):  $\chi^2(7) = 43.99$ ,  $p < 0.001$ ; Fig. 19). Regulated Y(NPQ) increased with warming and remained high until the end of the

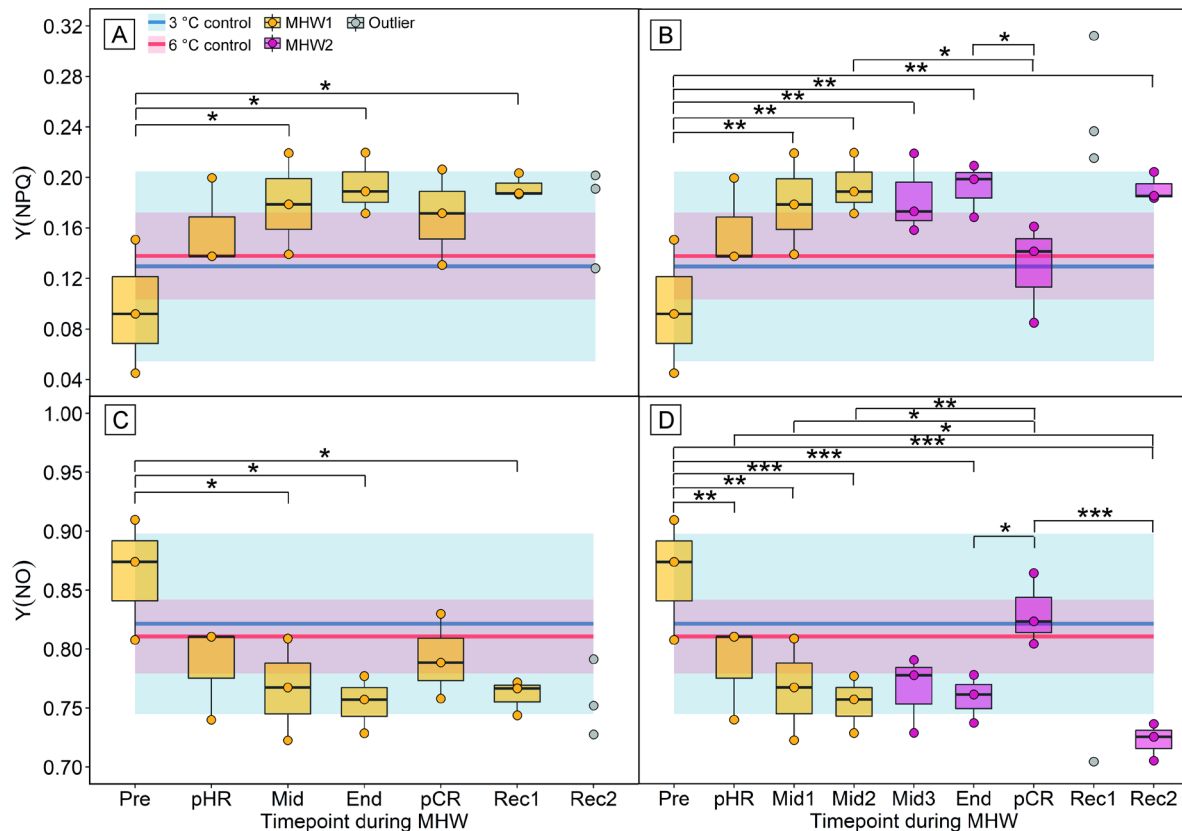


**Figure 19.** Capacity for non-photochemical quenching of *Phaeocystis pouchetii* under the different temperature treatments. Quantum yield of regulated ( $Y(NPQ)$ ) and nonregulated non-photochemical energy loss in PS II ( $Y(NO)$ ) in MHW1 (yellow; **A, C**) and MHW2 treatments (violet; **B, D**) are separately displayed for the different timepoints prior, during and after the MHW. Timepoints Rec2 of MHW1 and Rec1 of MHW2 are eliminated from statistical analysis due to an instrumental failure (grey dots). Mean (solid line)  $\pm$  SD (shaded area) of parameters are indicated as baselines on the plots for the 3 °C control (blue) and 6 °C control cultures (red). Statistical significance between the different timepoints revealed by post hoc tests is expressed in asterisks (\*:  $p \leq 0.05$ , \*\*:  $p \leq 0.01$ , \*\*\*:  $p \leq 0.001$ ). Abbreviations: Pre = pre-MHW, pHR = post heating ramp, Mid = during MHW, End = end of MHW, pCR = post cooling ramp, Rec = recovery.

MHW (post hoc tests, MHW1:  $t = 4.13$ ,  $p = 0.018$  MHW2:  $t = 5.45$ ,  $p = 0.002$ ). Non-regulated  $Y(NO)$  showed an opposing trend, with decreasing values during the MHW exposure (post hoc tests, MHW1:  $t = -4.42$ ,  $p = 0.012$  MHW2:  $t = -6.17$ ,  $p < 0.001$ ). With the sudden cooling from 6 to 3 °C after the MHW,  $Y(NPQ)$  started to decrease and  $Y(NO)$  started to increase (post hoc tests,  $Y(NPQ)$ :  $t = 1.01$ ,  $p = 0.904$ ;  $Y(NO)$ :  $t = -1.53$ ,  $p = 0.658$ ; Fig. 19). This trend was clearly more pronounced in MHW2 cultures (post hoc tests,  $Y(NPQ)$ :  $t = 3.57$ ,  $p = 0.047$ ;  $Y(NO)$ :  $t = -4.22$ ,  $p = 0.014$ ). During the recovery, however, this trend did not continue and  $Y(NPQ)$  remained significantly higher (post hoc tests, MHW1:  $t = -4.09$ ,  $p = 0.020$ , MHW2:  $t = -5.40$ ,  $p = 0.002$ ) and  $Y(NO)$  significantly lower than pre-MHW values (post hoc tests, MHW1:  $t = 4.16$ ,  $p = 0.018$ ; MHW2:  $t = 8.31$ ,  $p < 0.001$ ).

### 3.5. Intracellular levels of reactive oxygen species

*P. pouchetii* cells experiencing long-term exposure to 6 °C showed a significant increase in intracellular hydrogen peroxide levels by 18 % (LMM,  $\chi^2(1)= 6.99$ ,  $p = 0.008$ ), but not in superoxide anion levels (LMM,  $\chi^2(1)= 0.15$ ,  $p = 0.699$ ). Temperature fluctuations during the course of the MHW treatments resulted in a significant change in H<sub>2</sub>O<sub>2</sub> (LMM, MHW1:  $\chi^2(6)= 42.60$ ,  $p < 0.001$ ; MHW2:  $\chi^2(7)= 46.32$ ,  $p < 0.001$ ; Fig. 20A+B) and O<sub>2</sub><sup>-</sup> concentrations (LMM, MHW1:  $\chi^2(6)= 23.59$ ; MHW2:  $\chi^2(7)= 49.40$ ,  $p < 0.001$ ; Fig. 20C+D). For both reactive oxygen species, intracellular levels did not change directly with the abrupt temperature rise, but rather increased during the course of MHW1 until they reached a maximum after 6 days of heat exposure (post hoc tests, H<sub>2</sub>O<sub>2</sub>:  $t = -6.09$ ,  $p < 0.001$ ; O<sub>2</sub><sup>-</sup>:  $t = -3.09$ ,  $p = 0.098$ ). O<sub>2</sub><sup>-</sup> levels at this timepoint were ~ 55 % and those of H<sub>2</sub>O<sub>2</sub> ~ 93 % higher than the average ROS level of the 3 °C

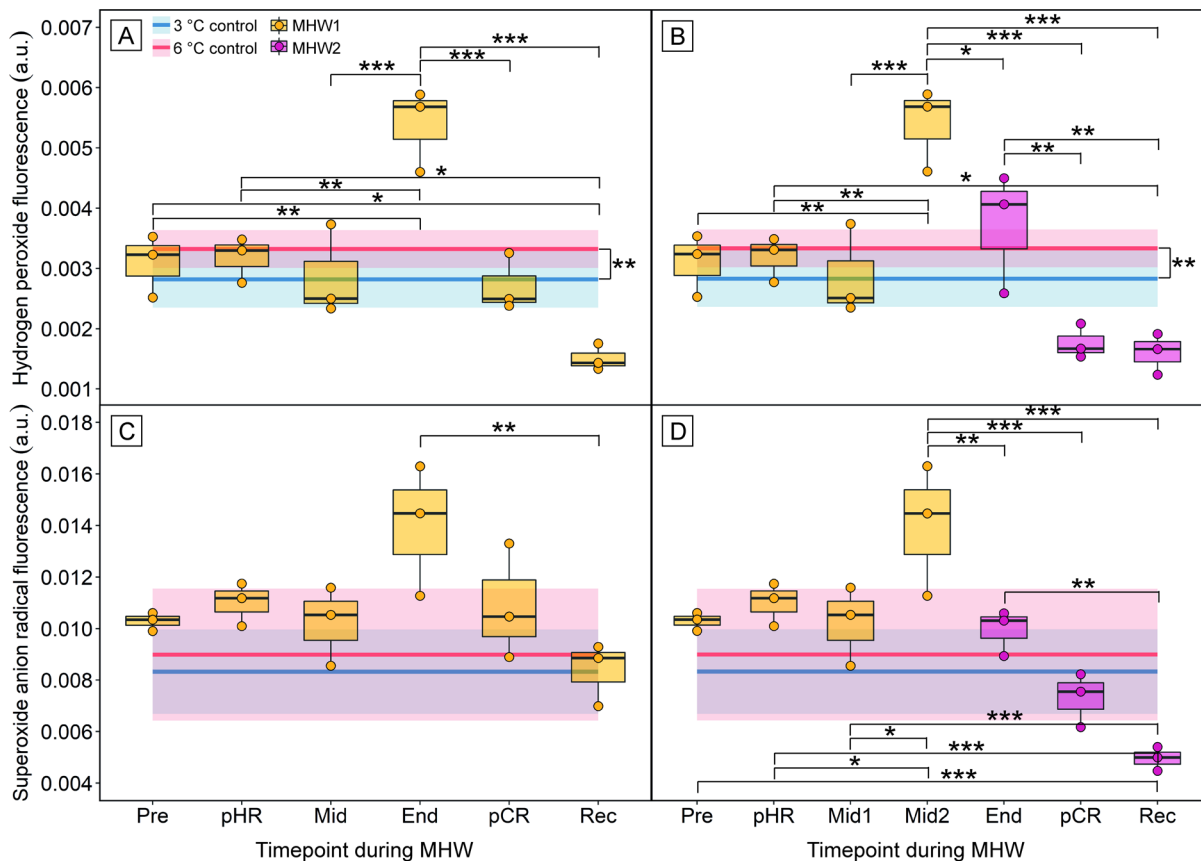


**Figure 20.** Intracellular levels of reactive oxygen species in *Phaeocystis pouchetii* under the different temperature treatments. Relative fluorescence of hydrogen peroxide (A, B) and superoxide anion radical (C, D) in MHW1 (yellow) and MHW2 cultures (violet) are separately displayed for the different timepoints prior, during and after the MHW. Mean (solid line)  $\pm$  SD (shaded area) of the 3 °C control (blue) and 6 °C control cultures (red) are indicated as baselines on the plots. Statistical significance between the different timepoints revealed by post hoc tests is expressed in asterisks (\*:  $p \leq 0.05$ , \*\*:  $p \leq 0.01$ , \*\*\*:  $p \leq 0.001$ ). Abbreviations: Pre = pre-MHW, pHR = post heating ramp, Mid = during MHW, End = end of MHW, pCR = post cooling ramp, Rec = recovery.

control. Cells that experienced an extended MHW of 10 days (MHW2), exhibited a gradual but significant decrease in intracellular ROS levels after the maximum on day 6 (post hoc tests,  $\text{H}_2\text{O}_2$ :  $t = 3.92$ ,  $p = 0.025$ ;  $\text{O}_2^{\cdot-}$ :  $t = 4.52$ ,  $p = 0.008$ ). The sudden temperature decline from 6 to 3 °C caused  $\text{H}_2\text{O}_2$  levels to drop clearly (post hoc tests, MHW1:  $t = 6.44$ ,  $p < 0.001$ ; MHW2:  $t = 4.56$ ,  $p = 0.007$ ), while  $\text{O}_2^{\cdot-}$  levels decreased only slightly (post hoc tests, MHW1:  $t = 2.55$ ,  $p = 0.224$ ; MHW2:  $t = 2.92$ ,  $p = 0.142$ ). After 5 days of recovery, both ROS decreased below pre-MHW values for the MHW1 (post hoc tests,  $\text{H}_2\text{O}_2$ :  $t = -3.81$ ,  $p = 0.030$ ;  $\text{O}_2^{\cdot-}$ :  $t = -1.56$ ,  $p = 0.710$ ) as well as the MHW2 treatment (post hoc tests,  $\text{H}_2\text{O}_2$ :  $t = -3.50$ ,  $p = 0.053$ ;  $\text{O}_2^{\cdot-}$ :  $t = -5.92$ ,  $p < 0.001$ ).

## 4. Discussion

Exposure of *Phaeocystis pouchetii* to MHW scenarios revealed surprisingly minor, but nevertheless important physiological responses, that include short-term stimulation of growth rates, altered Chl *a* concentrations and a rapid photoprotective capacity as well as high thresholds for oxidative stress. For the discussion of the results, it is important to consider the different timescales of these responses. A distinction must be made between the acute response to immediate exposure to temperature changes (heating/cooling ramps, see section 4.1. and 4.6.) and the long-term response to continued heat exposure (MHW1, MHW2 and 6 °C control, see section 4.2.-4.5.). On short timescales, physiology is mainly shaped by the instant effect of temperature on enzyme kinetics and diffusion processes. Over longer timescales of several days to weeks, physiological adjustments via acclimation increasingly play a role. By comparing the MHW treatments with the later timepoints of the 6 °C controls, the non-acclimated vs the acclimated response can be compared.

### 4.1. Acute response to rapidly increasing temperature

Growth rates more than tripled upon heat exposure from  $0.19 \pm 0.03 \text{ d}^{-1}$  to  $0.65 \pm 0.16 \text{ d}^{-1}$  within just one day (Fig. 15C), indicating a high physiological plasticity towards fast warming. This stimulation is accompanied by increased light harvest efficiency instantly after the temperature ramp (1-2 h) as evidenced through higher relative PSII electron transfer rate rETR (Fig. 18A) and absorption cross-section  $\sigma_{\text{PII}}$  (Fig 18E). The increased  $\sigma_{\text{PII}}$  implies a larger antenna size resulting in more excitation energy to be transferred to the PSII reaction centres (Falkowski and Raven, 2007). The steep rise in rETR corresponds to a  $Q_{10}$  value of 3.6, which might be an effect of the increased fluidity of the thylakoid membrane at elevated temperatures (Falkowski and Raven, 2007). Increased membrane fluidity facilitates the diffusion of electron carriers like plastoquinone and plastocyanin between PSII and PSI (Yamori *et al.*, 2008), thereby enhancing the rate of electron transfer. Furthermore, the reopening rate of PSII  $\tau$  decreased directly following the temperature ramp (Fig. 18G), which is a proxy for the rate at which downstream processes can remove electrons from PSII (Kolber *et al.*, 1998). The increased rETR and decreased  $\tau$  imply that more absorbed light energy reached PSII reaction centres and these were re-opening at a faster rate, because of a quicker drainage of electrons away from PSII by the plastoquinone pool. Enhanced C-fixation might contribute to the drainage of electrons, because the increase in temperature accelerates also reaction rates of enzymes, resulting in the

stimulation of the Calvin cycle (Raven and Geider, 1988). The resulting surplus of available energy but also reductant and carbon seems to be initially allocated into growth and cell division within the first day following temperature elevation. This is evidenced by the overshoot of growth rates that were observed in the MHW cultures on the day following the temperature rise.

The transition into the heatwave was monitored by FRRF measurements. Comparing  $F_v/F_m$  values shortly before and after the immediate temperature rise from 3 to 6 °C did not reveal significant changes of the photosynthetic capacity in *P. pouchetii* (Fig. 17). Hence, the applied temperature shift neither improved, nor damaged PSII reaction centres or provoked heat-stress in the short-term. This finding is surprising, because a change in temperature can cause a mismatch between energy absorption and consumption. The underlying reason for this assumption is that photosynthetic reactions associated with the thylakoid membranes and enzymes are temperature-dependent, while this is not the case for light absorption and excitation energy transfer (Falkowski and Raven, 2007; Raven and Geider, 1988). *P. pouchetii* seems to adjust to this potential mismatch in the short-term by enhancing light harvesting capacity as indicated by increased connectivity  $\rho$  of reaction centres (Fig 18C). A higher fraction of reaction centres are energetically connected and can re-distribute shared excitons, which migrate from closed to open reaction centres (Blankenship, 2014). The increased  $\rho$  may therefore help to channel energy into electron transport, which consequently builds up a proton gradient ( $\Delta pH$ ) that drives ATP synthesis and contributes to the stimulation of growth rates.

#### 4.2. Warming triggers accumulation of reactive oxygen species

Following the sudden growth stimulation after the temperature rise, growth rates already started to decline again 2 days later and approached values observed prior to the MHW (Fig. 15C). Even though ATP and carbohydrate production of cells is often accelerated under higher temperature, there is usually also an increase in energy demand (Raven and Geider, 1988). A possible cause, which may prevent *P. pouchetii* to maintain enhanced growth rates over several generations could be the accumulation of reactive oxygen species (ROS) and increases in cellular damage associated with more rapid reproduction (Collins, 2016). The ROS measurements performed in this study revealed that exposure to MHWs increased intracellular  $O_2^{\cdot -}$  levels by ~ 55 % and those of  $H_2O_2$  by ~ 93 % by the end of MHW1 (after 6 days) compared to the mean ROS levels in the 3 °C controls (Fig. 20). Such an increase in ROS production associated with elevated temperatures have also been observed in numerous other studies on

microalgae (Chokshi *et al.*, 2015; Chokshi *et al.*, 2020; Hu *et al.*, 2021; Murik *et al.*, 2019; Yakovleva *et al.*, 2009).  $\text{H}_2\text{O}_2$  levels increased almost twice as much as  $\text{O}_2^{\cdot-}$  levels, which could have either resulted from the incomplete oxidation of water at PSII (Pospíšil, 2009) or the transformation of generated  $\text{O}_2^{\cdot-}$  to  $\text{H}_2\text{O}_2$ . Most of the ROS in chloroplasts is produced at the site of PSI (Pospíšil, 2009), for example through the Mehler reaction, which reduces  $\text{O}_2$  to  $\text{O}_2^{\cdot-}$  (Mehler, 1951).  $\text{O}_2^{\cdot-}$  is very short-lived (sec–min) and might have dissociated spontaneously to  $\text{H}_2\text{O}_2$  (Marklund, 1976), or this reaction was catalysed by the antioxidant enzyme superoxide dismutase SOD (McCord and Fridovich, 1969), both leading to significantly higher  $\text{H}_2\text{O}_2$  levels. When cells divide, the daughter cells can inherit such high ROS levels and also the associated parental damage. A reallocation of energy from growth to repair processes or detoxification could result in a shift from producing many damaged offspring to producing less daughter cells of higher viability, as was shown in experiments by Lindberg and Collins (2020). Hence, accelerated metabolic rates and thus cell division rates entail a trade-off between high productivity and oxidative stress (Dowling and Simmons, 2009; Monaghan *et al.*, 2009).

The accumulation of ROS suggest that an increase of temperature by 3 °C caused an imbalance between the production and suppression of ROS in *P. pouchetii* cells. Assuming that enzymatic reactions of the dark reactions are stimulated more strongly with elevated temperatures than the light harvesting and electron transport of the light reactions, one could have expected the photosynthetic electron chain in a less reduced state. However, the results suggest the opposite, i.e. a higher stimulation of photosynthetic electron transport than  $\text{CO}_2$  fixation, which transfers the photosynthetic electron transport chain in a highly reduced state and increases the risk of ROS production (Allahverdiyeva *et al.*, 2005; Grieco *et al.*, 2012). Moreover, ROS production could also simply be scaled with the rate of electron transport. As a consequence, since the exposure to the MHW caused intensified electron traffic, cells might experience more oxidative stress. Furthermore,  $\text{O}_2^{\cdot-}$  and  $\text{H}_2\text{O}_2$  production can also be derived from respiratory instead of photosynthetic processes (Dröse and Brandt, 2012; Palenik *et al.*, 1987; Twiner and Trick, 2000). An accelerated electron transport chain in the mitochondria as a response to temperature rise may result in a high proton motive force that could potentially increase the probability of ROS formation (Collins *et al.*, 2012; Korshunov *et al.*, 1997).

### 4.3. MHWs reduce photosynthetic efficiency

Apart from the significant increase of intracellular ROS levels and changes of photophysiological parameters during MHW1, the elemental composition and pigmentation of *P. pouchetii* cells were only marginally affected (Fig. 16). Observed trends are discussed in the following, but because these effects were statistically not significant, weighting of these results has to be done with care.

In contrast to the acute response to warming, extended exposure to 6 °C resulted in a lower quantum yield of electron transport through PSII, as indicated by the trend of declining  $F_v/F_m$  values towards the end of MHW1 (Fig. 17A). However, increased POC production rates (Fig. 16C) as well as lowered  $\tau$  at the end of MHW1 (Fig. 18G) both point to higher rates of C-fixation. This is likely caused by the acceleration of catalytic rates of enzymes at higher temperature, including RuBisCO in the Calvin cycle (Galmés *et al.*, 2015). The higher production rates are mainly reflected in higher POC quota (Fig. 18A), while growth rates remained constant over the duration of the MHW. The required higher energy demand for biomass accumulation appear to result from optimized light harvesting through enhanced pigment abundance of the photosynthetic unit. Cultures exposed to the MHWs exhibited slightly higher Chl *a* quota compared to the control cultures growing at 3 °C (Fig. 16E). Rising Chl *a* content with increasing temperature was also observed in the diatoms *Chaetoceros calcitrans* (Anning *et al.*, 2001), *Thalassiosira pseudonana* (Stramski *et al.*, 2002) and *Phaeodactylum tricornutum* (Feijão *et al.*, 2018). This upregulation of pigment content may partly contribute to the rebalancing of the light and dark reactions of photosynthesis by providing more ATP and NADPH for C-fixation (Kana *et al.*, 1997).

However, Chl *a*:POC ratios increased under exposure to MHW1 in comparison to cultures merely experiencing a temperature of 3 °C (Fig. 16F). This indicates a reduced photosynthetic efficiency, because more Chl *a* was needed for the same biomass build-up, i.e. a relatively higher cost of energy input. These results are in accordance with the study of Feijão *et al.* (2018), who exposed *Phaeodactylum tricornutum* to heatwaves and discovered a less efficient PSII. A higher Chl *a*:POC ratio, only marginally higher POC quota and unaltered growth rates during the exposure to the MHW (Fig. 15C+D), may also imply that the additional ATP and NADPH generated through enhanced light harvesting and electron transport was not allocated one-to-one to the Calvin cycle, but a fraction was likely required for other cellular processes. These include cell maintenance and repair through selective degradation and new synthesis of damaged proteins, but also the detoxification of ROS. The latter was likely triggered during

MHW1, when a prominent increase of intracellular ROS levels were observed (see section 4.2; Fig. 20A+C). As a consequence, oxidative damage can be induced in cells by oxidizing membrane lipids and causing the denaturing of nucleic acids and proteins (Lesser, 2006; Sharma *et al.*, 2012). To prevent such deleterious effects, photosynthetic organisms evolved an array of scavenging and defence mechanisms (Asada, 1999, 2006; Noctor and Foyer, 1998; Rezayian *et al.*, 2019). These include the already mentioned SOD, but also other enzymatic antioxidants like catalase and ascorbate peroxidase (Asada, 2006; Rezayian *et al.*, 2019) and non-enzymatic scavengers like ascorbate and glutathione (Noctor and Foyer, 1998). Stimulated activity of SOD and catalase under higher temperature was for example observed in the diatom *Thalassiosira weissflogii* (Gao *et al.*, 2018). Furthermore, Antarctic microalga exposed to heat stress demonstrated increased activities of catalase, SOD, glutathione reductase, aldehyde dehydrogenase, and ascorbate peroxidase (Choi and Lee, 2012). However, the rise of  $O_2^{\cdot-}$  and  $H_2O_2$  levels during MHW1 imply, that such detoxification mechanisms were not sufficiently activated in *P. pouchetii* after 6 days.

Apart from inducing ROS scavenging systems, cells can also prevent harmful effects of ROS by reducing light harvesting. The slightly elevated Chl *a* content in MHW1 (Figure 16E), however, rather contributed to an increase in light harvesting, but may in turn also enable a higher energy availability for ROS detoxification. As a parallel adjustment to the rising Chl *a* content, Y(NPQ) values under high light significantly increased during the course of MHW1 and reached a maximum after 6 days of heat exposure (Fig. 19A). This upregulation of regulated NPQ is indicative for a high photoprotective capacity (Klughammer and Schreiber, 2008). *P. pouchetii* may compensate the vulnerability to photoinhibition under sudden high light exposure due to their more efficient harvesting system with a high capacity to dissipate surplus light energy and prevent the formation of ROS in the first place.

#### 4.4. Stress responses are enhanced during longer MHWs

It was hypothesized, that longer MHWs exert more thermal stress on cells than shorter ones. Even though the exposure to an extended MHW of 10 days (MHW2) did not have an effect on growth (Fig. 15D), the photosynthetic capacity of *P. pouchetii* was reduced compared to the shorter MHW of 6 days (MHW1). This trend of declining  $F_v/F_m$  values already started towards the end of MHW1, but progressed significantly during MHW2 (Fig. 17B). Hence, the longer MHW provoked more heat-stress than MHW1 by damaging PSII reaction centres. In addition, the photosynthetic efficiency, as represented by Chl *a*:POC values, was lowered in MHW2

cultures (Fig. 16F). Similar Chl *a* production rates for both MHW treatments indicate the same upregulation of light harvesting capacity of the photosynthetic units (Fig. 16D), but higher Chl *a*:POC ratio and lower POC production rates in MHW2 compared to MHW1 cultures (Fig. 16C+F) suggest that less of the absorbed energy was invested into C-fixation in MHW2 cultures.

Measurements of intracellular  $O_2^{\cdot-}$  and  $H_2O_2$  levels revealed, that after ROS accumulated during MHW1, they clearly declined with extended heat exposure during MHW2 (Fig. 20B+D). This is indicative for a lively activity of detoxifying mechanisms and may have been a potential energy sink explaining the reduced photosynthetic efficiency, as already described in section 4.3. Even though gene expression or activity of antioxidant enzymes were not investigated in this study, the significant decrease in cellular ROS concentration measured here is a clear indication for active defence mechanisms and that these take ~1 week to be fully activated. Another possible mechanism for the disposal of ROS, but which might have also contributed to the decreased cellular POC quota in MHW2 cultures in relation to the MHW1 cultures, is the water-water cycle or Mehler-ascorbate-peroxidase reaction. During this process,  $O_2^{\cdot-}$  generated at PSI by the Mehler reaction is converted to  $H_2O$  with an intermediate transformation step from  $O_2^{\cdot-}$  to  $H_2O_2$  (Asada, 1999). A pH gradient is generated and consequently ATP is synthesised, but no NADPH is produced. The operation of the water-water cycle therefore likely results in reduced NADPH production, which is essentially needed for C-fixation in the Calvin cycle. To draw further conclusions about the activity of the ROS scavenging system, more measurements of oxidative stress markers could be conducted like the redox state of the NAD(P)-pools (Schaefer *et al.*, 2019), as well as SOD activity and lipid peroxidation (Bischof *et al.*, 2006).

An explanation why POC quota were not enhanced at higher temperatures might also be that the Calvin cycle was already running at the maximum possible rate at the given light availability and the upregulation of Chl *a* reached the possible upper limit. Even though the photosynthetic electron transport is sensitive to temperature due to the diffusion of electron carriers and the dependency on membrane fluidity (Los *et al.*, 2013; Raven and Geider, 1988), photosynthesis is ultimately limited by how many photons are captured by light harvesting complexes. As a result, the stimulation of the Calvin cycle may be limited by insufficient supply with reductants generated in the light-dependent reactions of photosynthesis. Photorespiration could principally also play a role explaining a higher energy demand and lowered biomass build-up. Higher temperatures do not only accelerate the rate of RuBisCO (Galmés *et al.*, 2015), but they also

decrease its affinity for CO<sub>2</sub> (Jordan and Ogren, 1984; Young *et al.*, 2015). Hence, under higher temperature increased oxygenase activity of RuBisCO could lead to decreased C-fixation and increased photorespiration (Hermida-Carrera *et al.*, 2016), which consumes ATP and reductants (Peterhansel *et al.*, 2010). However, the genus *Phaeocystis* possess highly efficient CO<sub>2</sub>-concentrating mechanisms (Reinfelder, 2011; Rost *et al.*, 2006), which increase the concentration of CO<sub>2</sub> at the site of C-fixation, thereby presumably suppressing the oxygenase activity of RuBisCO and consequently photorespiration.

It can be concluded that the performance during MHWs is dependent on the duration of heat exposure and that longer MHWs exert more thermal stress on cells than shorter ones. PSII reaction centres seem to be damaged more strongly during the MHW of 10 days compared to the MHW of 6 days. In addition, the lower POC quota in MHW2 cultures are indicative for a more reduced biomass build-up compared to MHW1 cultures, even though the light harvesting capacity is the same in both MHW treatments. Future studies could examine the capacity of *P. pouchetii* to respond to a second heatwave after a short recovery period. Previous thermal experience may weaken the capacity to respond to further stress (Striebel *et al.*, 2016) and hamper performance in a second heatwave (Samuels *et al.*, 2021) or the thermal history provides a heat-hardening effect that results in a better performance than in the first heatwave.

#### 4.5. Acclimated response to continued heat stress

The comparison of the acclimated response to 3 and 6 °C is feasible after growth rates and physiological parameters have stabilized at the respective temperatures. Cell cultures were considered acclimated to 6 °C after ~14 days. In contrast to the unchanged growth rates during the MHWs of 6 and 10 days, continued exposure to 6 °C resulted in a slight decline of growth rates from 0.40 d<sup>-1</sup> at 3 °C to 0.34 d<sup>-1</sup> at 6 °C (Fig. 15A+B). A study on the same *P. pouchetii* strain using equal light levels reported similar growth rates of ~0.3 d<sup>-1</sup> at 3 °C and slightly lower rates at 7 °C (Pfaff *et al.*, 2016). However, the comparison between cultures acclimated to 3 and 6 °C furthermore reveals unchanged Chl *a*:POC (Fig. 16F) and F<sub>v</sub>/F<sub>m</sub> values (Fig. 17), suggesting that *P. pouchetii* has managed to adjust its physiology in a way that photosynthetic efficiency can be maintained at a higher temperature. This is in line with Wang *et al.* (2010) who also found no drastic changes in F<sub>v</sub>/F<sub>m</sub> among the temperatures 4, 6 and 8 °C in *P. pouchetii*. While POC quota only increased marginally during the MHWs, continuous exposure to 6 °C stimulated POC quota significantly by ~20% (Fig. 16A). Chl *a* content, rETR, σ<sub>PII</sub> and ρ increased, while τ decreased compared to cultures growing at 3 °C (Fig. 16E+18), likely as

an acclimation mechanism to match the energy supply of the light phase of photosynthesis to the demand of the dark phase. More electrons are harvested through enhanced light absorption and they are shuttled into C-fixation more quickly, as indicated by the higher cellular C content of cells. However, temperature had no effect on C:N ratios in 3 and 6 °C control cultures, as was also observed recently in phytoplankton communities by Kling *et al.* (2020).

Warming seems to cause significantly higher H<sub>2</sub>O<sub>2</sub> levels in cells growing constantly at 6 °C than in those growing at 3 °C (Fig. 20A+B). However, O<sub>2</sub><sup>•-</sup> levels were not significantly different between these two temperatures (Fig. 20C+D), which could indicate an increased activity of SOD. In comparison to the MHW cultures, intracellular ROS levels did not accumulate to such high concentrations (Fig. 20). The trend towards declining ROS levels with prolonged heat exposure was already apparent in the comparison of MHW1 and MHW2 cultures (see section 4.4.) and is in line with the study by Buerger *et al.* (2020), who also reported lowered intracellular ROS in thermally acclimated cells. It seems feasible that acclimation to higher temperatures involves the adjustment of mechanisms that rebalance intracellular levels of ROS. This might have been achieved by increasing scavenging through the operation of a highly efficient detoxifying system, as described earlier (see section 4.3 + 4.4). A highly effective scavenging system, however, would demand a high energy supply to cover the associated energetic costs. Microalgae evolved a number of alternative electron pathways to balance the energy supply to meet demands including cyclic electron flow around PSI, the water-water cycle, the malate valve and the plastoquinol oxidase (Curien *et al.*, 2016; Kramer and Evans, 2011). However, the slight decrease of growth rates at elevated temperature implies that *P. pouchetii* may not be able to realize these alternative metabolic pathways to an extent that matches the energy supply with demands. Maintaining Chl *a*:POC ratios, i.e. a high photosynthetic efficiency and a high capacity for ROS scavenging may thus allow *P. pouchetii* to tolerate increased temperature stress, but reduces performance in the long-term.

#### 4.6. Impact of the post-MHW cooling – a relief or additional stressor?

After the exposure to 6 °C for several days, the MHW cultures were exposed to a cooling ramp from 6 to 3 °C (-1 °C h<sup>-1</sup>), followed by a recovery period of 5 days (Fig. 7). The response of cells to cooling changed over time, with the acute (1-2 h) response differing enormously from the performance after 5 days of recovery. Immediately after the sudden cooling,  $\tau$  increased and rETR decreased at the same time (Fig. 18A, B, G, H). Hence, the temperature drop of 3 °C caused the slowing down of electron removal from PSII, which can be explained by reduced

enzyme activity, slower diffusion due to increased electrochemical turnover time of electron carriers and the increased viscosity of membranes, which in turn hampers the movement of membrane-associated components at lower temperatures (Falkowski and Raven, 2007; Raven and Geider, 1988).

Since light harvesting was still upregulated through higher Chl *a* quota from the exposure to higher temperature during the MHWs, an imbalance of energy absorption and consumption can be expected with the lowering of temperature. Directly after the cooling ramp (1-2 h) an increase in  $Y(NO)$  and decrease in  $Y(NPQ)$  was observed (Fig. 19), which is indicative for a suboptimal capacity of photoprotective reactions (Klughammer and Schreiber, 2008).  $Y(NO)$  implies unregulated dissipation of excess energy as heat, which results primarily from the fraction of closed reaction centres (Kramer *et al.*, 2004). When cells are suddenly exposed to lower temperatures, more light energy is absorbed than can be used by downstream processes. Under high light stress, this mismatch between light and dark reactions may result in the presence of excess energy in the photosynthetic apparatus and cause slower re-opening of PSII reaction centres, thus increasing unregulated NPQ. The trend of increasing  $Y(NO)$  and decreasing  $Y(NPQ)$  after the cooling ramp was more pronounced after the longer MHW (Fig. 19B+D), where more profound acclimation processes had already taken place.

Furthermore, a sharp decrease of ROS levels was detected right after the cooling ramp (Fig. 20). These results contradict the initial hypothesis that the mismatch between light and dark reactions caused by cooling generates an electron jam that facilitates ROS production. This unexpected outcome can be partly explained by the decelerated electron transport, because the electron transport chain was in a less reduced state thereby minimizing the potential of  $O_2$  reduction. Moreover, the antioxidant scavenging system was likely still upregulated from exposure to high temperature and thus contributed to the decline of ROS levels. With the continued recovery at 3 °C, ROS levels of cells declined even further and reached even lower levels than those of 3 °C control cultures after 5 days of recovery (Fig. 20). These results might be partly explained by the significant reduction in Chl *a* quota of both MHW cultures compared to quota during the MHW exposure (Fig. 16E). This physiological adjustment of minimizing light absorption decreases excitation pressure in the photosynthetic reactions and thereby limits ROS production. In addition, the decreased  $\sigma_{PII}$  during the recovery of MHW1 cultures (Fig. 18E) reflects lower efficiency in exciton delivery to the reaction centres and thus may reduce light capture efficiency further.

Lower Chl *a* production is also in line with the lower POC production rates at the end of the recovery period (Fig. 16C+D). Reduced enzyme activity at lower temperatures might cause a slowing down of the Calvin cycle and as a consequence, lower C-fixation rates. By decreasing cellular Chl *a* content, cells can facilitate a rebalancing of light and dark reactions of photosynthesis, i.e. energy absorption and consumption. However, rETR increased and  $\tau$  decreased significantly again at the end of the recovery period of MHW cultures (Fig. 18A, B, G, H). In combination with the observed low POC production rates, this indicates that the drainage of electrons from PSII must be achieved by additional electron acceptors next to the Calvin cycle, e.g. via the water-water cycle (Hirotzu *et al.*, 2004). Alternative electron pathways are sinks for excess energy and thereby help to maintain PSII reaction centres open and avoid photodamage (Wilhelm and Jakob, 2011). This is supported by the significant increase in Y(NPQ) and decrease in Y(NO) at the end of the recovery period of MHW2 (Fig. 19B+D). Even though it is unlikely that cells experience photoinhibition under the experimental light conditions used here ( $30 \mu\text{mol photons m}^{-2} \text{ s}^{-1}$ ), an upregulated water-water cycle decreases the pH in the thylakoid lumen and therefore may enable a higher capacity to activate regulated NPQ quickly and alleviate photoinhibition under high light stress. The partitioning of excess energy towards dissipation mechanisms seems to be a common response of phytoplankton to a decrease in temperature. This was, for example, observed in freshwater diatoms and cyanobacteria (Fanesi *et al.*, 2016), but also in the polar diatom *Fragilariopsis cylindrus* (Mock and Hoch, 2005). Enhanced xanthophyll cycle mediated NPQ under lower temperatures is further supported by the pigment analysis of *F. cylindrus* exposed to a temperature shift from  $+5 \text{ }^\circ\text{C}$  to  $-1.8 \text{ }^\circ\text{C}$ , which revealed that the ratio of diatoxanthin to diadinoxanthin increased from 0.7 to 5.0 (Mock and Valentin, 2004).

The duration of the MHW seems to have an impact on the capacity of recovery. In MHW2 cultures, POC and Chl *a* production was significantly reduced while this was only a slight trend in MHW1 cultures (Fig. 16C+D). In addition, growth rates in MHW1 cultures did not change post-MHW, but rather ranged around  $0.39 \text{ d}^{-1}$  with a large standard deviation of  $0.20 \text{ d}^{-1}$  (Fig. 15C). In MHW2 cultures, however, they declined slightly from  $0.40 \pm 0.08 \text{ d}^{-1}$  during the MHW to  $0.34 \pm 0.12 \text{ d}^{-1}$  post-MHW (Fig. 15D). Even though this reduction in growth was statistically not significant, it indicates a trend for reduced performance post-MHW. Hence, decreased Chl *a* content can cause reduced energy absorption and C-fixation and less energy and carbon is available to maintain growth rates after longer MHWs. Reduced performance after exposure to MHWs has already been demonstrated for diatoms (Bedolfe, 2015; Samuels *et al.*, 2021) and kelp (Nepper-Davidsen *et al.*, 2019). In addition, Samuels *et al.* (2021) showed that hotter and

longer heatwaves increased mortality and decreased post-MHW growth rates relative to shorter MHWs. However,  $F_v/F_m$  values of *P. pouchetii* increased to the baseline level of the 3 °C controls during recovery, suggesting that the temperature fluctuations induced by the MHWs did not damage PSII reaction centres severely and impose high stress levels on cells. In conclusion, the cooling post-MHW represents a relief in regard to oxidative stress, but it nevertheless requires re-acclimation and reduces performance as indicated by the trend of declining growth rates during recovery.

#### 4.7. Performance of *Phaeocystis pouchetii* in the future Arctic Ocean and implications for future research

The results of this study indicate that *P. pouchetii* performs well at 3 °C, which is a possible future spring temperature in Arctic waters and a current summer sea surface temperature. This is in line with the study by Thomas *et al.* (2012) and Coello-Camba and Agustí (2017), who reported that the average  $T_{opt}$  of polar phytoplankton is positioned above ambient Arctic temperatures. The acclimation to 6 °C, which represents the intensity of future Arctic MHWs based on predictions by (Frölicher *et al.*, 2018), seems possible but with a trade-off between biomass build-up and necessary physiological adjustments to avoid oxidative damage that resulted in decreased growth rates at 6 °C. As a general rule, growth rates below  $T_{opt}$  increase with rising temperature and rapidly decrease once they surpass this temperature (Boyd *et al.*, 2013; Eppley, 1972). Therefore, 6 °C is likely close to or already above the optimal temperature of *P. pouchetii* but still located within their thermal niche. The tolerance of *P. pouchetii* in that region to warming may be influenced by the ongoing Atlantification in the Fram Strait, where this strain was originally isolated. Northward-flowing Atlantic water masses are the major source of heat into the Arctic Ocean (Menze *et al.*, 2020; Wassmann *et al.*, 2015). This Atlantic water flows around the Svalbard shelf as the so-called West Spitsbergen Current (WSC), which is also rapidly warming (Norwegian Polar Institute, 2022). As a result, temperatures in the Fram Strait can geographically vary from 5 °C to -2 °C based on measurements made between September 2002 to August 2003 (Schauer *et al.*, 2008). Hence, strains like the one used here may have already adapted to higher temperature and also higher variability of this region, or they originated from lower latitudes and advected into the Arctic Ocean by northward-flowing water masses.

Before the start of this experiment, I tried to acclimate *P. pouchetii* cultures to 9 °C. While the experimental temperatures of 3 and 6 °C controls yielded mean growth rates of 0.40 d<sup>-1</sup> and 0.34 d<sup>-1</sup>, respectively, further warming to 9 °C caused growth to drop close to zero (0.01 ± 0.12 d<sup>-1</sup>; data not shown), making this temperature unsuitable to carry out the physiological experiments. This implies a very steep decline in thermal tolerance of *P. pouchetii*. High sensitivity to heat stress beyond the here tested 6 °C is in line with Degerlund and Eilertsen (2010) who reported that *P. pouchetii* was present in the Fram Strait between -1.7 and 9 °C, but that there was a weak trend towards lower abundances above approximately 5 °C. Furthermore, Wang *et al.* (2010) observed that *P. pouchetii* only grew from 4 to 8 °C, but stated that its physiological responses were relatively insensitive to temperature within this range. While a lot of species optimize the allocation of photosynthetic resources to maximize growth, *P. pouchetii* rather seems to follow a strategy of maintaining growth around a certain rate within its thermal scope.

It is expected that thermal tolerance determines the response of an organism to global warming (Pörtner and Farrell, 2008). Nevertheless, phytoplankton have a certain capacity for evolutionary responses to climate change due to their short generation times and high population densities (Collins *et al.*, 2014). They can compensate unfavourable environmental conditions like elevated temperatures by physiological adjustments via acclimation (phenotypic changes occurring after a few generations) or adaptation (phenotypic changes through evolution). The results of this study show that acclimation to higher temperatures and temperature fluctuations are associated with great energetic costs that can decrease the fitness of cells. Cell populations could overcome these costs through adaptation. Even though thermal tolerance of phytoplankton species reflects an evolutionary adaptation to their mean thermal growth environment (Thomas *et al.*, 2012), results of long-term experiments indicate that phytoplankton are indeed able to adapt to temperature changes over longer timescales and raise their optimal temperature (Schaum *et al.*, 2017; Schlüter *et al.*, 2014). In the future oceans, however, organisms will not only be exposed to a gradual temperature rise over several decades, but they will also experience MHWs more frequently, especially in the Arctic Ocean (Frölicher *et al.*, 2018). The intensity and sudden temperature fluctuations associated with these extremes can push species beyond their physiological thresholds on short timescales and could therefore impose strong limitations on the capacity of evolutionary adaptation. Especially on short timescales, high intraspecific diversity has a great potential to buffer the detrimental effects of MHWs by selecting between cell lineages with wider thermal tolerance ranges. Strock and Menden-Deuer (2020) observed an exponential increase of the intraspecific variability in

growth rates as response to cumulative thermal shifts and Samuels *et al.* (2021) showed that the effect of a simulated MHW on growth of the Southern Ocean diatom *Actinocyclus actinochilus* varied between genotypes. For *P. pouchetii* in particular, Pfaff *et al.* (2016) reported high physiological plasticity due to genotypic differentiation after they analysed the response of 7 different *P. pouchetii* strains to different salinity gradients and temperatures. Since this study only investigated a single strain, further experiments on more strains could be used to verify, whether a high intraspecific diversity can broaden the population's physiological plasticity and perhaps also improve the ecological success of *P. pouchetii* under the thermal conditions predicted for the future Arctic Ocean.

However, the ecological success of a species does not only depend on its individual performance, but also on how it compares to other competing species. Several studies have shown that MHWs cause species loss (Rasconi *et al.*, 2017; Stefanidou *et al.*, 2019) and induce changes in the composition of phytoplankton community structures (Remy *et al.*, 2017; Soulié *et al.*, 2022; Weisse *et al.*, 2016; Wernberg *et al.*, 2016). These changes can be explained by different temperature tolerances between phylogenetic groups (Huertas *et al.*, 2011), but also different speeds of acclimation to fluctuating conditions. When temperature thresholds are exceeded and/or a species is outcompeted by another, the organisms most sensitive to thermal changes will be excluded and the most resistant species become favoured. Therefore, the resilience of species to MHWs and the resulting differences in organismal fitness exerts a strong selection pressure that may induce changes in population sizes and community composition. Temperature fluctuations may push the system towards the dominance of fast-growing species that can acclimate rapidly to such abrupt temperature changes (Rasconi *et al.*, 2017). *P. pouchetii* exhibited lowered growth rates in response to future temperature regimes. It is therefore questionable whether *P. pouchetii* can compete with other faster growing species that can adjust more quickly to fluctuating temperatures. In addition, global warming causes a poleward shift in the range of species (Parmesan, 2006; Thomas *et al.*, 2012) and these species advected into the Arctic Ocean will exert additional selection pressure, as they are probably already adapted to warmer temperatures than resident Arctic species. In conclusion, this study only allows predictions about the physiological capacity of a single species to respond to MHWs. While this is advantageous to resolve underlying physiological principles that take place under temperature fluctuations, further studies on other ecologically relevant key species are needed to draw conclusions about the competitiveness between different species.

Even though maximizing growth rates does not seem to be the ecological strategy of *P. pouchetii*, many studies reported an increased *Phaeocystis* sp. dominance in Arctic phytoplankton assemblages in recent years (Assmy *et al.*, 2017; Lafond *et al.*, 2019; Nöthig *et al.*, 2015; Orkney *et al.*, 2020). Blooms of *P. pouchetii* were observed in association with a warm water anomaly in Kongsfjorden (Hegseth and Tverberg, 2013) and in Fram Strait (Nöthig *et al.*, 2015; Saiz *et al.*, 2013). Hence, other factors than optimized growth must come into play that explain the ecological success of this species. The results of this study suggest that *P. pouchetii* exhibits a high capacity for protection against oxidative stress and photodamage, which may enable its resilience in variable environments, including sudden temperature fluctuations. A study on xanthophyll cycling in *Phaeocystis globosa* and *Thalassiosira* sp. observed faster xanthophyll cycling rates in *P. globosa*, and the authors suggested that this ability gives *P. globosa* a possible competitive advantage over *Thalassiosira* sp. (Meyer *et al.*, 2000).

Moreover, the top-down control by grazing is important to consider, because an increase of grazing may be more pronounced than photosynthetic activity, thereby altering the metabolic balance of ecosystems (Boscolo-Galazzo *et al.*, 2018; Yvon-Durocher *et al.*, 2010). As a consequence, the minimisation of loss terms by avoiding grazing may be as important, or even more important as growth optimisation in structuring phytoplankton communities. *Phaeocystis* can function as a nanoplanktonic solitary cell, as well as a micro- to macroplanktonic colony (Verity *et al.*, 2007), thereby taking advantage of the benefits of both of these life stages. Colonies likely reduce the exposure to predation either due to size mismatches with grazers or the production of a chemical deterrent (Turner, 2002; Verity, 2000). On the other hand, it appears that colony cells can become motile and leave colonies under stressful environmental conditions (Marchant and Thomsen, 1994; Parke *et al.*, 1971; Verity *et al.*, 1988), implying a physiological advantage of the solitary life cycle stage. Hence, the complex heteromorphic life cycle of *P. pouchetii* could hold the secret to the success of this species.

To realistically predict the resilience of Arctic phytoplankton populations to future heatwaves, co-occurring environmental factors and holistic community responses need to be considered. Under global warming, not only temperature but also many other environmental factors will change in the Arctic Ocean, including nutrient limitation, higher pCO<sub>2</sub> and irradiance (Wassmann, 2011). In addition, stimulated metabolic rates due to higher temperatures raise the demand for nutrients and thereby intensify the likelihood of nutrient limitation further (Rhee and Gotham, 1981). Several studies have already shown that nutrient availability exerted a

much stronger influence on shaping phytoplankton community composition than temperature (Filiz *et al.*, 2020; Staehr and Sand-Jensen, 2006; Weisse *et al.*, 2016). In the future, a multifactorial experimental approach could be used to study the impact of nutrient and light availability and higher pCO<sub>2</sub> on the physiological capacity to respond to MHWs. In addition, diverse phytoplankton communities may respond differently than single species, because ecological compensatory processes may stabilize the community to prevent change (Connell and Ghedini, 2015) or biotic interactions like competition with other species and grazing pose additional stress. Mesocosm experiments including different functional groups and top-down processes like grazing could be used to investigate the response of Arctic communities to respond to MHWs, which will occur more frequently in the future. Increased *Phaeocystis* dominance and changed community compositions in general may alter marine food webs (Biela *et al.*, 2019; Jones *et al.*, 2018; Peña *et al.*, 2019), influence the resilience of entire marine ecosystems and would have major implications for the biological carbon pump (Reigstad and Wassmann, 2007; Wassmann *et al.*, 1990; Wollenburg *et al.*, 2018) and biogeochemical cycling in general.

## References

- Allahverdiyeva, Y., Mamedov, F., Mäenpää, P., Vass, I. and Aro, E.-M. (2005) Modulation of photosynthetic electron transport in the absence of terminal electron acceptors: characterization of the *rbcL* deletion mutant of tobacco. *Biochimica et Biophysica Acta*, **1709**, 69–83.
- Allakhverdiev, S. I., Kreslavski, V. D., Klimov, V. V., Los, D. A., Carpentier, R. and Mohanty, P. (2008) Heat stress: an overview of molecular responses in photosynthesis. *Photosynthesis Research*, **98**, 541–550.
- Ananyev, G., Renger, G., Wacker, U. and Klimov, V. (1994) The photoproduction of superoxide radicals and the superoxide dismutase activity of Photosystem II. The possible involvement of cytochrome b559. *Photosynthesis Research*, **41**, 327–338.
- Anning, T., Harris, G. and Geider, R. (2001) Thermal acclimation in the marine diatom *Chaetoceros calcitrans* (Bacillariophyceae). *European Journal of Phycology*, **36**, 233–241.
- Ardyna, M. and Arrigo, K. R. (2020) Phytoplankton dynamics in a changing Arctic Ocean. *Nature Climate Change*, **10**, 892–903.
- Arrigo, K. R., van Dijken, G. and Pabi, S. (2008) Impact of a shrinking Arctic ice cover on marine primary production. *Geophysical Research Letters*, **35**.
- Årthun, M., Eldevik, T., Smedsrud, L. H., Skagseth, Ø. and Ingvaldsen, R. B. (2012) Quantifying the influence of Atlantic heat on Barents sea ice variability and retreat. *Journal of Climate*, **25**, 4736–4743.
- Asada, K. (1999) The water-water cycle in chloroplasts: Scavenging of active oxygens and dissipation of excess photons. *Annual Review of Plant Physiology and Plant Molecular Biology*, **50**, 601–639.
- Asada, K. (2006) Production and scavenging of reactive oxygen species in chloroplasts and their functions. *Plant Physiology*, **141**, 391–396.
- Asada, K. and Takahashi, M. (1987) Production and scavenging of active oxygen in chloroplasts. In Kyle, D. J., Osmond, C. B. and Arntzen, C. J. (eds), *Photoinhibition*. Elsevier, Amsterdam, pp. 227–287.
- Asbjørnsen, H., Årthun, M., Skagseth, Ø. and Eldevik, T. (2020) Mechanisms underlying recent Arctic Atlantification. *Geophysical Research Letters*, **47**.
- Assmy, P., Fernández-Méndez, M., Duarte, P., Meyer, A., Randelhoff, A., Mundy, C. J., Olsen, L. M. and Kauko, H. M. et al. (2017) Leads in Arctic pack ice enable early phytoplankton blooms below snow-covered sea ice. *Scientific Reports*, **7**, 40850.
- Badger, M. R., Andrews, T. J., Whitney, S. M., Ludwig, M., Yellowlees, D. C., Leggat, W. and Price, G. D. (1998) The diversity and coevolution of Rubisco, plastids, pyrenoids, and chloroplast-based CO<sub>2</sub>-concentrating mechanisms in algae. *Canadian Journal of Botany*, **76**, 1052–1071.
- Barber, D. G., Hop, H., Mundy, C. J., Else, B., Dmitrenko, I. A., Tremblay, J.-E., Ehn, J. K. and Assmy, P. et al. (2015) Selected physical, biological and biogeochemical implications of a rapidly changing Arctic Marginal Ice Zone. *Progress in Oceanography*, **139**, 122–150.
- Basu, S. and Mackey, K. (2018) Phytoplankton as key mediators of the biological carbon pump: Their responses to a changing climate. *Sustainability*, **10**, 869.
- Beardall, J. and Raven, J. A. (2004) The potential effects of global climate change on microalgal photosynthesis, growth and ecology. *Phycologia*, **43**, 26–40.
- Beardall, J. and Raven, J. A. (2020) Structural and biochemical features of carbon acquisition in algae. In Larkum, A. W., Grossman, A. R. and Raven, J. A. (eds), *Photosynthesis in Algae: Biochemical and Physiological Mechanisms*. Springer International Publishing, Cham, pp. 141–160.
- Beck, L. J., Sarnela, N., Junninen, H., Hoppe, C. J. M., Garmash, O., Bianchi, F., Riva, M. and Rose, C. et al. (2021) Differing mechanisms of new particle formation at two Arctic sites. *Geophysical Research Letters*, **48**.
- Bedolfe, S. (2015): *Heatwaves decrease production in benthic diatom communities*, Master Thesis.
- Behrenfeld, M. J., Halsey, K. H. and Milligan, A. J. (2008) Evolved physiological responses of phytoplankton to their integrated growth environment. *Philosophical Transactions of the Royal Society of London. Series B, Biological Sciences*, **363**, 2687–2703.

- Bekker, A., Holland, H. D., Wang, P.-L., Rumble, D., Stein, H. J., Hannah, J. L., Coetzee, L. L. and Beukes, N. J. (2004) Dating the rise of atmospheric oxygen. *Nature*, **427**, 117–120.
- Berger, W. H., Fischer, K., Lai, C. and Wu, G. (1987) Ocean productivity and organic carbon flux. Part I. Overview and maps of primary production and export production: University of California, San Diego. SIO Reference, 87-30.
- Bernhardt, J. R., Sunday, J. M., Thompson, P. L. and O'Connor, M. I. (2018) Nonlinear averaging of thermal experience predicts population growth rates in a thermally variable environment. *Proceedings. Biological Sciences*, **285**.
- Biela, V. R. von, Arimitsu, M. L., Piatt, J. F., Heflin, B., Schoen SK Trowbridge, J. L. and Clawson, C. M. (2019) Extreme reduction in nutritional value of a key forage fish during the Pacific marine heatwave of 2014-2016. *Marine Ecology Progress Series*, **613**, 171–182.
- Bindokas, V. P., Jordan, J., Lee, C. C. and Miller, R. J. (1996) Superoxide production in rat hippocampal neurons: selective imaging with hydroethidine. *J. Neurosci.*, **16**, 1324–1336.
- Bischof, K., Rautenberger, R., Brey, L. and Pérez-Lloréns, J. L. (2006) Physiological acclimation to gradients of solar irradiance within mats of the filamentous green macroalga *Chaetomorpha linum* from southern Spain. *Marine Ecology Progress Series*, **306**, 165–175.
- Bissinger, J. E., Montagnes, D. J. S., harples, J. and Atkinson, D. (2008) Predicting marine phytoplankton maximum growth rates from temperature: Improving on the Eppley curve using quantile regression. *Limnology and Oceanography*, **53**, 487–493.
- Blankenship, R. E. (2014) *Molecular mechanisms of photosynthesis*. Wiley Blackwell, Chichester.
- Boscolo-Galazzo, F., Crichton, K. A., Barker, S. and Pearson, P. N. (2018) Temperature dependency of metabolic rates in the upper ocean: A positive feedback to global climate change? *Global and Planetary Change*, **170**, 201–212.
- Boyd, P. W., Rynearson, T. A., Armstrong, E. A., Fu, F., Hayashi, K., Hu, Z., Hutchins, D. A. and Kudela, R. M. et al. (2013) Marine phytoplankton temperature versus growth responses from polar to tropical waters—outcome of a scientific community-wide study. *PLOS one*, **8**, e63091.
- Breuer, G., Lamers, P. P., Martens, D. E., Draaisma, R. B. and Wijffels, R. H. (2012) The impact of nitrogen starvation on the dynamics of triacylglycerol accumulation in nine microalgae strains. *Bioresource Technology*, **124**, 217–226.
- Brewer, P. G., Bradshaw, A. L. and Williams, R. T. (1986) Measurements of total carbon dioxide and alkalinity in the North Atlantic Ocean in 1981. In Trabalka, J. R. and Reichle, D. E. (eds), *The changing carbon cycle*. Springer, New York, pp. 348–370.
- Brown, J. H., Gillooly, J. F., Allen, A. P., van Savage, M. and West, G. B. (2004) Toward a metabolic theory of ecology. *Ecology*, **85**, 1771–1789.
- Buerger, P., Alvarez-Roa, C., Coppin, C. W., Pearce, S. L., Chakravarti, L. J., Oakeshott, J. G., Edwards, O. R. and van Oppen, M. J. H. (2020) Heat-evolved microalgal symbionts increase coral bleaching tolerance. *Science Advances*, **6**, eaba2498.
- Burrows, M. T., Schoeman, D. S., Buckley, L. B., Moore, P., Poloczanska, E. S., Brander, K. M., Brown, C. and Bruno, J. F. et al. (2011) The pace of shifting climate in marine and terrestrial ecosystems. *Science*, **334**, 652–655.
- Carter, W. O., Narayanan, P. K. and Robinson, J. P. (1994) Intracellular hydrogen peroxide and superoxide anion detection in endothelial cells. *Journal of Leukocyte Biology*, **55**, 253–258.
- Carvalho, K. S. and Wang, S. (2020) Sea surface temperature variability in the Arctic Ocean and its marginal seas in a changing climate: Patterns and mechanisms. *Global and Planetary Change*, **193**, 103265.
- Chen, B. (2015) Patterns of thermal limits of phytoplankton. *Journal of Plankton Research*, **37**, 285–292.
- Cheng, L., Trenberth, K. E., Fasullo, J., Boyer, T., Abraham, J. and Zhu, J. (2017) Improved estimates of ocean heat content from 1960 to 2015. *Science Advances*, **3**, e1601545.
- Choi, K. M. and Lee, M. Y. (2012) Differential protein expression associated with heat stress in Antarctic microalga. *BioChip Journal*, **6**, 271–279.

- Chokshi, K., Pancha, I., Trivedi, K., George, B., Maurya, R., Ghosh, A. and Mishra, S. (2015) Biofuel potential of the newly isolated microalgae *Acutodesmus dimorphus* under temperature induced oxidative stress conditions. *Bioresource Technology*, **180**, 162–171.
- Chokshi, K., Pancha, I., Trivedi, K., Maurya, R., Ghosh, A. and Mishra, S. (2020) Physiological responses of the green microalga *Acutodesmus dimorphus* to temperature induced oxidative stress conditions. *Physiologia Plantarum*, **170**, 462–473.
- Cleland, R. E. and Grace, S. C. (1999) Voltammetric detection of superoxide production by photosystem II. *FEBS Letters*, **457**, 348–352.
- Coello-Camba, A. and Agustí, S. (2017) Thermal thresholds of phytoplankton growth in polar waters and their consequences for a warming polar ocean. *Frontiers in Marine Science*, **4**.
- Cohen, J., Screen, J. A., Furtado, J. C., Barlow, M., Whittleston, D., Coumou, D., Francis, J. and Dethloff, K. et al. (2014) Recent Arctic amplification and extreme mid-latitude weather. *Nature Geoscience*, **7**, 627–637.
- Collins, S. (2016) Growth rate evolution in improved environments under Prodigal Son dynamics. *Evolutionary Applications*, **9**, 1179–1188.
- Collins, S., Pi, J. and Yehuda-Shnaidman, E. (2012) Uncoupling and reactive oxygen species (ROS)-a double-edged sword for  $\beta$ -cell function? “Moderation in all things”. *Best Practice & Research. Clinical Endocrinology & Metabolism*, **26**, 753–758.
- Collins, S., Rost, B. and Rynearson, T. A. (2014) Evolutionary potential of marine phytoplankton under ocean acidification. *Evolutionary Applications*, **7**, 140–155.
- Connell, S. D. and Ghedini, G. (2015) Resisting regime-shifts: the stabilising effect of compensatory processes. *Trends in Ecology & Evolution*, **30**, 513–515.
- Coruzzi, G. and Last, R. (2000) Amino Acids. In Buchanan, B., Gruissem, W. and Jones, R. (eds), *Biochemistry and Molecular Biology of Plants*. American Society of Plant Biologists, Rockville, pp. 358–410.
- Curien, G., Flori, S., Villanova, V., Magneschi, L., Giustini, C., Forti, G., Matringe, M. and Petroutsos, D. et al. (2016) The water to water cycles in microalgae. *Plant & Cell Physiology*, **57**, 1354–1363.
- Degerlund, M. and Eilertsen, H. C. (2010) Main species characteristics of phytoplankton spring blooms in NE Atlantic and Arctic waters (68–80° N). *Estuaries and Coasts*, **33**, 242–269.
- Diaz, J. M. and Plummer, S. (2018) Production of extracellular reactive oxygen species by phytoplankton: past and future directions. *Journal of Plankton Research*, **40**, 655–666.
- Dickson, A. G. (1981) An exact definition of total alkalinity and a procedure for the estimation of alkalinity and total inorganic carbon from titration data. *Deep Sea Research Part A. Oceanographic Research Papers*, **28**, 609–623.
- Dickson, A. G. (1990) Standard potential of the reaction:  $\text{AgCl(s)} + 12\text{H}_2(\text{g}) = \text{Ag(s)} + \text{HCl(aq)}$ , and the standard acidity constant of the ion  $\text{HSO}_4^-$  in synthetic sea water from 273.15 to 318.15 K. *The Journal of Chemical Thermodynamics*, **22**, 113–127.
- Dickson, A. G. and Millero, F. J. (1987) A comparison of the equilibrium constants for the dissociation of carbonic acid in seawater media. *Deep Sea Research Part A. Oceanographic Research Papers*, **34**, 1733–1743.
- Dlugokencky, E. and Tans, P. (2022) *Trends in atmospheric carbon dioxide, National Oceanic and Atmospheric Administration, Earth System Research Laboratory (NOAA/ESRL)*. <https://gml.noaa.gov/ccgg/trends/global.html>. Accessed January 28, 2022.
- Dröse, S. and Brandt, U. (2012) Molecular mechanisms of superoxide production by the mitochondrial respiratory chain. *Advances in Experimental Medicine and Biology*, **748**, 145–169.
- Eikrem, W., Medlin, L. K., Henderiks, J., Rokitta, S., Rost, B., Probert, I., Throndsen, J. and Edvardsen, B. (2016) Haptophyta. In Archibald, J. M., Simpson, A. G., Slamovits, C. H., Margulis, L., Melkonian, M., Chapman, D. J. and Corliss, J. O. (eds), *Handbook of the Protists*. Springer International Publishing, Cham, pp. 1–61.
- Eppley, R. W. (1972) Temperature and phytoplankton growth in the sea. *Fishery Bulletin*, **70**.
- Falkowski, P. G., Barber, R. T. and Smetacek, V. (1998) Biogeochemical controls and feedbacks on ocean primary production. *Science*, **281**, 200–207.
- Falkowski, P. G., Katz, M. E., Knoll, A. H., Quigg, A., Raven, J. A., Schofield, O. and Taylor, F. J. R. (2004) The evolution of modern eukaryotic phytoplankton. *Science*, **305**, 354–360.

- Falkowski, P. G. and Raven, J. A. (2007) *Aquatic Photosynthesis*. Princeton University Press.
- Fanesi, A., Wagner, H., Becker, A. and Wilhelm, C. (2016) Temperature affects the partitioning of absorbed light energy in freshwater phytoplankton. *Freshw Biol*, **61**, 1365–1378.
- Feijão, E., Gameiro, C., Franzitta, M., Duarte, B., Caçador, I., Cabrita, M. T. and Matos, A. R. (2018) Heat wave impacts on the model diatom *Phaeodactylum tricorutum*: Searching for photochemical and fatty acid biomarkers of thermal stress. *Ecological Indicators*, **95**, 1026–1037.
- Field, A., Miles, J. and Field, Z. (2012) *Discovering statistics using R*. Sage, Los Angeles, London, New Delhi, Singapore, Washington, DC.
- Field, C. B., Behrenfeld, M. J., Randerson, J. T. and Falkowski, P. (1998) Primary production of the biosphere: integrating terrestrial and oceanic components. *Science*, **281**, 237–240.
- Filiz, N., Işık, U., Beklioğlu, M., Öglü, B., Cao, Y., Davidson, T. A., Søndergaard, M. and Lauridsen, T. L. et al. (2020) Phytoplankton Community Response to Nutrients, Temperatures, and a Heat Wave in Shallow Lakes: An Experimental Approach. *Water*, **12**, 3394.
- Foyer, C. H., Descourvieres, P. and Kunert, K. J. (1994) Protection against oxygen radicals: an important defence mechanism studied in transgenic plants. *Plant, Cell and Environment*, **17**, 507–523.
- Foyer, C. H. and Noctor, G. (2000) Tansley Review No. 112 Oxygen processing in photosynthesis: regulation and signalling. *The New Phytologist*, **146**, 359–388.
- Foyer, C. H. and Noctor, G. (2005) Oxidant and antioxidant signalling in plants: a re-evaluation of the concept of oxidative stress in a physiological context. *Plant, Cell and Environment*, **28**, 1056–1071.
- French, C. S., Smith, J. H., Virgin, H. I. and Airth, R. L. (1956) Fluorescence-spectrum curves of chlorophylls, pheophytins, phycoerythrins, phycocyanins and hypericin. *Plant Physiology*, **31**, 369–374.
- Fridovich, I. (1998) Oxygen toxicity: a radical explanation. *The Journal of Experimental Biology*, **201**, 1203–1209.
- Frölicher, T. L., Fischer, E. M. and Gruber, N. (2018) Marine heatwaves under global warming. *Nature*, **560**, 360–364.
- Galmés, J., Kapralov, M. V., Copolovici, L. O., Hermida-Carrera, C. and Niinemets, Ü. (2015) Temperature responses of the Rubisco maximum carboxylase activity across domains of life: phylogenetic signals, trade-offs, and importance for carbon gain. *Photosynthesis Research*, **123**, 183–201.
- Gao, G., Shi, Q., Xu, Z., Xu, J., Campbell, D. A. and Wu, H. (2018) Global warming interacts with ocean acidification to alter PSII function and protection in the diatom *Thalassiosira weissflogii*. *Environmental and Experimental Botany*, **147**, 95–103.
- Geider, R. J., Moore, C. M. and Ross, O. N. (2009) The role of cost–benefit analysis in models of phytoplankton growth and acclimation. *Plant Ecology & Diversity*, **2**, 165–178.
- Genty, B., Briantais, J.-M. and Baker, N. R. (1989) The relationship between the quantum yield of photosynthetic electron transport and quenching of chlorophyll fluorescence. *Biochimica et Biophysica Acta (BBA) - General Subjects*, **990**, 87–92.
- Goiris, K., van Colen, W., Wilches, I., León-Tamariz, F., Cooman, L. de and Muylaert, K. (2015) Impact of nutrient stress on antioxidant production in three species of microalgae. *Algal Research*, **7**, 51–57.
- Goldman, J. C. and Carpenter, E. J. (1974) A kinetic approach to the effect of temperature on algal growth. *Limnology and Oceanography*, **19**, 756–766.
- Grieco, M., Tikkanen, M., Paakkanen, V., Kangasjärvi, S. and Aro, E.-M. (2012) Steady-state phosphorylation of light-harvesting complex II proteins preserves photosystem I under fluctuating white light. *Plant Physiology*, **160**, 1896–1910.
- Guillard, R. R. and Ryther, J. H. (1962) Studies of marine planktonic diatoms. I. *Cyclotella nana* Hustedt, and *Detonula confervacea* (Cleve) Gran. *Canadian Journal of Microbiology*, **8**, 229–239.
- Halliwell, B. (2015) *Free Radicals in Biology and Medicine*. OUP Oxford, Oxford.
- Halsey, K. H. and Jones, B. M. (2015) Phytoplankton strategies for photosynthetic energy allocation. *Annual Review of Marine Science*, **7**, 265–297.
- Hamm, C. (2000) Architecture, ecology and biogeochemistry of *Phaeocystis* colonies. *Journal of Sea Research*, **43**, 307–315.

- Hegseth, E. N. and Sundfjord, A. (2008) Intrusion and blooming of Atlantic phytoplankton species in the high Arctic. *Journal of Marine Systems*, **74**, 108–119.
- Hegseth, E. N. and Tverberg, V. (2013) Effect of Atlantic water inflow on timing of the phytoplankton spring bloom in a high Arctic fjord (Kongsfjorden, Svalbard). *Journal of Marine Systems*, **113-114**, 94–105.
- Henderson, L. M. and Chappell, J. B. (1993) Dihydrorhodamine 123: a fluorescent probe for superoxide generation? *European Journal of Biochemistry*, **217**, 973–980.
- Hermida-Carrera, C., Kapralov, M. V. and Galmés, J. (2016) Rubisco catalytic properties and temperature response in crops. *Plant Physiology*, **171**, 2549–2561.
- Herndl, G. J. and Reinthaler, T. (2013) Microbial control of the dark end of the biological pump. *Nature Geoscience*, **6**, 718–724.
- Hirotsu, N., Makino, A., Ushio, A. and Mae, T. (2004) Changes in the thermal dissipation and the electron flow in the water-water cycle in rice grown under conditions of physiologically low temperature. *Plant & Cell Physiology*, **45**, 635–644.
- Hobday, A. J., Alexander, L. V., Perkins, S. E., Smale, D. A., Straub, S. C., Oliver, E. C., Benthuysen, J. A. and Burrows, M. T. et al. (2016) A hierarchical approach to defining marine heatwaves. *Progress in Oceanography*, **141**, 227–238.
- Hoppe, C. J. M., Langer, G., Rokitta, S. D., Wolf-Gladrow, D. A. and Rost, B. (2010) On CO<sub>2</sub> perturbation experiments: over-determination of carbonate chemistry reveals inconsistencies. *Biogeosciences Discussions*, **7**, 1707–1726.
- Horton, P., Ruban, A. V. and Walters, R. G. (1994) Regulation of light harvesting in green plants (indication by nonphotochemical quenching of chlorophyll fluorescence). *Plant Physiology*, **106**, 415–420.
- Hu, S., Zhang, L. and Qian, S. (2020) Marine heatwaves in the Arctic region: variation in different ice covers. *Geophysical Research Letters*, **47**.
- Hu, X., Tang, X., Bi, Z., Zhao, Q. and Ren, L. (2021) Adaptive evolution of microalgae *Schizochytrium* sp. under high temperature for efficient production of docosahexaenoic acid. *Algal Research*, **54**, 102212.
- Huertas, I. E., Rouco, M., López-Rodas, V. and Costas, E. (2011) Warming will affect phytoplankton differently: evidence through a mechanistic approach. *Proceedings. Biological Sciences*, **278**, 3534–3543.
- Hutchinson, G. E. (1961) The paradox of the plankton. *The American Naturalist*, **95**, 137–145.
- IPCC, 2014: Climate Change 2014: Synthesis Report. Contribution of Working Groups I, II and III to the Fifth Assessment Report of the Intergovernmental Panel on Climate Change [Core Writing Team, R.K. Pachauri and L.A. Meyer (eds.)]. IPCC, Geneva, Switzerland, 151 pp.
- IPCC, 2019: IPCC Special Report on the Ocean and Cryosphere in a Changing Climate [H.-O. Pörtner, D.C. Roberts, V. Masson-Delmotte, P. Zhai, M. Tignor, E. Poloczanska, K. Mintenbeck, A. Alegría, M. Nicolai, A. Okem, J. Petzold, B. Rama, N.M. Weyer (eds.)]. In press.
- IPCC, 2021: Climate Change 2021: The Physical Science Basis. Contribution of Working Group I to the Sixth Assessment Report of the Intergovernmental Panel on Climate Change [Masson-Delmotte, V., P. Zhai, A. Pirani, S.L. Connors, C. Péan, S. Berger, N. Caud, Y. Chen, L. Goldfarb, M.I. Gomis, M. Huang, K. Leitzell, E. Lonnoy, J.B.R. Matthews, T.K. Maycock, T. Waterfield, O. Yelekçi, R. Yu, and B. Zhou (eds.)]. Cambridge University Press. In press.
- Jacobsen, A. (2002) Morphology, relative DNA content and hypothetical life cycle of *Phaeocystis pouchetii* (Prymnesiophyceae); with special emphasis on the flagellated cell type. *Sarsia*, **87**, 338–349.
- Jones, T., Parrish, J. K., Peterson, W. T., Bjorkstedt, E. P., Bond, N. A., Ballance, L. T., Bowes, V. and Hipfner, J. M. et al. (2018) Massive mortality of a planktivorous seabird in response to a marine heatwave. *Geophysical Research Letters*, **45**, 3193–3202.
- Joos, F. and Spahni, R. (2008) Rates of change in natural and anthropogenic radiative forcing over the past 20,000 years. *Proceedings of the National Academy of Sciences of the United States of America*, **105**, 1425–1430.
- Jordan, D. B. and Ogren, W. L. (1984) The CO<sub>2</sub>/O<sub>2</sub> specificity of ribulose 1,5-bisphosphate carboxylase/oxygenase : Dependence on ribulosebisphosphate concentration, pH and temperature. *Planta*, **161**, 308–313.
- Kana, T. M., Geider, R. J. and Critchley, C. (1997) Regulation of photosynthetic pigments in micro-algae by multiple environmental factors: a dynamic balance hypothesis. *New Phytologist*, **137**, 629–638.

- Kim, K. and Portis, A. R. (2004) Oxygen-dependent H<sub>2</sub>O<sub>2</sub> production by Rubisco. *FEBS Letters*, **571**, 124–128.
- Klimov, V., Ananyev, G., Zastrzhnaya, O., Wydrzynski, T. and Renger, G. (1993) Photoproduction of hydrogen peroxide in Photosystem II membrane fragments: A comparison of four signals. *Photosynthesis Research*, **38**, 409–416.
- Kling, J. D., Lee, M. D., Fu, F., Phan, M. D., Wang, X., Qu, P. and Hutchins, D. A. (2020) Transient exposure to novel high temperatures reshapes coastal phytoplankton communities. *The ISME Journal*, **14**, 413–424.
- Klughammer, C. and Schreiber, U. (2008) Complementary PS II quantum yields calculated from simple fluorescence parameters measured by PAM fluorometry and the Saturation Pulse method. *PAM Application Notes*, **1**, 27–35.
- Knap, A., Michaels, A., Close, A. and Ducklow, H. (eds) (1996) *Protocols for the Joint Global Ocean Flux Study (JGOFS) core measurements*. Vol. 19. UNESCO.
- Kolber, Z. S., Prášil, O. and Falkowski, P. G. (1998) Measurements of variable chlorophyll fluorescence using fast repetition rate techniques: defining methodology and experimental protocols. *Biochimica et Biophysica Acta (BBA) - Bioenergetics*, **1367**, 88–106.
- Korshunov, S. S., Skulachev, V. P. and Starkov, A. A. (1997) High protonic potential actuates a mechanism of production of reactive oxygen species in mitochondria. *FEBS Letters*, **416**, 15–18.
- Kováčik, J., Klejdus, B. and Backor, M. (2010) Physiological responses of *Scenedesmus quadricauda* (Chlorophyceae) to UV-A and UV-C light. *Photochemistry and Photobiology*, **86**, 612–616.
- Kramer, D. M. and Evans, J. R. (2011) The importance of energy balance in improving photosynthetic productivity. *Plant Physiology*, **155**, 70–78.
- Kramer, D. M., Johnson, G., Kiirats, O. and Edwards, G. E. (2004) New fluorescence parameters for the determination of QA redox state and excitation energy fluxes. *Photosynthesis Research*, **79**, 209.
- Ku, S. B. and Edwards, G. E. (1977) Oxygen inhibition of photosynthesis: I. Temperature dependence and relation to O<sub>2</sub>/CO<sub>2</sub> solubility ratio. *Plant Physiology*, **59**, 986–990.
- Lafond, A., Leblanc, K., Quéguiner, B., Moriceau, B., Leynaert, A., Cornet, V., Legras, J. and Ras, J. et al. (2019) Late spring bloom development of pelagic diatoms in Baffin Bay. *Elementa: Science of the Anthropocene*, **7**.
- Lenth, R. V. (2021) *emmeans: Estimated Marginal Means, aka Least-Squares Means*.
- Lesser, M. P. (2006) Oxidative stress in marine environments: biochemistry and physiological ecology. *Annual Review of Physiology*, **68**, 253–278.
- Lewis, K. M., van Dijken, G. L. and Arrigo, K. R. (2020) Changes in phytoplankton concentration now drive increased Arctic Ocean primary production. *Science*, **369**, 198–202.
- Li, W. K. W. (1980) Temperature adaptation in phytoplankton: cellular and photosynthetic characteristics. In Falkowski, P. G. (ed.), *Primary Productivity in the Sea*. Springer US, Boston, MA, pp. 259–279.
- Liang, Y., Koester, J. A., Liefer, J. D., Irwin, A. J. and Finkel, Z. V. (2019) Molecular mechanisms of temperature acclimation and adaptation in marine diatoms. *The ISME Journal*, **13**, 2415–2425.
- Litchman, E., Tezanos Pinto, P. de, Edwards, K. F., Klausmeier, C. A., Kremer, C. T. and Thomas, M. K. (2015) Global biogeochemical impacts of phytoplankton: a trait-based perspective. *Journal of Ecology*, **103**, 1384–1396.
- Liu, W., Au, D. W., Anderson, D. M., Lam, P. K. and Wu, R. S. (2007) Effects of nutrients, salinity, pH and light:dark cycle on the production of reactive oxygen species in the alga *Chattonella marina*. *Journal of Experimental Marine Biology and Ecology*, **346**, 76–86.
- Los, D. A., Mironov, K. S. and Allakhverdiev, S. I. (2013) Regulatory role of membrane fluidity in gene expression and physiological functions. *Photosynthesis Research*, **116**, 489–509.
- Lovejoy, C., Quillfeldt, C. von, Hopcroft, R. R., Poulin, M., Thaler, M., Arendt, K., Debes, H. and Gíslan, Á. et al. (2017) Plankton. In Arctic Council Secretariat (ed.), *State of the Arctic Marine Biodiversity Report*. Akureyri, Iceland, pp. 63–83.
- Marchant, H. J. and Thomsen, H. A. (1994) Haptophytes in polar waters. In Green, J. C. and Leadbeater, B. (eds), *The haptophyte algae*. Vol. 51. Clarendon Press, Oxford, pp. 209–228.
- Marklund, S. (1976) Spectrophotometric study of spontaneous disproportionation of superoxide anion radical and sensitive direct assay for superoxide dismutase. *Journal of Biological Chemistry*, **251**, 7504–7507.

- Maxwell, K. and Johnson, G. N. (2000) Chlorophyll fluorescence—a practical guide. *Journal of Experimental Botany*, **51**, 659–668.
- McCord, J. M. and Fridovich, I. (1969) Superoxide Dismutase. *Journal of Biological Chemistry*, **244**, 6049–6055.
- Mehler, A. H. (1951) Studies on reactions of illuminated chloroplasts. *Archives of Biochemistry and Biophysics*, **33**, 65–77.
- Mehrbach, C., Culbertson, C. H., Hawley, J. E. and Pytkowicz, R. M. (1973) Measurement of the apparent dissociation constants of carbonic acid in seawater at atmospheric pressure. *Limnology and Oceanography*, **18**, 897–907.
- Menze, S., Ingvaldsen, R. B., Nikolopoulos, A., Hattermann, T., Albretsen, J. and Gjørseter, H. (2020) Productive detours – Atlantic water inflow and acoustic backscatter in the major troughs along the Svalbard shelf. *Progress in Oceanography*, **188**, 102447.
- Meyer, A., Tackx, M. and Daro, N. (2000) Xanthophyll cycling in *Phaeocystis globosa* and *Thalassiosira* sp.: a possible mechanism for species succession. *Journal of Sea Research*, **43**, 373–384.
- Mock, T. and Hoch, N. (2005) Long-term temperature acclimation of photosynthesis in steady-state cultures of the polar diatom *Fragilariopsis cylindrus*. *Photosynthesis Research*, **85**, 307–317.
- Mock, T. and Valentin, K. (2004) Photosynthesis and cold acclimation: Molecular evidence from a polar diatom. *Journal of Phycology*, **40**, 732–741.
- Moller, I. M. (2001) Plant mitochondria and oxidative stress: Electron transport, NADPH turnover, and metabolism of reactive oxygen species. *Annual Review of Plant Physiology and Plant Molecular Biology*, **52**, 561–591.
- Morel, F. M. M. (1987) Kinetics of nutrient uptake and growth in phytoplankton. *Journal of Phycology*, **23**, 137–150.
- Müller, P., Li, X. P. and Niyogi, K. K. (2001) Non-photochemical quenching. A response to excess light energy. *Plant Physiology*, **125**, 1558–1566.
- Murik, O., Tirichine, L., Prihoda, J., Thomas, Y., Araújo, W. L., Allen, A. E., Fernie, A. R. and Bowler, C. (2019) Downregulation of mitochondrial alternative oxidase affects chloroplast function, redox status and stress response in a marine diatom. *New Phytologist*, **221**, 1303–1316.
- Navari-Izzo, F., Pinzino, C., Quartacci, M. F. and Sgherri, C. L. (1999) Superoxide and hydroxyl radical generation, and superoxide dismutase in PSII membrane fragments from wheat. *Free Radical Research*, **31 Suppl**, S3-9.
- Nepper-Davidsen, J., Andersen, D. T. and Pedersen, M. F. (2019) Exposure to simulated heatwave scenarios causes long-term reductions in performance in *Saccharina latissima*. *Marine Ecology Progress Series*, **630**, 25–39.
- Niyogi, K. K. (1999) Photoprotection revisited: Genetic and molecular approaches. *Annual Review of Plant Physiology and Plant Molecular Biology*, **50**, 333–359.
- Noctor, G. and Foyer, C. H. (1998) Ascorbate and glutathione: Keeping active oxygen under control. *Annual Review of Plant Physiology and Plant Molecular Biology*, **49**, 249–279.
- Norwegian Polar Institute (2022) *Annual maximum temperature in the West Spitsbergen Current: Environmental monitoring of Svalbard and Jan Mayen (MOSJ)*. <http://www.mosj.no/en/climate/ocean/temperature-salinity-fram-strait.html>. Accessed February 20, 2022.
- Nöthig, E.-M., Bracher, A., Engel, A., Metfies, K., Niehoff, B., Peeken, I., Bauerfeind, E. and Cherkasheva, A. et al. (2015) Summertime plankton ecology in Fram Strait—a compilation of long- and short-term observations. *Polar Research*, **34**, 23349.
- Oliver, E. C. J., Burrows, M. T., Donat, M. G., Sen Gupta, A., Alexander, L. V., Perkins-Kirkpatrick, S. E., Benthuyssen, J. A. and Hobday, A. J. et al. (2019) Projected marine heatwaves in the 21<sup>st</sup> century and the potential for ecological impact. *Frontiers in Marine Science*, **6**.
- Orkney, A., Platt, T., Narayanaswamy, B. E., Kostakis, I. and Bouman, H. A. (2020) Bio-optical evidence for increasing *Phaeocystis* dominance in the Barents Sea. *Philosophical Transactions. Series A, Mathematical, Physical, and Engineering Sciences*, **378**, 20190357.
- Oxborough, K., Moore, C. M., Suggett, D. J., Lawson, T., Chan, H. G. and Geider, R. J. (2012) Direct estimation of functional PSII reaction center concentration and PSII electron flux on a volume basis: a new approach to

- the analysis of Fast Repetition Rate fluorometry (FRRf) data. *Limnology and Oceanography: Methods*, **10**, 142–154.
- Oziel, L., Baudena, A., Ardyna, M., Massicotte, P., Randelhoff, A., Sallée, J.-B., Ingvaldsen, R. B. and Devred, E. et al. (2020) Faster Atlantic currents drive poleward expansion of temperate phytoplankton in the Arctic Ocean. *Nature Communications*, **11**, 1705.
- Oziel, L., Sirven, J. and Gascard, J.-C. (2016) The Barents Sea frontal zones and water masses variability (1980–2011). *Ocean Science*, **12**, 169–184.
- Palenik, B., Zafiriou, O. C. and Morel, F. M. M. (1987) Hydrogen peroxide production by a marine phytoplankton 1. *Limnology and Oceanography*, **32**, 1365–1369.
- Parke, M., Green, J. C. and Manton, I. (1971) Observations on the fine structure of zooids of the genus *Phaeocystis* [Haptophyceae]. *Journal of the Marine Biological Association of the United Kingdom*, **51**, 927–941.
- Parmesan, C. (2006) Ecological and evolutionary responses to recent climate change. *Annual Review of Ecology, Evolution, and Systematics*, **37**, 637–669.
- Pearle, P., Collett, B., Bart, K., Bilderback, D., Newman, D. and Samuels, S. (2010) What Brown saw and you can too. *American Journal of Physics*, **78**, 1278–1289.
- Peña, M. A., Nemcek, N. and Robert, M. (2019) Phytoplankton responses to the 2014–2016 warming anomaly in the northeast subarctic Pacific Ocean. *Limnology and Oceanography*, **64**, 515–525.
- Perovich, D. K., Light, B., Eicken, H., Jones, K. F., Runciman, K. and Nghiem, S. V. (2007) Increasing solar heating of the Arctic Ocean and adjacent seas, 1979–2005: Attribution and role in the ice-albedo feedback. *Geophysical Research Letters*, **34**.
- Peterhansel, C., Horst, I., Niessen, M., Blume, C., Kebeish, R., Kürkcüoglu, S. and Kreuzaler, F. (2010) Photorespiration. *The Arabidopsis Book*, **8**, e0130.
- Pfaff, S., Gustavs, L., Reichardt, A., Jaskulke, R., Ewald, H., Gäbler-Schwarz and Karsten, U. (2016) Ecophysiological plasticity in the Arctic phytoplankton species *Phaeocystis pouchetii* (Prymnesiophyceae, Haptophyta). *Algological Studies*, **151–152**, 87–102.
- Pierrot, D. E., Wallace, D. and Lewis, E. (2006) *MS Excel Program Developed for CO2 System Calculations*.
- Pinheiro, J., Bates, D., DebRoy, S., Sarkar, D. and R Core Team (2021) *nlme: Linear and Nonlinear Mixed Effects Models*.
- Polyakov, I. V., Pnyushkov, A. V., Alkire, M. B., Ashik, I. M., Baumann, T. M., Carmack, E. C., Goszczko, I. and Guthrie, J. et al. (2017) Greater role for Atlantic inflows on sea-ice loss in the Eurasian Basin of the Arctic Ocean. *Science*, **356**, 285–291.
- Polyakov, I. V., Pnyushkov, A. V. and Timokhov, L. A. (2012) Warming of the intermediate Atlantic water of the Arctic Ocean in the 2000s. *Journal of Climate*, **25**, 8362–8370.
- Pörtner, H. O. and Farrell, A. P. (2008) Ecology. Physiology and climate change. *Science*, **322**, 690–692.
- Pospíšil, P. (2009) Production of reactive oxygen species by photosystem II. *Biochimica et Biophysica Acta*, **1787**, 1151–1160.
- Pospíšil, P., Arató, A., Krieger-Liszkay, A. and Rutherford, A. W. (2004) Hydroxyl radical generation by photosystem II. *Biochemistry*, **43**, 6783–6792.
- Prado, R., Rioboo, C., Herrero, C., Suárez-Bregua, P. and Cid, A. (2012) Flow cytometric analysis to evaluate physiological alterations in herbicide-exposed *Chlamydomonas moewusii* cells. *Ecotoxicology*, **21**, 409–420.
- Qin, Y., Lu, M. and Gong, X. (2008) Dihydrorhodamine 123 is superior to 2,7-dichlorodihydrofluorescein diacetate and dihydrorhodamine 6G in detecting intracellular hydrogen peroxide in tumor cells. *Cell Biology International*, **32**, 224–228.
- Quinn, G. P. and Keough, M. J. (2012) *Experimental Design and Data Analysis for Biologists*. Cambridge University Press.
- Rasconi, S., Winter, K. and Kainz, M. J. (2017) Temperature increase and fluctuation induce phytoplankton biodiversity loss - Evidence from a multi-seasonal mesocosm experiment. *Ecology and Evolution*, **7**, 2936–2946.
- Raven, J. A. and Geider, R. J. (1988) Temperature and algal growth. *New Phytologist*, **110**, 441–461.

- Redfield, A. C. (1934) On the proportions of organic derivatives in sea water and their relation to the composition of plankton. *James Johnstone Memorial Volume*, 176–192.
- Redfield, A. C. (1958) The biological control of chemical factors in the environment. *American Scientist*, **46**, 205–221.
- Regaudie-de-Gioux, A. and Duarte, C. M. (2012) Temperature dependence of planktonic metabolism in the ocean. *Global Biogeochemical Cycles*, **26**.
- Reigstad, M. and Wassmann, P. (2007) Does *Phaeocystis* spp. contribute significantly to vertical export of organic carbon? *Biogeochemistry*, **83**, 217–234.
- Reinfelder, J. R. (2011) Carbon concentrating mechanisms in eukaryotic marine phytoplankton. *Annual Review of Marine Science*, **3**, 291–315.
- Remy, M., Hillebrand, H. and Flöder, S. (2017) Stability of marine phytoplankton communities facing stress related to global change: Interactive effects of heat waves and turbidity. *Journal of Experimental Marine Biology and Ecology*, **497**, 219–229.
- Rezayian, M., Niknam, V. and Ebrahimzadeh, H. (2019) Oxidative damage and antioxidative system in algae. *Toxicology Reports*, **6**, 1309–1313.
- Rhee, G.-Y. and Gotham, I. J. (1981) The effect of environmental factors on phytoplankton growth: Temperature and the interactions of temperature with nutrient limitation. *Limnology and Oceanography*, **26**, 635–648.
- Riebesell, U., Schulz, K. G., Bellerby, R. G. J., Botros, M., Fritsche, P., Meyerhöfer, M., Neill, C. and Nondal, G. et al. (2007) Enhanced biological carbon consumption in a high CO<sub>2</sub> ocean. *Nature*, **450**, 545–548.
- Rokitta, S. D., Kranz, S. A. and Rost, B. (2021) Inorganic carbon acquisition of aquatic primary producers. In Marberly, S. and Gontero, B. (eds), *Blue planet, red and green photosynthesis*. accepted.
- Rost, B. and Riebesell, U. (2004) Coccolithophores and the biological pump: responses to environmental changes. In Thierstein, H. R. and Jeremy, R. Y. (eds), *Coccolithophores: from molecular processes to global impact*. Springer, Berlin [u.a.], pp. 99–125.
- Rost, B., Riebesell, U. and Sültemeyer, D. (2006) Carbon acquisition of marine phytoplankton: Effect of photoperiod length. *Limnology and Oceanography*, **51**, 12–20.
- Rost, B., Zondervan, I. and Wolf-Gladrow, D. (2008) Sensitivity of phytoplankton to future changes in ocean carbonate chemistry: current knowledge, contradictions and research directions. *Marine Ecology Progress Series*, **373**, 227–237.
- Rothe, G. and Valet, G. (1990) Flow cytometric analysis of respiratory burst activity in phagocytes with hydroethidine and 2',7'-dichlorofluorescein. *Journal of Leukocyte Biology*, **47**, 440–448.
- Rousseau, V., Vaulot, D., Casotti, R., Cariou, V., Lenz, J., Gunkel, J. and Baumann, M. (1994) The life cycle of *Phaeocystis* (Prymnesiophyceae): evidence and hypotheses. *Journal of Marine Systems*, **5**, 23–39.
- Saiz, E., Calbet, A., Isari, S., Antó, M., Velasco, E. M., Almeda, R., Movilla, J. and Alcaraz, M. (2013) Zooplankton distribution and feeding in the Arctic Ocean during a *Phaeocystis pouchetii* bloom. *Deep Sea Research Part I: Oceanographic Research Papers*, **72**, 17–33.
- Sakshaug, E. (2004) Primary and secondary production in the Arctic seas. In Stein, R. and MacDonald, R. W. (eds), *The organic carbon cycle in the Arctic Ocean*. Springer, Berlin, Heidelberg, pp. 57–81.
- Samuels, T., Rynearson, T. A. and Collins, S. (2021) Surviving heatwaves: thermal experience predicts life and death in a Southern Ocean diatom. *Frontiers in Marine Science*, **8**.
- Sanz-Luque, E., Chamizo-Ampudia, A., Llamas, A., Galvan, A. and Fernandez, E. (2015) Understanding nitrate assimilation and its regulation in microalgae. *Frontiers in Plant Science*, **6**, 899.
- Schaefer, P. M., Kalinina, S., Rueck, A., Arnim, C. A. F. von and Einem, B. von (2019) NADH autofluorescence—A marker on its way to boost bioenergetic research. *Cytometry. Part A : The Journal of the International Society for Analytical Cytology*, **95**, 34–46.
- Schauer, U., Beszczynska-Möller, A., Walczowski, W., Fahrbach, E., Piechura, J. and Hansen, E. (2008) Variation of measured heat flow through the Fram Strait between 1997 and 2006. In Dickson, Robert R., Meincke, Jens and Rhines, P. (eds), *Arctic-subarctic ocean fluxes: Defining the role of the northern seas in climate*. Springer, Dordrecht, pp. 65–85.

- Schaum, C.-E., Barton, S., Bestion, E., Buckling, A., Garcia-Carreras, B., Lopez, P., Lowe, C. and Pawar, S. et al. (2017) Adaptation of phytoplankton to a decade of experimental warming linked to increased photosynthesis. *Nature Ecology & Evolution*, **1**, 94.
- Schlüter, L., Lohbeck, K. T., Gutowska, M. A., Gröger, J. P., Riebesell, U. and Reusch, T. B. H. (2014) Adaptation of a globally important coccolithophore to ocean warming and acidification. *Nature Climate Change*, **4**, 1024–1030.
- Schoemann, V., Becquevort, S., Stefels, J., Rousseau, V. and Lancelot, C. (2005) *Phaeocystis* blooms in the global ocean and their controlling mechanisms: a review. *Journal of Sea Research*, **53**, 43–66.
- Schuback, N., Tortell, P. D., Berman-Frank, I., Campbell, D. A., Ciotti, A., Courtecuisse, E., Erickson, Z. K. and Fujiki, T. et al. (2021) Single-turnover variable chlorophyll fluorescence as a tool for assessing phytoplankton photosynthesis and primary productivity: opportunities, caveats and recommendations. *Frontiers in Marine Science*, **8**.
- Serreze, M. C. and Barry, R. G. (2011) Processes and impacts of Arctic amplification: A research synthesis. *Global and Planetary Change*, **77**, 85–96.
- Sharma, P., Jha, A. B., Dubey, R. S. and Pessarakli, M. (2012) Reactive oxygen species, oxidative damage, and antioxidative defense mechanism in plants under stressful conditions. *Journal of Botany*, **2012**, 1–26.
- Simon, N., Cras, A.-L., Foulon, E. and Lemée, R. (2009) Diversity and evolution of marine phytoplankton. *Comptes Rendus Biologies*, **332**, 159–170.
- Smale, D. A., Wernberg, T., Oliver, E. C. J., Thomsen, M., Harvey, B. P., Straub, S. C., Burrows, M. T. and Alexander, L. V. et al. (2019) Marine heatwaves threaten global biodiversity and the provision of ecosystem services. *Nature Climate Change*, **9**, 306–312.
- Smetacek, V. (1999) Diatoms and the ocean carbon cycle. *Protist*, **150**, 25–32.
- Smith, W. O., Codispoti, L. A., Nelson, D. M., Manley, T., Buskey, E. J., Niebauer, H. J. and Cota, G. F. (1991) Importance of *Phaeocystis* blooms in the high-latitude ocean carbon cycle. *Nature*, **352**, 514–516.
- Soulié, T., Vidussi, F., Mas, S. and Mostajir, B. (2022) Functional stability of a coastal Mediterranean plankton community during an experimental marine heatwave. *Frontiers in Marine Science*, **9**.
- Staeher, P. A. and Sand-Jensen, K. A. (2006) Seasonal changes in temperature and nutrient control of photosynthesis, respiration and growth of natural phytoplankton communities. *Freshwater Biology*, **51**, 249–262.
- Stefanidou, N., Genitsaris, S., Lopez-Bautista, J., Sommer, U. and Moustaka-Gouni, M. (2019) Response of a coastal Baltic Sea diatom-dominated phytoplankton community to experimental heat shock and changing salinity. *Oecologia*, **191**, 461–474.
- Stoll, M. H., Bakker, K., Nobbe, G. H. and Haese, R. R. (2001) Continuous-flow analysis of dissolved inorganic carbon content in seawater. *Analytical Chemistry*, **73**, 4111–4116.
- Stramski, D., Sciandra, A. and Claustre, H. (2002) Effects of temperature, nitrogen, and light limitation on the optical properties of the marine diatom *Thalassiosira pseudonana*. *Limnology and Oceanography*, **47**, 392–403.
- Striebel, M., Schabhüttl, S., Hodapp, D., Hingsamer, P. and Hillebrand, H. (2016) Phytoplankton responses to temperature increases are constrained by abiotic conditions and community composition. *Oecologia*, **182**, 815–827.
- Strock, J. P. and Menden-Deuer, S. (2020) Temperature acclimation alters phytoplankton growth and production rates. *Limnology and Oceanography*.
- Sun, A.-Z. and Guo, F.-Q. (2016) Chloroplast retrograde regulation of heat stress responses in plants. *Frontiers in Plant Science*, **7**, 398.
- Taiz, L. and Zeiger, E. (2006) *Plant physiology*. Sinauer, Sunderland, Massachusetts.
- Thomas, M. K., Kremer, C. T., Klausmeier, C. A. and Litchman, E. (2012) A global pattern of thermal adaptation in marine phytoplankton. *Science*, **338**, 1085–1088.
- Turner, J. T. (2002) Zooplankton feeding ecology: does a diet of *Phaeocystis* support good copepod grazing, survival, egg production and egg hatching success? *Journal of Plankton Research*, **24**, 1185–1195.

- Twiner, M. J. and Trick, C. (2000) Possible physiological mechanisms for production of hydrogen peroxide by the ichthyotoxic flagellate *Heterosigma akashiwo*. *Journal of Plankton Research*, **22**, 1961–1975.
- Verity, P. G. (2000) Grazing experiments and model simulations of the role of zooplankton in *Phaeocystis* food webs. *Journal of Sea Research*, **43**, 317–343.
- Verity, P. G., Brussaard, C. P., Nejstgaard, J. C., van Leeuwe, M. A., Lancelot, C. and Medlin, L. K. (2007) Current understanding of *Phaeocystis* ecology and biogeochemistry, and perspectives for future research. *Biogeochemistry*, **83**, 311–330.
- Verity, P. G. and Medlin, L. K. (2003) Observations on colony formation by the cosmopolitan phytoplankton genus *Phaeocystis*. *Journal of Marine Systems*, **43**, 153–164.
- Verity, P. G., Villareal, T. A. and Smayda, T. J. (1988) Ecological investigations of blooms of colonial *Phaeocystis pouchetti*: I. Abundance, biochemical composition, and metabolic rates. *Journal of Plankton Research*, **10**, 219–248.
- Volk, T. and Hoffert, M. I. (1985) Ocean carbon pumps: Analysis of relative strengths and efficiencies in ocean-driven atmospheric CO<sub>2</sub> changes. In Sundquist, E. T. and Broecker, W. S. (eds), *The carbon cycle and atmospheric CO<sub>2</sub>*. American Geophysical Union, Washington, D. C., pp. 99–110.
- Wang, X., Tang, K. W., Wang, Y. and Smith, W. O. (2010) Temperature effects on growth, colony development and carbon partitioning in three *Phaeocystis* species. *Aquatic Biology*, **9**, 239–249.
- Wassmann, P. (2011) Arctic marine ecosystems in an era of rapid climate change. *Progress in Oceanography*, **90**, 1–17.
- Wassmann, P., Kosobokova, K. N., Slagstad, D., Drinkwater, K. F., Hopcroft, R. R., Moore, S. E., Ellingsen, I. and Nelson, R. J. et al. (2015) The contiguous domains of Arctic Ocean advection: Trails of life and death. *Progress in Oceanography*, **139**, 42–65.
- Wassmann, P., Reigstad, M., Haug, T., Rudels, B., Carroll, M. L., Hop, H., Gabrielsen, G. W. and Falk-Petersen, S. et al. (2006) Food webs and carbon flux in the Barents Sea. *Progress in Oceanography*, **71**, 232–287.
- Wassmann, P., Vernet, M., Mitchell, B. G. and Rey, F. (1990) Mass sedimentation of *Phaeocystis pouchetii* in the Barents Sea. *Marine Ecology Progress Series*, **66**, 183–195.
- Webb, W. L., Newton, M. and Starr, D. (1974) Carbon dioxide exchange of *Alnus rubra*: A mathematical model. *Oecologia*, **17**, 281–291.
- Weisse, T., Gröschl, B. and Bergkemper, V. (2016) Phytoplankton response to short-term temperature and nutrient changes. *Limnologia*, **59**, 78–89.
- Wernberg, T., Bennett, S., Babcock, R. C., Bettignies, T. de, Cure, K., Depczynski, M., Dufois, F. and Fromont, J. et al. (2016) Climate-driven regime shift of a temperate marine ecosystem. *Science*, **353**, 169–172.
- Wilhelm, C. and Jakob, T. (2011) From photons to biomass and biofuels: evaluation of different strategies for the improvement of algal biotechnology based on comparative energy balances. *Applied Microbiology and Biotechnology*, **92**, 909–919.
- Wolf, K. K. E., Hoppe, C. J. M. and Rost, B. (2018) Resilience by diversity: Large intraspecific differences in climate change responses of an Arctic diatom. *Limnology and Oceanography*, **63**, 397–411.
- Wolf-Gladrow, D. A., Zeebe, R. E., Klaas, C., Körtzinger, A. and Dickson, A. G. (2007) Total alkalinity: The explicit conservative expression and its application to biogeochemical processes. *Marine Chemistry*, **106**, 287–300.
- Wollenburg, J. E., Katlein, C., Nehrke, G., Nöthig, E.-M., Matthiessen, J., Wolf-Gladrow, D. A., Nikolopoulos, A. and Gázquez-Sanchez, F. et al. (2018) Ballasting by cryogenic gypsum enhances carbon export in a *Phaeocystis* under-ice bloom. *Scientific Reports*, **8**, 7703.
- Yakovleva, I. M., Baird, A. H., Yamamoto, H. H., Bhagooli, R., Nonaka, M. and Hidaka, M. (2009) Algal symbionts increase oxidative damage and death in coral larvae at high temperatures. *Marine Ecology Progress Series*, **378**, 105–112.
- Yamori, W., Noguchi, K., Kashino, Y. and Terashima, I. (2008) The role of electron transport in determining the temperature dependence of the photosynthetic rate in spinach leaves grown at contrasting temperatures. *Plant & Cell Physiology*, **49**, 583–591.
- Yang, X., Liu, L., Yin, Z., Wang, X., Wang, S. and Ye, Z. (2020) Quantifying photosynthetic performance of phytoplankton based on photosynthesis–irradiance response models. *Environmental Sciences Europe*, **32**.

- Young, J. N., Goldman, J. A. L., Kranz, S. A., Tortell, P. D. and Morel, F. M. M. (2015) Slow carboxylation of Rubisco constrains the rate of carbon fixation during Antarctic phytoplankton blooms. *New Phytologist*, **205**, 172–181.
- Yvon-Durocher, G., Jones, J. I., Trimmer, M., Woodward, G. and Montoya, J. M. (2010) Warming alters the metabolic balance of ecosystems. *Philosophical Transactions of the Royal Society of London. Series B, Biological Sciences*, **365**, 2117–2126.
- Zeebe, R. E. and Wolf-Gladrow, D. (2005) *CO<sub>2</sub> in seawater: Equilibrium, kinetics, isotopes*. Vol. 65. Elsevier, Amsterdam.
- Zhao, H., Kalivendi, S., Zhang, H., Joseph, J., Nithipatikom, K., Vásquez-Vivar, J. and Kalyanaraman, B. (2003) Superoxide reacts with hydroethidine but forms a fluorescent product that is distinctly different from ethidium: potential implications in intracellular fluorescence detection of superoxide. *Free Radical Biology and Medicine*, **34**, 1359–1368.
- Zhu, S., Huang, W., Xu, J., Wang, Z., Xu, J. and Yuan, Z. (2014) Metabolic changes of starch and lipid triggered by nitrogen starvation in the microalga *Chlorella zofingiensis*. *Bioresource Technology*, **152**, 292–298.